THIS THESIS IS SUBMITTED IN PARTIAL FULFILMENT OF THE REQUIREMENTS OF THE AWARD OF MSC BY RESEARCH

Development, Testing and Calibration of Oxford Brookes V-Twin Engine

Adam Christopher Stevens

Oxford Brookes University
Department of Mechanical Engineering and Mathematical Sciences

14/08/2020

INTENTIONALLY BLANK

“…I can’t design you the perfect engine, but I can design you the least worst, and that’s good to beat the pants off everybody…” Geoff Goddard

INTENTIONALLY BLANK

Abstract

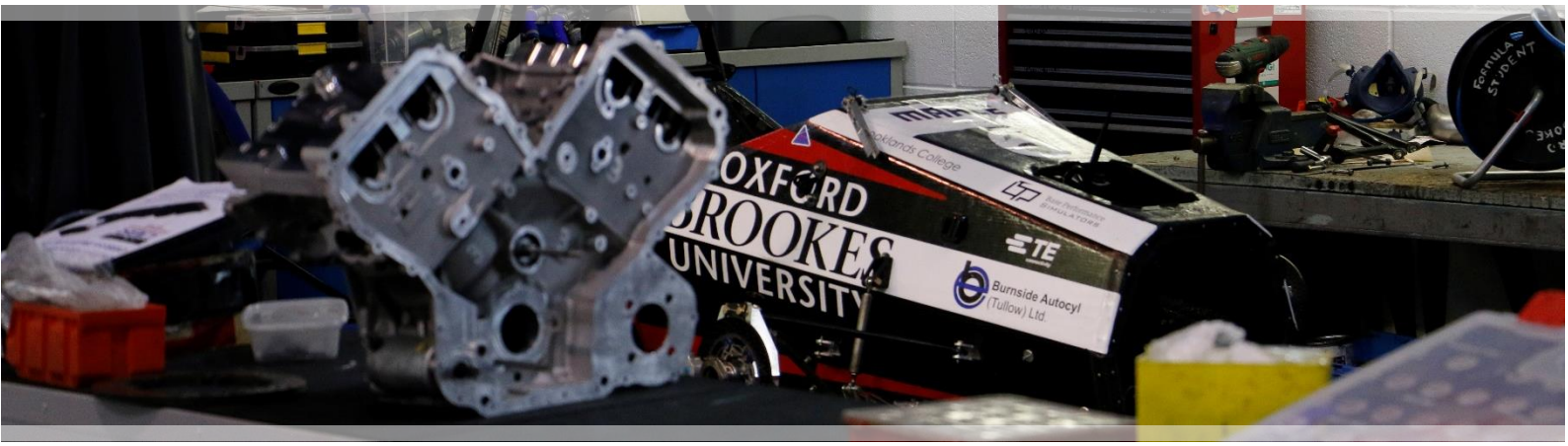

Figure 1: V-Twin Engine in OBU Autolab

The powertrain is one of the most distinguishable and, arguably, most important aspects of a high performance or competition vehicle. For over a decade, the V-Twin project aimed to provide a superior powertrain package for the Formula Student entry of the Oxford Brookes team, as a flagship for the capabilities and commitment of the students involved. This research built on the thousands of hours already invested into the programme by students until 2013, to complete the mechanical and electronic development of the engine to run, test and calibrate the engine for the first time.

This research investigated the mechanical development and calibration requirements of an otherwise blank sheet package, to derive a suitable base calibration for test cell operation.

A bespoke control system was designed and manufactured, with particular attention to reliability, redundancy and robustness. Calibration of sensors and actuators was conducted in accord with theoretical understanding to create a safe base configuration for start-up attempts. A comprehensive analysis of the drivetrain was conducted to ascertain safe operating ranges to minimise risk of integrity loss and component failure.

Datasets from each run were analysed to iteratively update the engine ancillaries, hardware and software, towards the objective of achieving acceptable idle quality at 3000 rev/min. Wide open throttle torque output at 3000 rev/min and 3500 rev/min was within 14% and 19% of one-dimension simulation results respectively. Encouraging BSFC (371g/kWh) and thermal efficiency figures (21%) were noted within this operating range, outside of the intended operating speed of such a high valve overlap configuration.

The conducted research and development represent a key milestone in the decade long development of the V-Twin package, as a basis and encouragement for future development towards a target of vehicle installation. Recommendations have been made with regards to test cell and rigging upgrades to safely expand the engine speed and load sites that can be tested beyond those recorded in this research

INTENTIONALLY BLANK

Acknowledgements

Sept 2016.

To list all those who have given their support, wisdom or shoulder over the past twelve months would require a supplement to this report. Rest assured your help has not gone unnoticed or without thanks.

INTENTIONALLY BLANK

Table of Contents

List of Figures

List of Tables

Acronyms and Abbreviations

ATDC	After Top Dead Centre
AV	Anti-Vibration
AW	Anti-Wear
BDC	Bottom Dead Centre
BTDC	Before Top Dead Centre
BMEP	Brake Mean Effective Pressure (bar)
BSFC	Brake Specific Fuel Consumption (g/kWh)
CAD	Computer Aided Design / Crank Angle Degrees
CFD	Computational Fluid Dynamics
CFR	Cooperative Fuel Research
CoV	Coefficient of Variation
CVI	Closed Valve Injection
DISI	Direct Injection, Spark Ignition
EIVC	Early Intake Valve Closing
Equivalence Ratio	$(A/F)_{Stoichiometric}$ divided by $(A/F)_{actual}$.
ET / ECT	Engine Coolant Temperature
EP	Extreme Protection
EGT	Exhaust Gas Temperature
EGR	Exhaust Gas Recirculation
FS	Formula Student
FSAE	Formula SAE
FSC	Formula Student (Combustion Engine Entries)
FSG	Formula Student Germany
GDI	Gasoline Direct Injection
HC	Hydrocarbons
HTHS	High Temperature, High Shear
IAT	Inlet Air Temperature (Celsius)
IJPU	Injector Scaling
IMEP	Indicated Mean Effective Pressure
KI	Knock Intensity
LA	Lambda
LH	Left-Hand
LNV	Lowest Normalised Value
MAP	Manifold Air Pressure (bar)
MBT	Point of Mean Best Torque
MFB	Mass Fraction Burned
MNV	Mean of Normalised Values
NA	Naturally Aspirated / Natural Aspiration
OBR	Oxford Brookes Racing
OBU	Oxford Brookes University
OVI	Open Valve Injection
PID	Proportional Integral Derivative
PFI	Port Fuel Injection
PW	Pulse Width (ms)
RH	Right-Hand
SI	Spark Ignition, Otto Cycle
SIT	Self-Ignition Temperature of the fuel used
SOC	Start of Combustion
SOI	Start of Injection
TDC	Top Dead Centre
Turbo	Turbocharger
UK	United Kingdom
WOT	Wide Open Throttle

Nomenclature

$\boldsymbol{A/F}$	Air to Fuel Ratio (Stoichiometric ≈ 14.7:1)
$\boldsymbol{C}$	System stiffness (Nm/rad)
$\boldsymbol{\overline{C}}$	Mean Piston Speed (m/sec)
$\boldsymbol{F_n}$	Natural Frequency (Hz)
$\boldsymbol{J_D}$	Polar Moment of Inertia, Dynamometer (m^4)
$\boldsymbol{J_E}$	Polar Moment of Inertia, Engine (m^4)
$\boldsymbol{\dot{m}_f}$	Mass Flow Rate of Fuel (Kg/sec)
$\boldsymbol{n}$	Constant (2 for 4-stroke SI engines)
$\boldsymbol{N}$	Engine Speed (rev/sec)
$\boldsymbol{r_c}$	Compression Ratio
$\boldsymbol{Q_{LHV}}$	Calorific Value of Fuel Used (44MJ/Kg)
$\boldsymbol{V_d}$	Displacement Volume per cylinder (m^3)
$\boldsymbol{\dot{W}}$	Indicated Power Output (W)
$\boldsymbol{\dot{W}_b}$	Brake Power Output (W)
$\boldsymbol{\lambda}$	Lambda. $(A/F)_{actual}$ divided by $(A/F)_{stoichiometric}$.
$\boldsymbol{\eta_c}$	Combustion efficiency
$\boldsymbol{\eta_f}$	Fuel combustion efficiency
$\boldsymbol{\eta_{f,ig}}$	Fuel combustion efficiency, indicated gross
$\boldsymbol{\eta_{th}}$	Thermal efficiency of process
$\boldsymbol{\eta_v}$	Volumetric Efficiency
$\boldsymbol{\rho_{air}}$	Density of Intake Air (kg/m^3)
$\boldsymbol{\tau}$	Brake Torque (Nm)
$\boldsymbol{\gamma}$	Ratio of specific heats of intake charge

1 | Introduction

Formula Student is a competition in which universities and colleges around the world design, and build, single seat race cars. Regarded as a 'breeding ground for engineers', the competition encourages a wide range of design concepts. A variety of different powertrain configurations are used, with each team striving to achieve the best compromise between cost, weight and performance from their system.

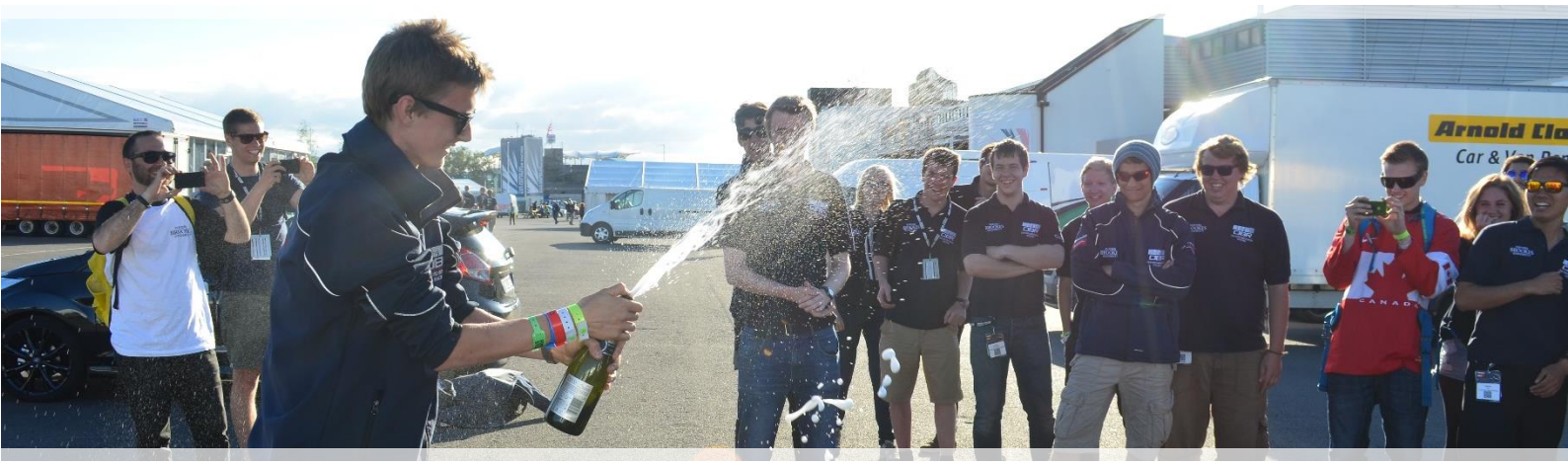

Figure 2: *OBR winning design event, FSUK 2014 [1].*

Oxford Brookes Racing, the formula student team of Oxford Brookes University, has been at the forefront of the competition, both in terms of innovation and performance. With an ethos of simple, lightweight design, capturing the spirit of the weekend racer, the 2014 team regained the title of *top UK entry*, winning the UK design event in the process (Figure 2). Despite significant work, the performance characteristics of the single-cylinder KTM engine used leave the team's entries at a disadvantage to 4-cylinder and electric rivals.

Started in 2006, the V-Twin development aimed to create the world's first student designed and built powertrain, consolidating the system to a semi-stressed package to improve vehicle dynamics and drivability.

The purpose of this research is to develop a control strategy and base calibration for the engine, such that torque and power output can be compared to simulation to iteratively optimise both.

1.1 | Aims and Objectives

The overall aim of the project was to perform base calibration of the Oxford Brookes V-Twin engine. This could be divided into the following subtasks, reflected in the structure of the report.

N1: Conduct a comprehensive literature review of high-performance engine design concepts and control system strategies. This is to understand and highlight the features of the project engine, and the accommodations that may need to be made to provide suitable control refinement.

N2: Mechanical development of engine unit and ancillaries in preparation for test cell installation.

N3: Development of an electronic control system utilising a third-party engine control unit

N4: Population of ECU calibratable parameters using theory and prior knowledge for first fire

N5: Collection of performance data to allow iterative optimisation of calibration.

The broad range of research conducted extends published work and theories in the application of the V-Twin engine, with additional resource constraints and complexities.

1.2 | Thesis Layout

Expanding on the title of the thesis, the first chapter introduces the context and background of the project, along with the aims and objectives specified at the start of the exercise. The second chapter gives a detailed overview of the work previously conducted in the subject area, and their relevance and influence on the system's previous development has been discussed.

The methodology of system development is presented in the third chapter, with base calibration and bedding in sequences collated in the fourth. Performance results from base mapping and their discussion are presented in the fifth chapter. Following project conclusions in the sixth chapter, recommendations for future work are outlined in the seventh.

2 | Literature Review

2.1 | Introduction

Figure 3: Render of OBU V-Twin Timing assembly

To minimise the risk to competitors, event organisers restrict many aspects of the powertrain configuration, most notably a displacement limit and restriction of the mass flow through the intake [2]. As such, teams strive to achieve the most volumetric and thermal efficient systems to improve the vehicle performance during dynamic competitions (Table A1). This also gives rise to engine downsizing, allowing the mass of the overall vehicle to be reduced for a target power output, to the preference of kinematics and resource conservation [3].

This section discusses the notable design and control strategies for improving specific power output, thermal efficiency and response characteristics in high performance powertrains, in particular the optimisation of components in response to intake restrictions [4] [5]. Whilst this review primarily concerns the 4-stroke spark ignited engine configuration of the V-Twin, electrification either in direct replacement or in conjunction with SI engines should be noted as an emerging area for increased conversion efficiency and power output [6] [7].

"There are many newly invented or resurrected ideas which are claimed to be beneficial to the performance of engines. Whether or not these features are of real benefit is often the subject of lively debate within the engineering community and even devices which offer a measurable advantage are sometimes difficult to justify" [8].

In a vehicle installation, the tractive effort of the powertrain unit is calculated as a function of the torque output of the engine across vehicle operating speeds: the culmination of engine design concepts and control strategies should be focused on delivering a smooth, uniform torque curve and, in high performance applications, the largest area underneath the power curve. Abrupt changes in torque output can produce undesirable vehicle responses, such as excessive wheel slip, understeer or oversteer, compromising the drivability of the package [9]

2.2 | Engine Design Concepts

Numerous studies have been conducted to understand the effect of individual component geometry on emissions, efficiency and engine response characteristics. Commonly, the engine acts as an air pump, in which the components are optimised to increase the volume, density and homogeneity of the charge entering the chamber. Whilst it is common for papers written on the subject to focus on one particular component or feature of the system, it is important to stress the interdependent nature of a powertrain unit: their influence on other aspects should be considered to provide the best compromise for the intended application

Whilst there is overlap between design concepts used to achieve maximum thermal efficiency and those aimed at peak performance, these two goals are discreet. Figure 4 identifies engine parameters that influence brake thermal efficiency: whilst this is not an exhaustive list, concepts such as exhaust gas recirculation and lean burn will be discussed as often detrimental to BMEP.

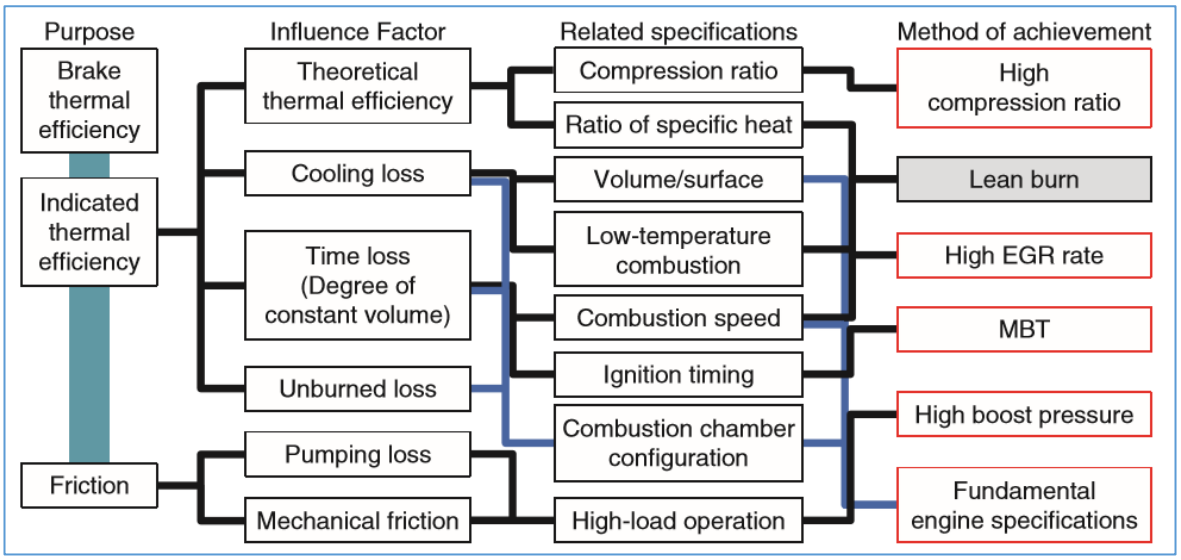

Figure 4: General Influences of Brake Thermal Efficiency [10]

As such, compromises within design concepts and decisions are inevitable: during the development of the V-Twin engine several areas have been designed with the additional constraints of component longevity, noise restrictions and fuel economy. Through this review it is important to identify the decisions previously made in the design of the project engine, so that it can be developed and calibrated accordingly.

2.2.1 | Engine Geometry

The brake power of a four-stroke internal combustion engine could be described with regards to BMEP, mean piston speed and engine displacement (Equation 1).

$$P_b \propto bmep \cdot \overline{C} \cdot \sqrt[3]{\left(\frac{V_d}{S/_B}\right)} \cdot N \qquad \textit{Equation 1 [12]}$$

For a fixed displacement Bianchi *et al* [11] explains how, in this simplified derivation, high engine speed, high compression ratio and high bore/stroke ratio are required to achieve high power output. In medium to high engine speed, their studies increasing the bore/stroke ratio yielded a volumetric improvement of up to 4%, to the detriment of low speed operation (Figure 5). However, the increased heat rejection to the chamber through the relationship between bore/stroke ratio and surface area per chamber volume leads to a reduction in thermal efficiency.

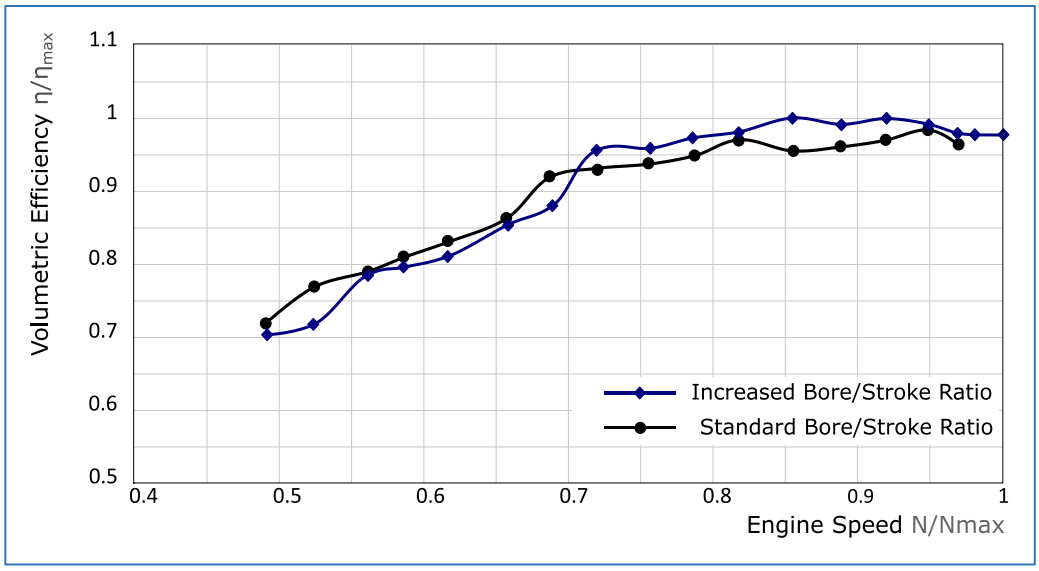

Figure 5: Effect of bore-to-stroke ratio on Volumetric Efficiency, adapted from [12]

Bianchi *et al* [11] noted the effect of compression ratio on recorded outputs, normally limited by increased propensity to knock [12]. Gerty; Heywood [13], and Ayala *et al* [14] separately concluded that raising the compression ratio of a test engine yielded increased brake, gross indicated and net indicated efficiencies by 5.1, 4.6 and 4.5% respectively, *as* hypothesised through Equation 2.

$$\eta_{f,ig} = 1 - \frac{1}{r_c^{\gamma-1}} \qquad \textit{Equation 2 [16]}$$

In production applications or instances where the vehicle is traction limited, further efficiency can be gained by reducing the engine's displacement as R_c is increased, to match torque output of the base engine (Figure 6).

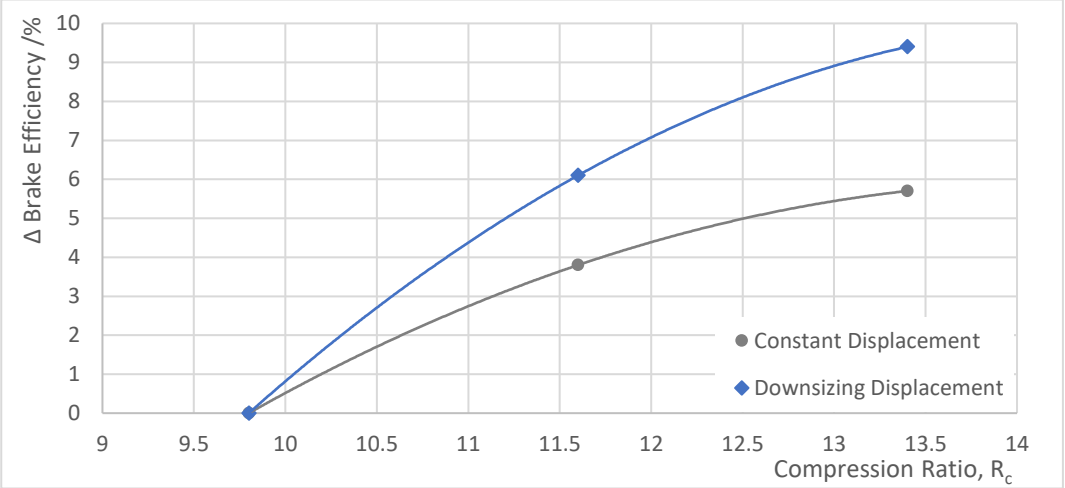

Figure 6: Relationship between R_c and Brake Efficiency, adapted from [13]

Whilst the total displacement of the four-stroke engine is stipulated within FS regulations, the number of cylinders and their arrangement are open for optimisation. However, the number of cylinders is realistically limited to four, given its proportionality to frictional losses and system complexity. Cylinder configuration and respective firing orders can lead to crankshaft imbalance through primary or secondary forces and moments, causing discomfort to the driver and, in extreme cases, fluctuation in vertical load on the tyres.

The chosen package is often a compromise between engine balancing, centre of gravity, lubrication properties, system mass and vehicle packaging. High performance, and high efficiency, engine design results in peak cylinder pressures above 200 bar [15], hence design of critical components have been carefully dimensioned and detailed in the previous stages of the V-Twin development to prevent premature failure.

2.2.2 | Engine Aspiration for Restricted Formulae

The feasibility of forced induction in restricted formulae has been widely researched, through increasing the density of the intake charge these systems aim to increase specific power output [16] [17]. Turbochargers can be used to achieve this, normally at the detriment of tip-in response and system reliability. Wastegate control is often implemented in order to provide additional volumetric efficiency when operating in conditions of high torque demand and low engine speed, resulting in a more uniform torque curve. The utilisation of energy from the expended gas can also advantageously reduce noise pollution.

Variable geometry turbochargers have been recently used to reduce the lag and resulting drivability flaws in conventional turbochargers [18]. Whilst their use has been historically focused in diesel engines, the technology is becoming readily available for gasoline engines, where the exhaust gas temperatures are significantly higher.

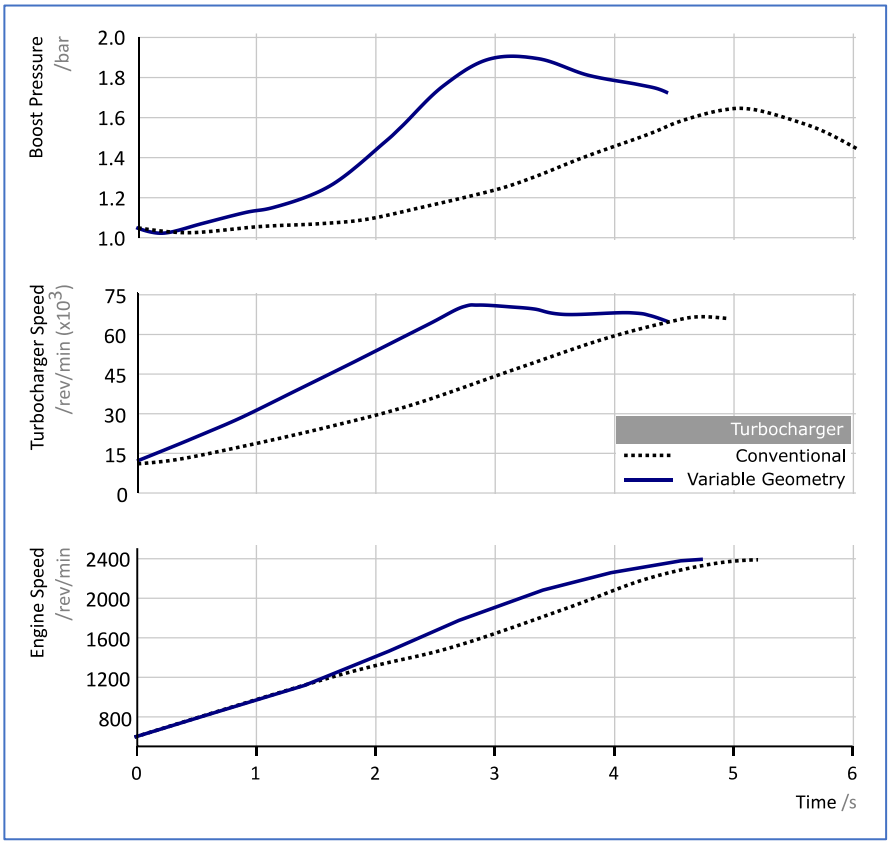

Figure 7: Fixed vs variable geometry turbocharger behaviour in response to tip-in [18]

Removing the dependency on sufficient energy in the exhaust gas, supercharged systems are rotated directly by the crankshaft to compress the intake air. Whilst the tip-in response is widely regarded to be improved compared to a turbocharger system the parasitic load often reduces thermal efficiency. E-superchargers are an emerging form of hybridisation [19], utilising a high speed motor to boost manifold pressure, providing significant benefit at low speed operation (Figure 8) [20].

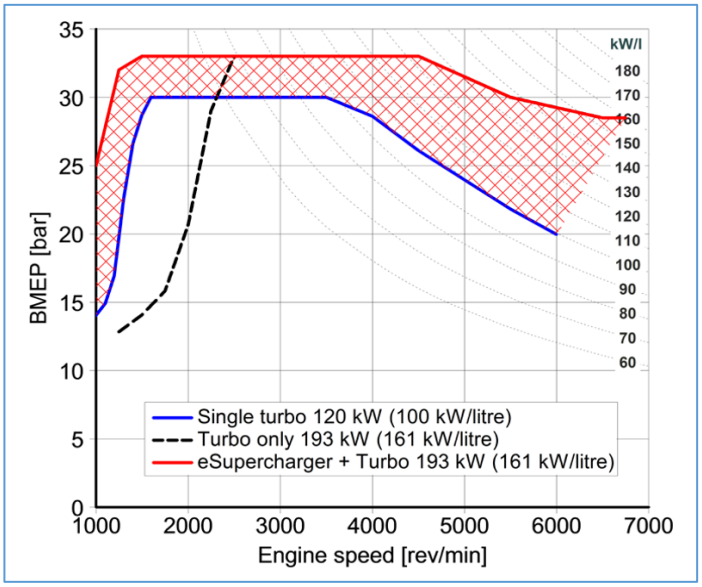

Figure 8: Characteristics of MAHLE eSupercharged downsized engine operating at 160kW/l [21]

Whilst research has focused on utilising energy from exhaust gas or the crankshaft, a re-emerging area of interest involves the compressed air in the crankcase. Installing reed valves between a baffled crankcase and the intake can achieve a small torque increase through normalising intake pressure

during the intake stroke [22]. Alternatively, crankcase geometry can be used to create an air spring, creating a diminishing force underneath the piston, reducing the negative work done during compression and exhaust strokes [23]. The project engine will naturally benefit from this phenomenon to a reduced effect as the displacements of the pistons are 75° out of phase.

2.2.3 | Manifold Geometry and the Requirement for Plenum Chambers

Formula Student regulations stipulate a maximum intake throat diameter of 20mm, downstream of the throttle [24]. Providing a large air reservoir upstream of the intake ports, a plenum acts to minimise this constraint by normalising the flow of air to design point at the restrictor, thus increasing the average intake pressure during the intake stroke at high engine speeds. Hamilton and Lee [25] noted a 14 per cent increase in WOT volumetric efficiency with a 4-cylinder engine conforming to the same regulations, focusing on steady-state testing (Figure 9).

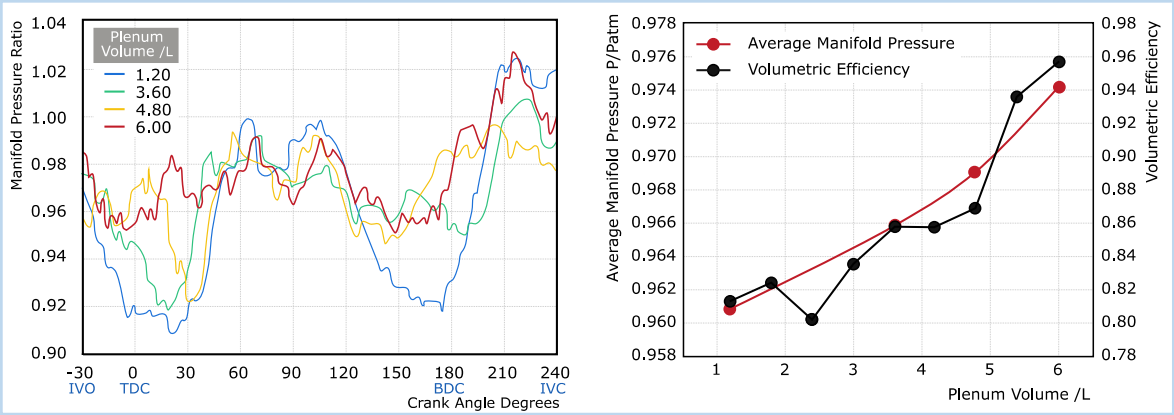

Figure 9: Effect of Plenum Volume on Manifold Pressure & Volumetric Efficiency. Adapted from [28]

Larger plenums give rise to notable tip-in and tip-out delay, given the time required for the manifold pressure to react to throttle adjustments. Plenum geometry is therefore a compromise between responsiveness and torque output at high engine speeds. Stationary volumes of air can be discretised from the central manifold, to the advantage of system packaging [26].

The number of cylinders has significant influence on plenum volume required to minimise choking before the operating speed limit; one reason why 4-cylinder engines have historically been preferred for the competition [27]. Single cylinder engines require the total displacement volume during one intake stroke, whereas twin, triple and 4-cylinder configurations ingest the displacement air more uniformly, assuming an even firing order.

Intake runner length tuning is a method of advantageously increasing pressure behind the valve during the intake stroke. Using a compressible flow model, longitudinal waves occur in the runner due to the cyclic flow of air to the chamber and the resulting pressure drop upstream. The speed of sound for intake air can be approximated, allowing the tuned length for resonance to be calculated with respect to engine speed (as a function of the period between valve openings) [23]. At each resonant order charge pressure at the runner increases, providing a light forced induction effect.

The intensity of the longitudinal wave diminishes with resonance order as a proportion of energy is lost at the end of the intake runner into the plenum on each reflection [28]. As such, torque gain through this phenomenon is greatest at first order resonance, but is often at the detriment of drivability. The range of engine speeds in which a given resonance occurs is inherently narrow; to provide a more even torque output across all engine operating speeds, a tuned length should be chosen that achieves 3.5 order resonance around the engine speed of peak power [23] (Figure 10).

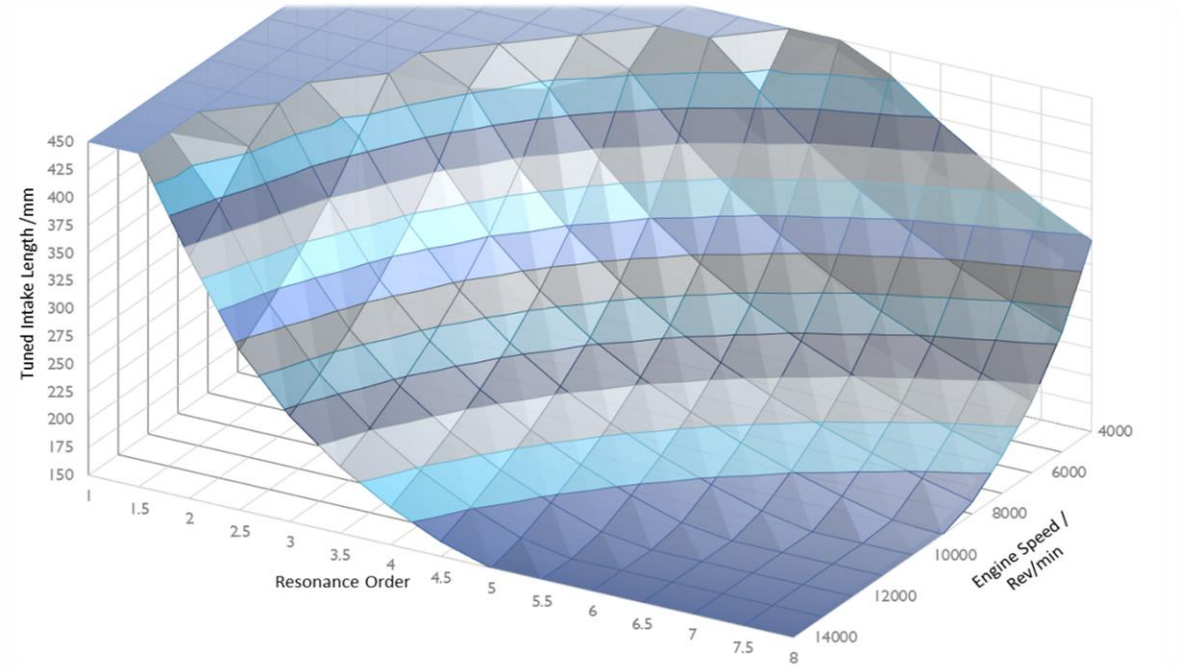

Figure 10: Repetition of Resonance with fixed intake runner length. Adapted from [29]

In multi-cylinder configurations, unequal intake or exhaust runner lengths can be used to disperse the resonance peaks in torque output [30]. Similar effects can be achieved when applied to exhaust manifold runners, with resonance occurring at longer tuned lengths due to the increased energy of the gas.

Complex manifold geometries can distort the aforementioned tuning calculations and often require a combination of computational modelling, physical validation and iterative tuning [31] [32]. Interactions between cylinders with overlapping intake strokes can provide additional challenge in accurate flow prediction [33].

Whilst precedence should be given to diffuser length, excessive diffuser half-angles can reduce flow attachment and hence manifold efficiency [34]. Given the difference in energy between the intake and exhaust charges, precedence is given to the inlet tract in the previous design of the project engine to minimise flow separation (Figure 11).

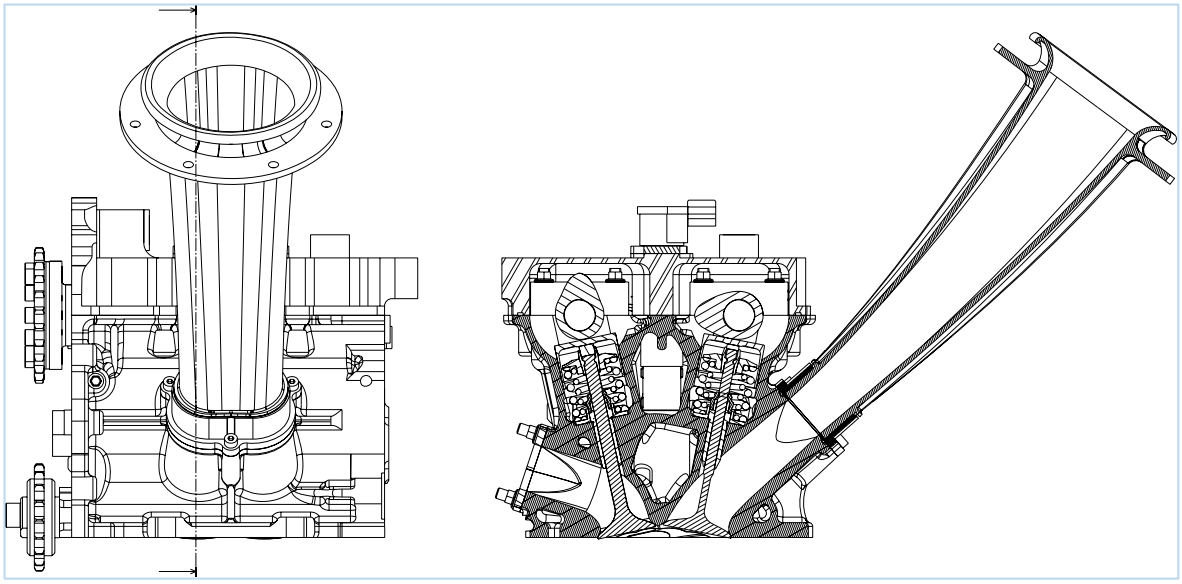

Figure 11: Representation of OBU V-Twin Cylinder Head [35].

Exhaust port and manifold design has considerable impact on back pressure, which can lead to high quantities of internal EGR and reduction in BMEP. Whilst noting a lower limit for exhaust runner diameter, Primus [36] concluded a wide range of diameters are suitable as reductions in frictional losses when manifold diameter is increased are countered by proportional valve throttling losses. Optimum exhaust diameter was hypothesised to increase with respect to engine speed, providing another area of system tuning to normalise torque characteristics.

Studies by Lakshmikantha; Kec [37] and Wade; Hsieh [38] note design considerations for thermal cyclic failure and exhaust quenching respectively, however the short design life for motorsport render the exhaust header and silencer consumable, and hence have not been primarily considered in their design.

2.2.4 | Valvetrain and Port Flow Regulation

Given the reduction in pressure upstream of the intake port compared to unrestricted engines, a longer duration of intake valve opening is generally used to compensate. Taylor *et al* [39] concluded that 'intake camshaft duration is one of the most significant factors affecting engine performance in its restricted format', resulting in a longer overlap between the two sets of valve openings.

A longer overlap can improve the scavenging effect in conditions of high mass flow, whereby the vacuum caused by the spent gas exiting the chamber increases the mass of fresh charge entering. This can lead to more valve lift at TDC, requiring piston geometry of engines with low squish clearance to be modified to suit. Using cams designed for an unrestricted engine, excessive valve duration can result in portions of negative flow during overlap and the start of the compression stroke when the intake pressure is reduced through intake choking [40]..

Increasing valve overlap can also reduce internal EGR, though the thermal efficiency of the engine may reduce as a larger quantity of port-injected fuel can be drawn through the exhaust port. Often the centre position of the valve overlap does not reside at TDC: a displacement of overlap centre position of 10 ^{O}BTDC was noted to reduce burn duration and regulate ignition delay [41].

Thermal efficiency can be improved by using either a late [42] or early intake valve closing strategy [43]: the expansion ratio remains mechanically constrained whilst the effective compression ratio is defined by valve timing. Forced induction is normally required on such configurations to maintain specific power output (creating a Millers Cycle configuration).

Port throttling allows the idle stability and BSFC of a high valve overlap arrangement to be maintained at values associated with low overlap in a conventionally throttled engine [44] (Figure 12). The main advantage for motorsport applications is the increased operating range of engine speeds and promotion of engine braking [45]. Tip-in response of large plenums can be improved and part-throttle charge dilution is reduced. However, to comply with FS regulations a conventionally located throttle is required in conjunction.

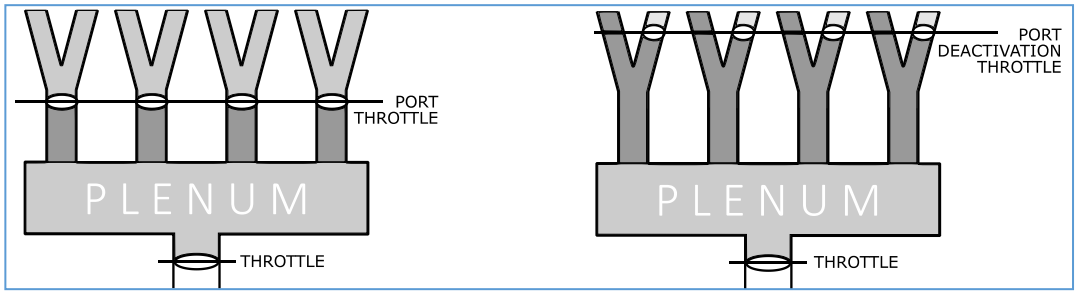

Figure 12: Port Throttled (left) and Port Deactivated Configurations. Adapted from [45]

Port deactivation can also be used to induce tumble and swirl to the intake charge entering the chamber, and give similar effects to port throttling. The increased complexity of the intake or valvetrain assemblies when employing port throttling or deactivation should however be noted, with focus on repeatable actuation their effect on unthrottled operation.

2.2.5 | Combustion Chamber Design

Of particular importance in chamber design is the minimisation of burn duration before knock regions (Section 2.3.3). This reduces the ignition advance required, the negative work done and the stress on the reciprocating components, maximising combustion efficiency. Creating axial swirl and tumble of the chamber gasses, through both cylinder head and piston geometry, is used to increase the homogeneity of the charge to promote uniform, predictable rate of combustion [46] [47].

In addition to affecting flow speed, valve lift significantly affects the turbulence of the charge downstream of the valve (Figure 13). Valve timing and chamber design are therefore synergistic to volumetric and thermal efficiency improvements. Chamber geometry modifications for the

improvement of turbulent kinetic energy can also impact the achievable compression ratio, as configurations similar to pent roofs increase the volume at TDC.

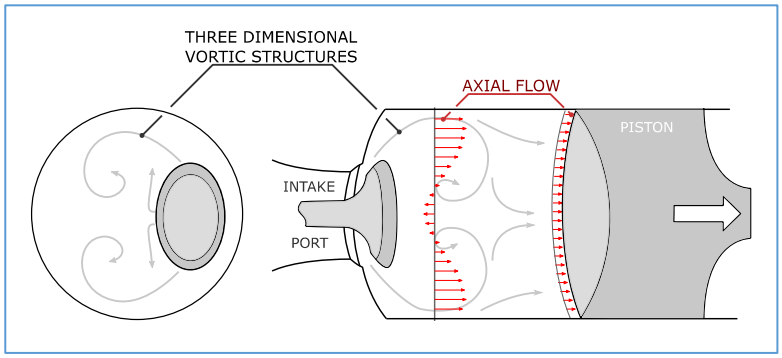

Figure 13: Representation of Vortices Induced through Small Valve Openings. Adapted from [48]

The geometry, quantity and layout of valves within the cylinder head has significant impact on volumetric efficiency and, through its effect on charge motion and dilution, burn duration and homogeneity of the intake charge. Precedence is given to the intake valves in terms of area and location, given the difference in energy between intake charge and exhaust gas (Figure 14).

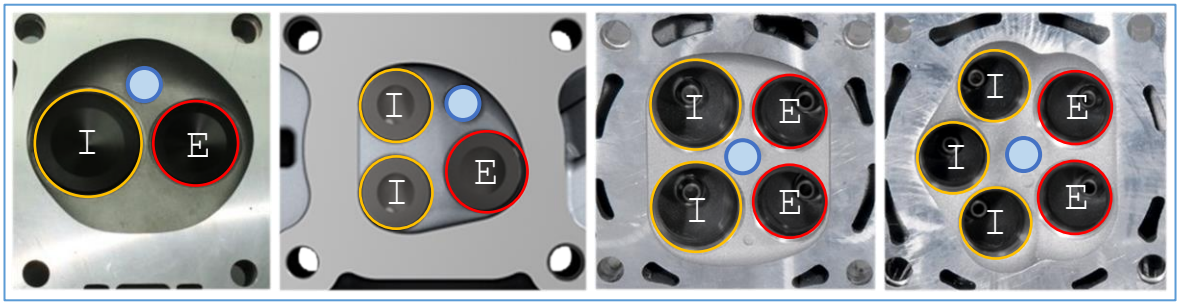

Figure 14: Comparison 2,3,4 and 5 valve single cylinder heads [49] [50] [51].

Most automotive applications utilise 4 or 5 valve per cylinder configurations. Applications where manufacturing cost and complexity are paramount may use 3-valve and 2-valve designs to the detriment of fuel efficiency, due in part to unfavourable spark plug position. The effectiveness of a 5-valve configuration is dependent on the bore diameter (Figure 15); at bores above 90mm diameter the increase in intake valve opening area outweighs the increased shrouding by the cylinder walls [52] (Figure 16). Negligible difference between a five-valve and four-valve configurations was observed at light load, with respect to burn rate, fuel consumption and EGR tolerance [8].

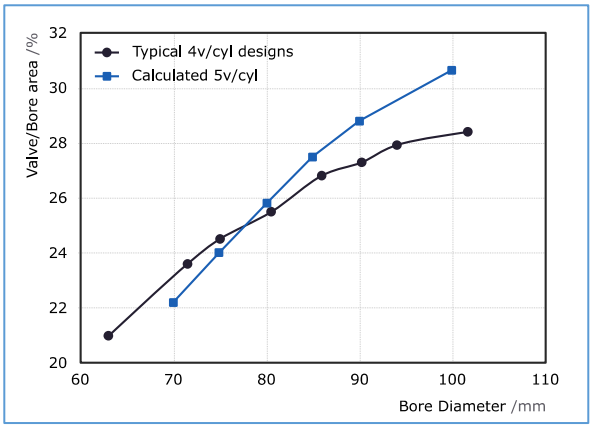

Figure 15: Comparison of Valve Area between 4-valve and 5-valve heads with respect to bore. Adapted from [8]

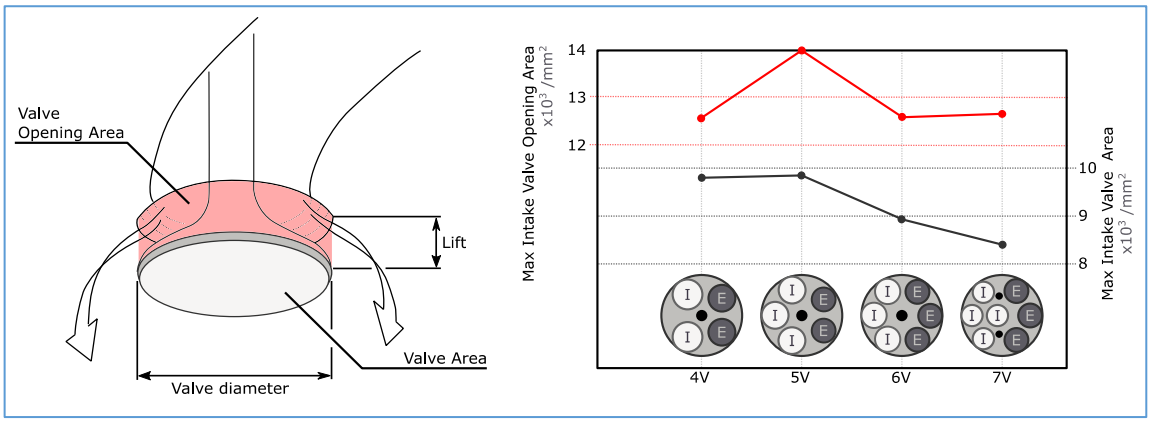

Figure 16: Relationship between valve configuration and opening area. Adapted from [52]

In addition to increased system complexity, a 5-valve design was observed to have gas velocity across the exhaust stroke approaching Mach 1, 'implying pressure losses due to friction and transonic choking effects would be a significant performance limiting factor' [53]. The V-twin engine employs a high lift 4-valve per cylinder design; the Vee configuration allows for preferential packaging of the inlet tract, and efficient design of valvetrain actuation for high speed, high temperature operation.

The type, location and installation angle of the spark plug in gasoline engines has influence on the flame propagation characteristics and knock tolerance, with several studies highlighting the importance of flame front concentricity and head symmetry [54] [55]. The project engine utilises a semi surface discharge design to minimise the shrouding of the electrode and minimise the intrusion in the combustion chamber. Viewed in cross section, the top surface of each piston is slanted, creating faces perpendicular to the inlet and exhaust valve centrelines. This is utilised by the valvetrain configuration to extend the duration and overlap of the cams, whilst minimising the risk of valve damage at low dynamic clearances [56] (Figure 17).

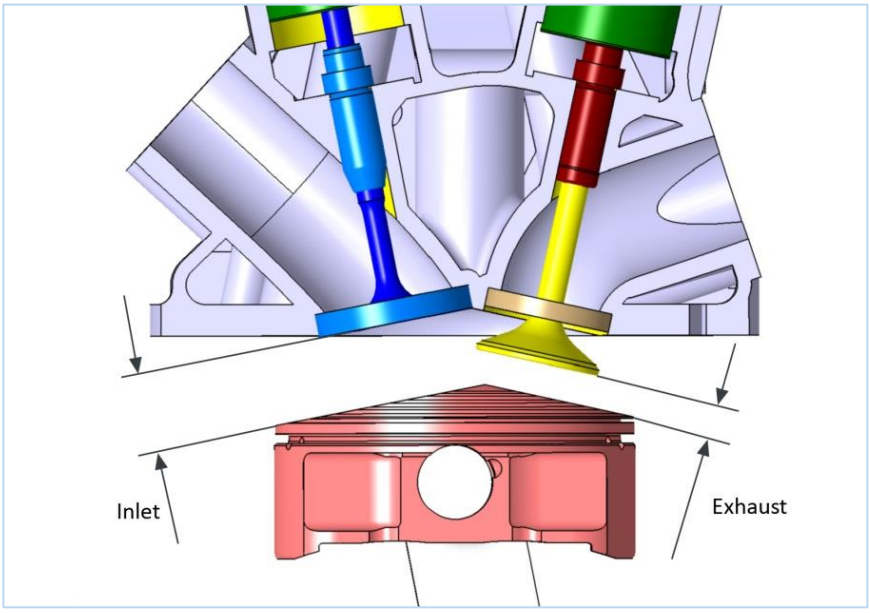

Figure 17: Representation of V-Twin Piston and Valve Clearance [57]

Care must be taken to design adequate heat rejection into the cylinder, head and piston crown; minimising areas of excessive surface temperature that may cause knock or component damage. Modern water-cooled IC engines include jackets designed for multiphase cooling, enhancing the heat transfer through convection [58] (Figure 18).

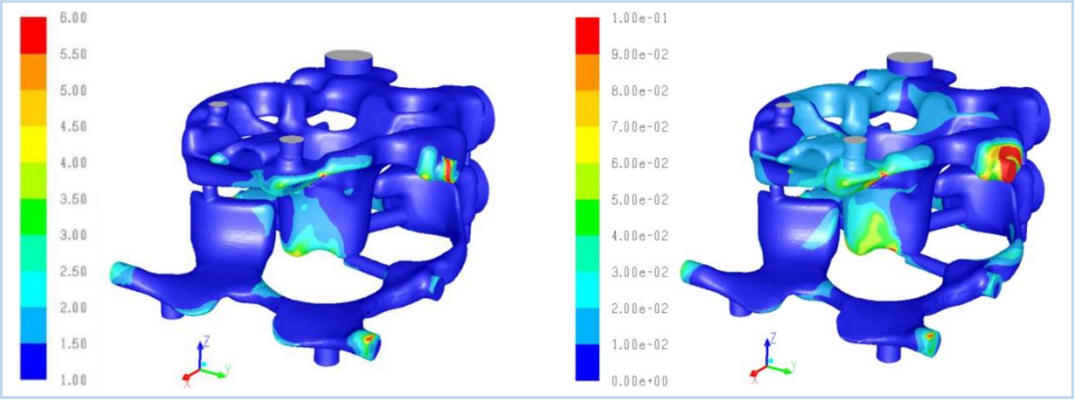

Figure 18: *Regions of Multiphase Cooling on Normalised Heat Transfer (Left) and Vapour Volume Fraction (Right) [58]*

2.2.6 | Lubrication System and Engine Oils

The lubrication system is an integral design with primary objectives of minimising wear and frictional losses, as well as conduction of heat. Arguably its importance is forgotten, particularly in the grade of oil specified, and can result in fundamental durability or performance complaints difficult to rectify if not properly considered.

Configurations are categorised as wet sump and dry sump systems, with the latter commonplace in motorsport. Wet sump systems house oil below the crank centreline and components are lubricated through splashing or positive displacement. The required sump depth increases the centre of gravity of the powertrain, and the displacement of oil away from the intended pickup points can lead to oil starvation and component damage (Figure 19). Conversely dry sump systems continually scavenge the oil from the sump, where it is de-aerated and reintroduced to the system under pressure. Providing sufficient oil pressure under a much wider range of vehicle conditions, the external reservoir can also to an extent act as an oil cooler, and vehicle kinematics is improved.

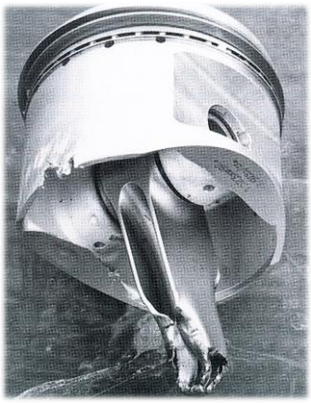

Figure 19: *Connecting rod bearing seizure due to oil starvation in high speed cornering [59]*

Within modern automotive applications, the reduction of friction and pumping losses is of primary concern, with the prerequisite of meeting longevity targets. The theory of bearing lubrication is based on the formation of an oil film between two cylindrical surfaces, and through its viscosity this film creates sufficient pressure to withstand loads that tend to bring these two surfaces together.

The lubrication phase corresponding to the conditions required for the formation of a sufficiently thick oil film to eliminate solid friction is known as hydrodynamic lubrication [60]. In this case, the friction coefficient and oil thickness are entirely determined for a given bearing diameter, diametrical clearance and length by the product:

$$\frac{\mu N}{\rho} \qquad \textit{Equation 3}$$

Where N is proportional to speed, μ is the viscosity of the lubricant and p is the specific pressure on the surfaces, with exception when the oil film is less than or equal to the surface roughness. Boundary and Mixed lubrication scenarios often lead to component wear if suitable extreme protection (EP) additives or coatings are not sufficient (Figure 20).

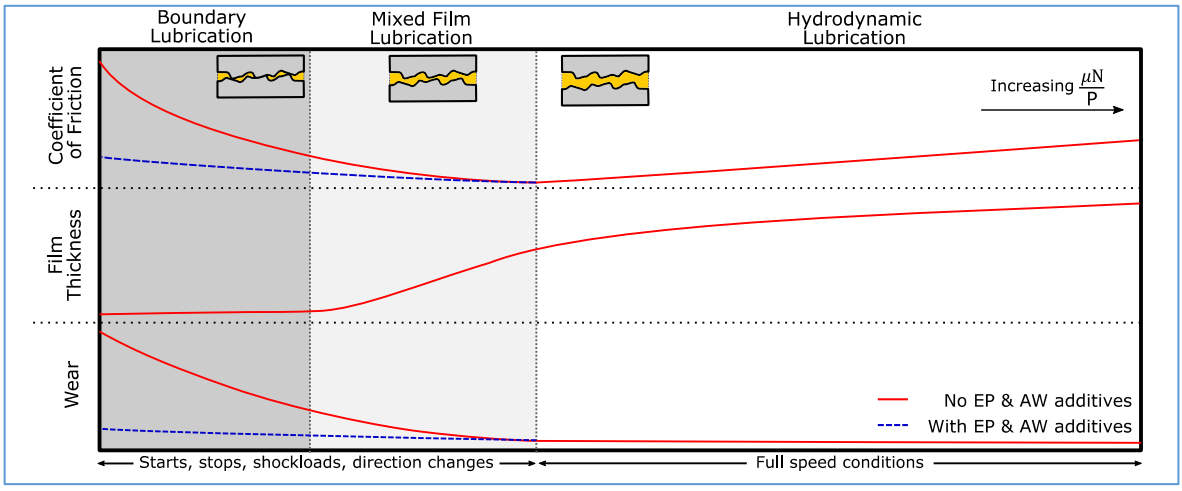

Figure 20: Stribech curve describing effect of lubrication modes. Adapted from [61]

Lubricating oil is an example of non-Newtonian fluid and hence its viscosity is dependent on temperature, pressure and shear rate. As such, critical components are often designed around the high temperature, high shear viscosity (HTHS) of an oil, as the test sequence for this parameter replicates the pressure and shear rate within crankshaft bearing journals.

A film of oil is naturally present along the cylinder walls and is constantly replenished as the more volatile constituents evaporate and (often) ignite. Whilst oil consumption is not of primary importance within motorsport, minimising this parameter is synonymous with efficiency and longevity expectations in automotive applications. Conversely, fuel and water droplets can enter the lubrication system and, over time, this dilution can significantly reduce the viscosity and performance of the oil.

2.3 | High Performance Engine Management and Control Strategies

Control system development is often an iterative process which requires significant prior knowledge and understanding of mechanical design concepts to provide suitable refinement. Whilst areas such as control algorithm development and transient calibration are outside the scope of this project, Figure 21 depicts a typical workstream for automotive applications.

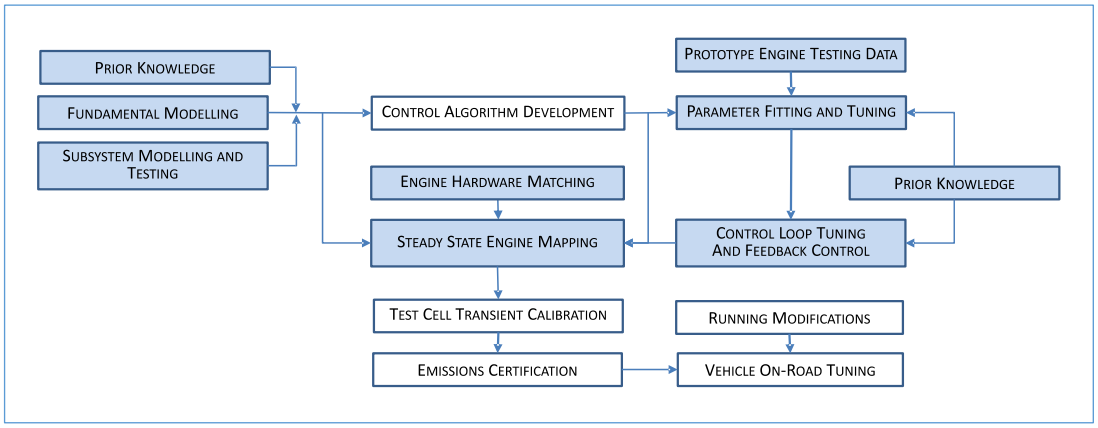

Figure 21: Engine Control System Development Flow Chart, adapted from [62]

This section of the review focusses on the fuelling and ignition strategies required for steady state calibration, highlighted blue in the above figure.

2.3.1 | Fuel Management Strategies

Regulation of the air/fuel ratio has long been a primary area for system calibration, and its effect on performance, emissions and efficiencies have been widely documented. Commonly for gasoline SI engines, power and BMEP follow a parabolic curve, with maxima positioned slightly rich of stoichiometric combustion [63]. Tang *et al* [64] observed benefit of spark timing adjustments to suit changes in flame speed with lambda (Figure 22).

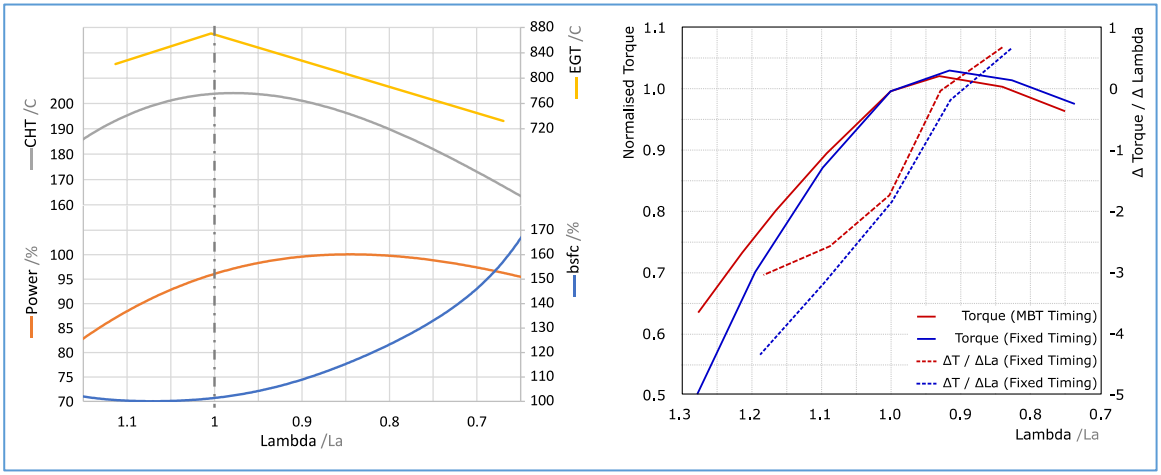

Figure 22: Effect of Lambda on Engine Outputs. Adapted from [63] [65]

Aside from carburetion, port fuelling and (more recently in SI engines) direct injection systems are used to introduce the fuel to the intake charge with focus on the homogeneity of resultant charge [46]. Port injected systems have the additional benefit of cooling the intake charge through the atomisation of the fuel, increasing the density and resulting mass flow into the chamber [8] [66]. Stratified charge configurations can also be implemented with a direct injection system, whereby the air-to-fuel ratio of the charge is varied in order to allow for combustion in an overall lean mixture, transitioning to homogenous charge operation under high loading to retain performance [67].

An emerging area of research is Jet Ignition [68], whereby a pre-chamber is used to ignite a small portion of the injected fuel before interaction with the intake charge (Figure 23). This allows for uniform flame propagation around the point of injection, and can be used in stratified charge applications to achieve thermal efficiencies of up to 45%. NO_x concentration in tailpipe emissions is also reduced; a concern in typical direct injection systems [69].

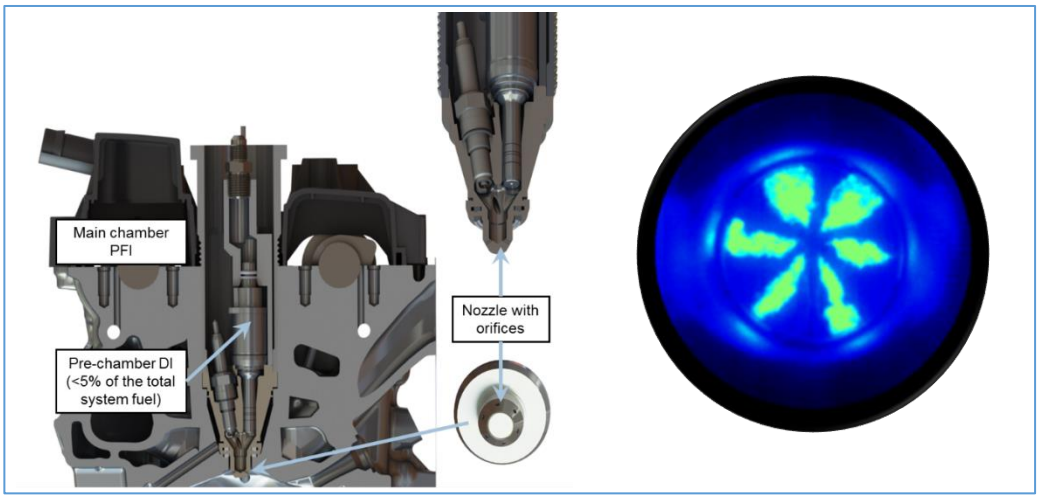

Figure 23: Schematic of MAHLE Jet Ignition System (Left) and Lomography of flame propagation [68]

With port injected systems a length of inlet port wall is covered by a film of wet fuel. Acting like a puddle, this film constantly evaporates and is replenished by the subsequent injections; under steady state conditions, the rates or evaporation and replenishment are equal.

Transient fuelling compensations are primarily required when a fuel/air mixture exists upstream of the inlet valves and downstream of the throttle; an arrangement common with port fuel injection systems. During tip-out, the manifold pressure is reduced and a greater rate of evaporation is noted for a reduction in quantity of air induced. This can provide an overly rich mixture, and a converse effect is present during tip-in. The mandatory restrictor plate in formula student inlet systems exasperates these phenomena, often leading to hesitation in no-load race, due to excessively rich, lean or inconsistent combustion.

To minimise wetted area, injectors are often positioned as close as possible to the intake valves. Many automotive designs mount the injector in the cylinder head rather than the manifold. Proximity to the valve is constrained by injector tip temperature, which if excessive will suffer lacquering

Given the packaging constraints on the cylinder head and the prioritisation of intake tract, the V-Twin utilises a port fuel injection system. As such, injection timing has significant impact on the combustion efficiency, emissions and engine stability; a result of variation between cycles of mixture homogeneity in the combustion chamber and intake runner [70]. Corti; Forte [71] continue, stating the probability of engine backfiring and idle stalling is proportional to the quantity of fuel that has fallen out of suspension and collected as liquid in the chamber, also indicating potential factors such as injector targeting and fuel pressure. Whilst often negated, the delay of injector actuation and effects of intake air velocity can result in fuel entering the chamber over more than twice the injection duration [72], presenting an argument for advancing the injection timing with engine speed.

Studies promote the use of closed valve injection in warm engines due to a more homogenous mixture at the runner and the effect of fuel atomisation through the conduction of heat from the head and valve [72] [73]. However under high speed and load operation, Whitelaw [74] noted that the high velocity of the intake air resulted in minimal fuel attachment to the walls of the runner in open valve injection, and hypothesised the reatomisation of droplets when colliding with the intake air (Figure 24). During cold start conditions, the fuel evaporation rate is often unpredictable and the engine is fuelled excessively rich in order to compensate and prevent stalling [75].

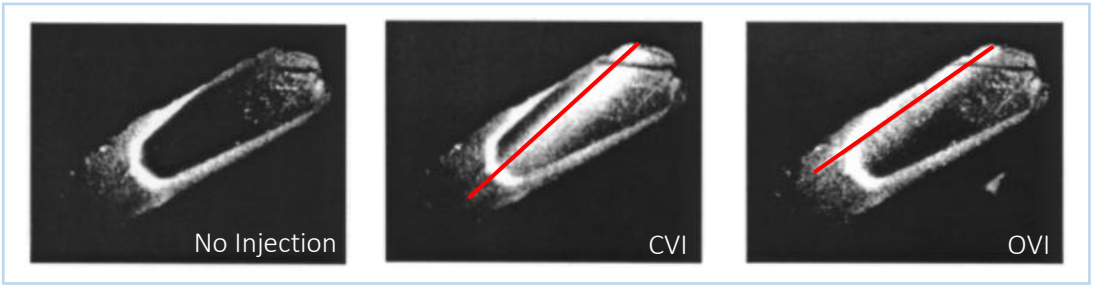

Figure 24: Fuel spray pattern with varying port injection timing [72]

Yumoto *et al* [70] summarise that the system's stability and sensitivity to injection timing is heavily dependant on injector targeting, orifice diameter and positioning, noting OVI has an advantageous effect on the transient throttle response. Given the intended motorsport application, the calibration of the engine in this report utilised OVI, to the potential detriment of steady-state hydrocarbon emissions and specific fuel consumption. Increasing the fuel pressure, as well as the tumble and swirl ratio of the intake charge through head and chamber modifications can be used to promote more homogeneous mixture in OVI mode.

To inject small quantities of fuel (particularly in DISI configurations) traditional injectors are forced to work in their ballistic region 'where the correlation between coil energising time and injected fuel amount becomes highly non-linear' [76]. However, this is applicable to idling conditions where required fuel quantity is minimal: injector size and rail pressure require consideration of anticipated idle fuel quantity to reduce injection quantity variance and hence improve idle stability. Common Rail diesel systems overcome this problem by reducing the fuel pressure at idle conditions, compensating lower flow rates with increased pulse widths that reside in linear operation [77].

Two port injectors can be used to minimise duty cycle: a small injector for fine control at idle and low mass flow [78], in conjunction with a large injector to supply large quantities of fuel for OVI at high mass flows. Given the cylinder displacement of the project engine, a secondary injector would pose little benefit and would provide additional calibration requirements to maintain engine stability and cycle-by-cycle variations. The fuel system also incorporates a common rail configuration for the injectors, for simplicity and capacity.

2.3.2 | Spark Timing Strategies

In an ideal Otto cycle, combustion happens instantaneously at TDC of the compression stroke, however the flame requires time to propagate (Figure 25) thus spark timing must be advanced to occur during the compression stroke to optimise thermal efficiency.

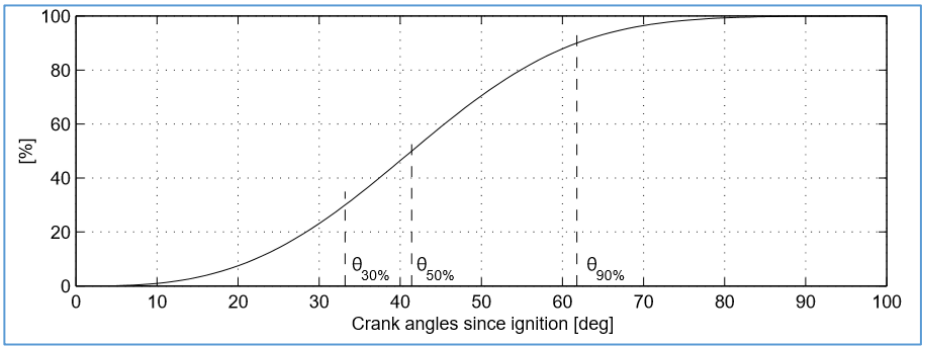

Figure 25: Typical mass fraction burned profile for an SI engine [79]

There are several different methods for determining the appropriate spark advance for an engine; a parameter affected primarily by volumetric efficiency, engine speed and air/fuel ratio [59]. Typically 50% of mass fraction burned should occur at 8-10 ^{O}ATDC to prevent component damage through magnitude and location of peak pressure [80] [81] (Figure 26).

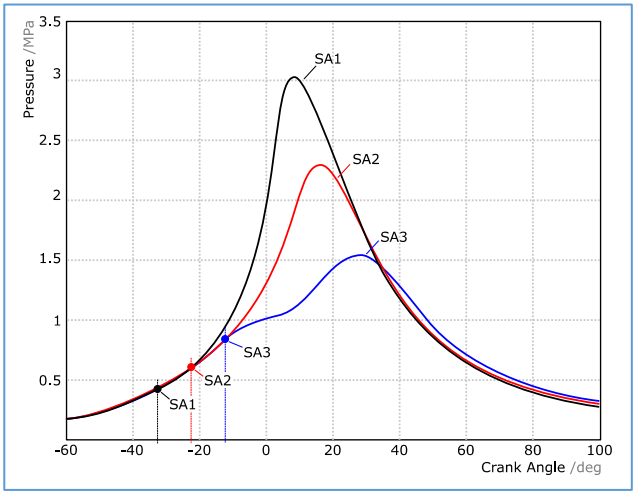

Figure 26: Pressure traces from incremental retardation of spark timing [79]

When the peak cylinder pressure rate of increase is not limited by engine components, for instance the head gasket or timing chain, ignition timing should be set for Mean Best Torque (MBT): a conservative advance gives minimal loss of power compared to ideal conditions [82]. The heat accumulation within the cylinder is noted to be inversely proportional to the spark advance toward MBT due to its relationship with fuel conversion efficiency [23] [83] (Figure 27).

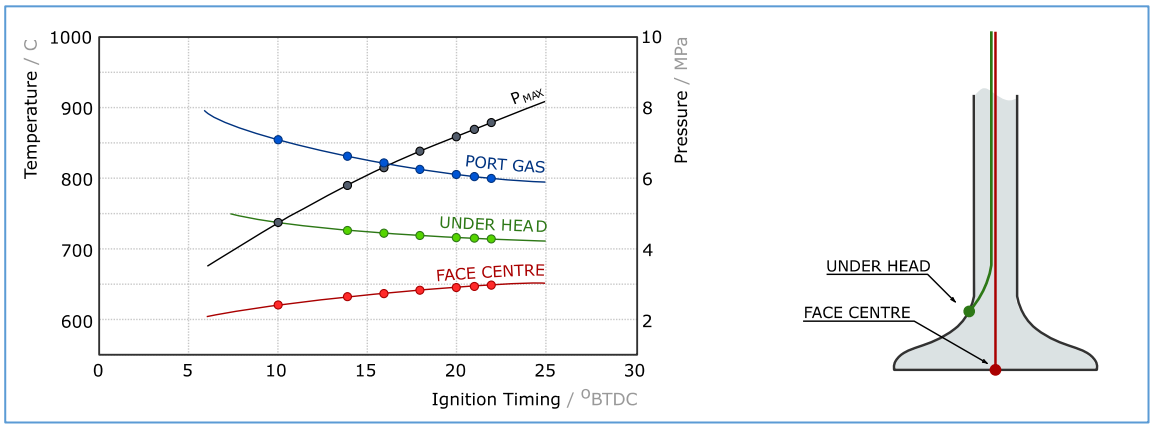

Figure 27: Influence of Injection Timing on Exhaust Valve Temperature. Adapted from [83]

Knock sensors allow the control system to incrementally advance the ignition timing from base values to accommodate for changes in fuel quality, carbon deposits and component wear. Within a test cell installation, a calibrated knock sensor or crank-angle-resolved pressure transducer should be fitted to aid tuning of ignition advance, with focus on the interdependent relationship between air/fuel ratio and ignition advance (through improved combustion efficiency).

2.3.3 | Knock Detection and Control

While increasing the compression ratio and spark advance can yield thermal efficiency improvements, extreme values can cause knock. Described as the progressive damage to internal engine components through abnormal combustion [84], knock primarily occurs through spark-based knock or surface ignition (Figure 28).

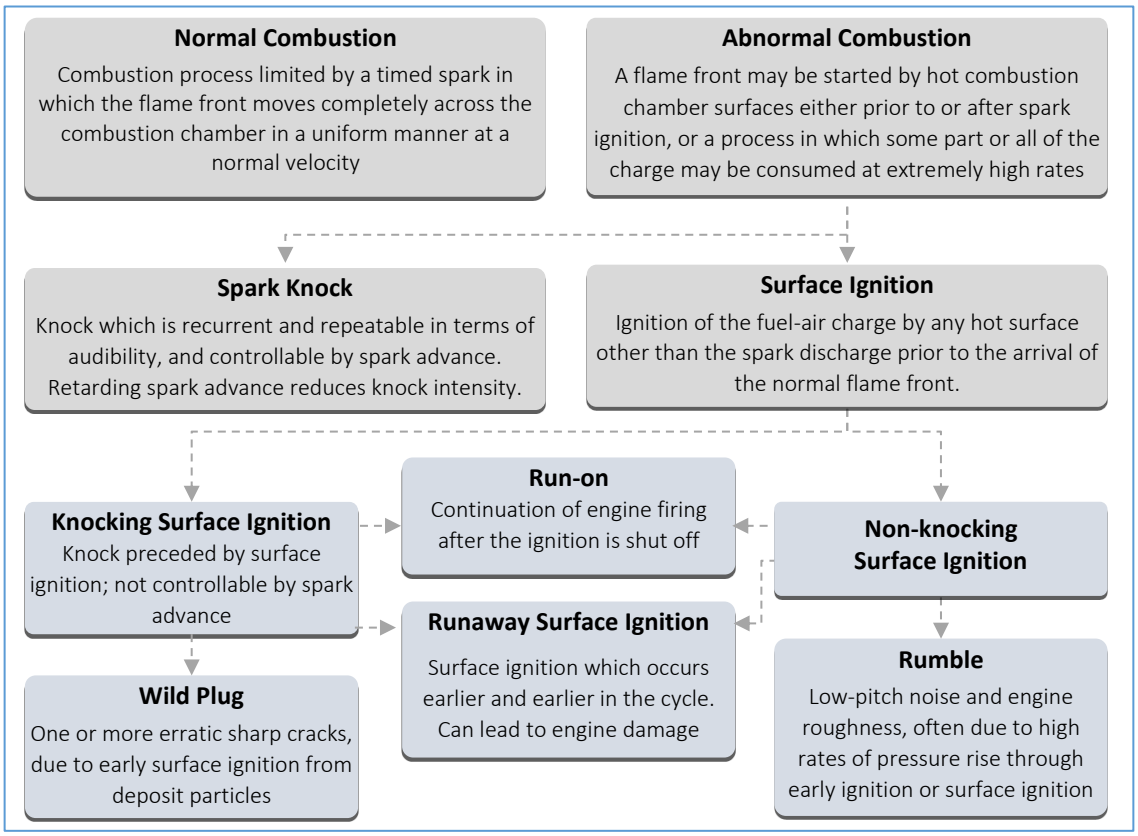

Figure 28: Categorisation of Knock Phenomena. Adapted from [84]

Though strongly influenced by installation location and chamber geometry [85], crank angle resolved cylinder pressure transducers can be used to identify knock regions during the calibration phase (Figure 29). In mainstream application on-board knock detection filters the vibrations from the engine block and compares to calibrated threshold values, behaving in a binary fashion to retard ignition and regulate knock. Conservative calibration can often lead to torque reduction based on insufficient data, to the detriment of efficiency [86].

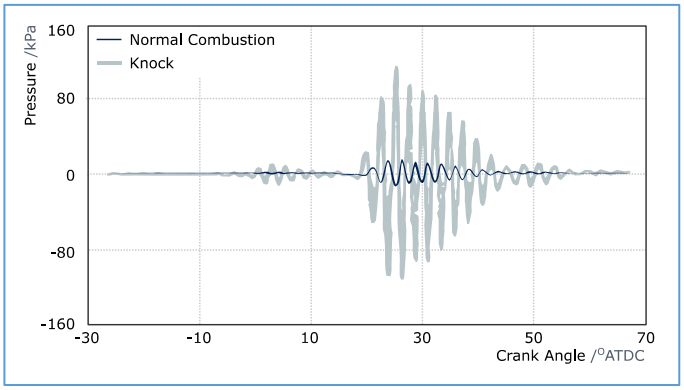

Figure 29: Transducer signal from normal combustion and knock event. Adapted from [85]

The project system cannot take advantage of such detection methods as a suitable transducer was not available, thus audible ques and the behaviour of measured outputs was used to identify incidents of knock.

2.3.4 | Electronic Throttle Actuation and Control Strategies

Decoupling the throttle pedal movement to valve actuation, electronic throttle control allows for torque demand to be characterised to various requirements [87] [88]. *Sport* and *comfort* pedal maps can be implemented, and the control system can compensate for the additional torque requirements of ancillary loading, pull away and crawl. Figure 30 depicts typical relationships between pedal angle and butterfly opening, although most automotive ECUs use *torque demand* as a load axis.

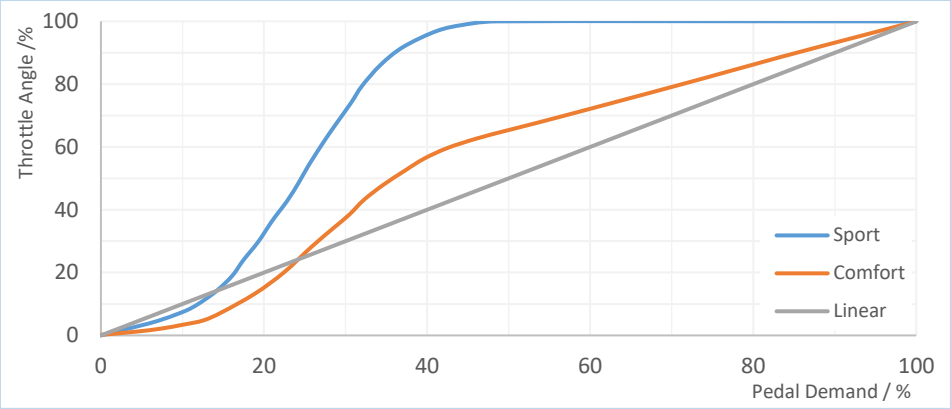

Figure 30: Accelerator Characteristic Profiles, Adapted from [89]

A PID system is often utilised to control the actuation of the valve motor [90]. Aggressive opening and closing of the throttle can require significant torque, particularly in the presence of stiction and contaminates [91] [92]. Such a system increases the dependency on sensor reliability; contactless position sensors are often installed to minimise mechanical wear and cumulative signal error [93].

ECUs often retard spark timing from MBT in given conditions to improve vehicle drivability. By creating a torque reserve that can be utilized quickly in response to torque demand, the system can compensate for the time required for the throttle to actuate and manifold pressure to increase [94]. In conjunction with ETC this gives a favourable mechanism for idle control, providing suitable throttle corrections with respect to engine temperature, lambda and auxiliary loading [95].

FS regulations stipulate the driver demanded torque may not be exceeded [24], however control strategies can lower torque output to provide intended throttle graduation or to regulate wheel slip.

Whilst a difference in tyre circumference speed and road speed is one method in which the tyre generates lateral and longitudinal forces [96], Hoffman [97] explains how excessive slip angle can be detrimental to the effective coefficient of friction and the resulting vehicle behaviour (Figure 31).

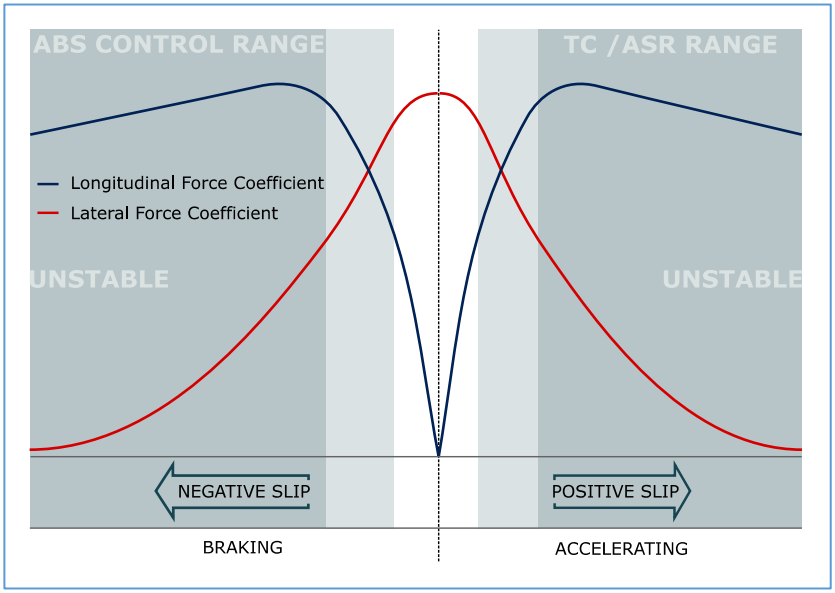

Figure 31: Lateral and Longitudinal Force as a function of wheel slip. Adapted from [97]

Launch control and ASR functionality can be integrated with an electronic throttle control system to maintain force generation and thus provide significant performance, stability and drivability benefits [98]. Moreover, ETC allows the intake air to be governed during overrun, reducing exotherm that can result when using fuel cut alone to cut torque.

Such systems are primarily advantageous in vehicle installations; electronic throttle control has not been chosen for this project to minimise control system complexity during base calibration.

2.4 | Summary of Literature Review

Several strategies and design concepts are implemented in modern high-performance engine design, to tailor the powertrain package to the requirements of the vehicle specification or governing regulations. Commonly, the engine unit acts as an air pump, with the design and configuration of the auxiliary systems tailored to give a balance between airpath optimisation, cost and packaging requirements: the priority of which is determined by the division entered. Within road applications, legislations push the efficiency, longevity and emission targets, often to the detriment of mass, power and cost

The pursuit of performance and efficiency gains from the internal combustion engine continued from its inception over a century ago, with modern advancements such as high-performance alloys, high pressure fuel injection and forced induction commonplace in production vehicles. Forms of hybridisation are used to improve the overall fuel conversion efficiency of the Powertrain system, providing a synergistic combination that suits the varied drive characteristics required in road or race applications.

Combining many of the advancements stemming from motorsport and research developments, the V-Twin engine used in this project is a notably advanced naturally aspirated engine. In the previous design of the package, extensive consideration has been made to optimise the airpath, packaging and drivability in light of the regulations governing formula student entrants. The large bore/stroke ratio allows for a high-speed engine, with the cylinder head, valvetrain and intake designed in synergy to provide a wide operating range and prevent the sacrifice of low-speed BMEP.

The drivability of the powertrain package when installed in a high-performance vehicle is an often-overlooked quality, which can be detrimental to the vehicle stability and driver confidence. The control system should manage the auxiliary components and actuators effectively to regulate the torque output to the minimum of driver demand and ASR intervention. To that end, electronic closed loop control of the fuel quantity, ignition advance, throttle angle and, in many applications, the valve timing are implemented. The V-twin engine in the project will benefit from a powerful electronic control unit, allowing a base calibration to be established and providing a platform for future strategy developments.

Using the literature review as a theoretical ground, the following sections of the report document the work, experimentation and analysis used in order to satisfy the objectives from Section 1.1.

3 | Methodology of Engine & System Development

This section discusses the development, testing procedure and experimental setup completed by the author in order to achieve the objectives of the project. In conjunction with data in the appendices, this is also aimed to serve as a reference for future students to aid knowledge transfer.

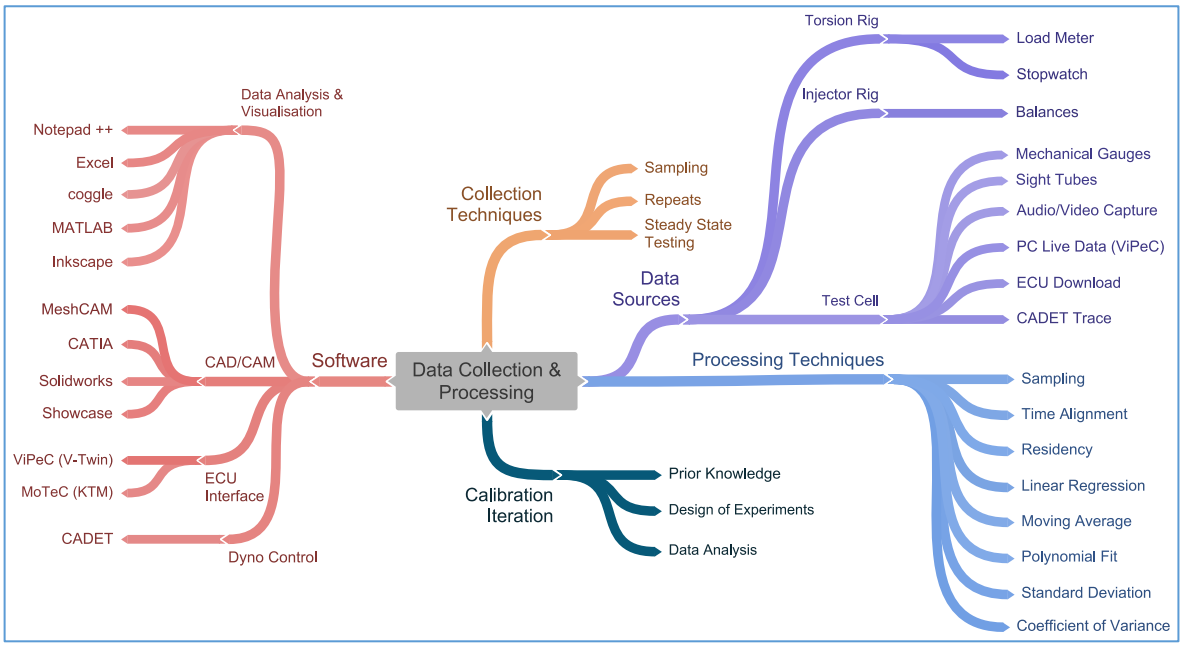

Figure 32: *Methods and tools for data acquisition and processing used in system development and calibration*

Each step is discretised within the report in accordance with the project objectives for clarity, however steps with few dependencies often occurred simultaneously or in a different sequence to minimise project lead times (Figure 33).

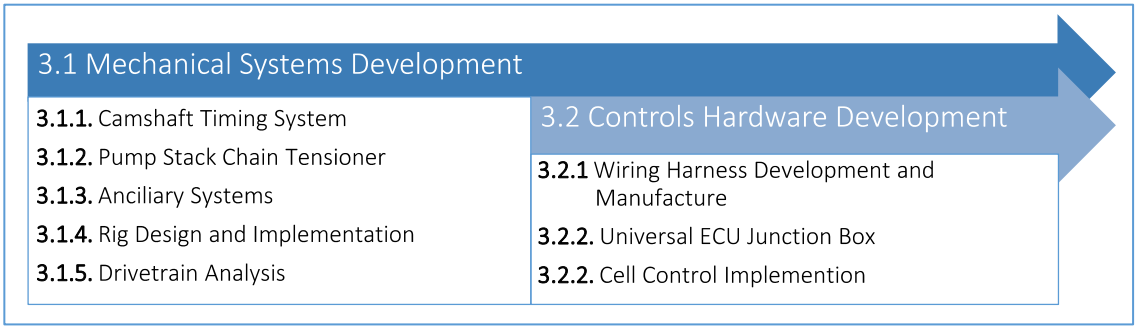

Figure 33: *Process for achieving project deliverables*

3.1 | Mechanical Systems Development

Several subsystems of the engine have been adapted or redesigned to accommodate for silent changes to previous components or for dynamometer ancillaries. Additional work was undertaken to accelerate engine inspection and validate alignment, minimising the risk to engine and associated capital. Resource was spent amending systems and components with unforeseeable complications, common with prototype systems of this magnitude. Drivetrain resonance analysis has been conducted to validate propshaft integrity and system safety during the anticipated operating regions.

3.1.1 | Camshaft Timing System & Procedure

The Importance of valvetrain timing and the strategies employed in modern high-performance engine design is widely discussed in section 2.2.4. To align the camshafts, and hence valve motion, appropriately with piston displacement, the camshaft profiles were initially measured using a depth clock, timing wheel and vee blocks. Camshaft position for maximum lift was found through averaging measurements 0.1mm either side of maximum recorded lift to minimise the effect of equipment accuracy (Figure 34). Lift was measured at each increment of shaft rotation, taking care to prevent the dislocation of the timing wheel to the camshaft (Figure 35).

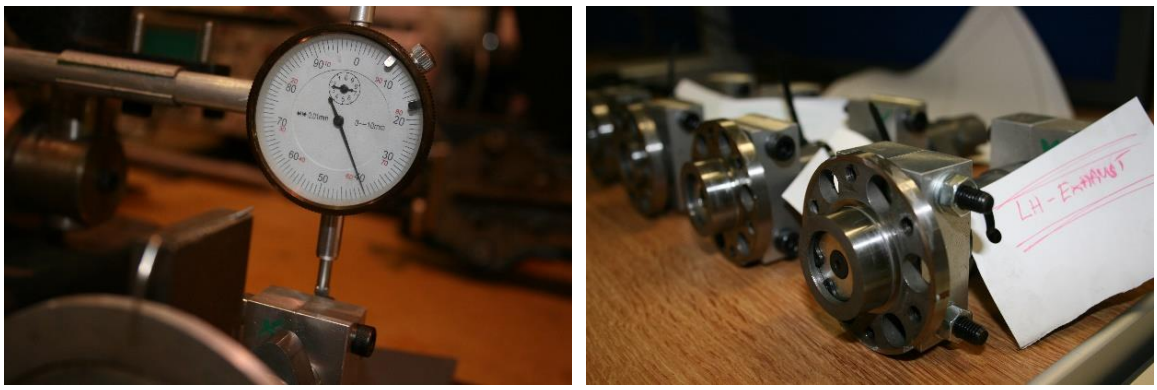

Figure 34: Setup of Camshaft Position for External Marking

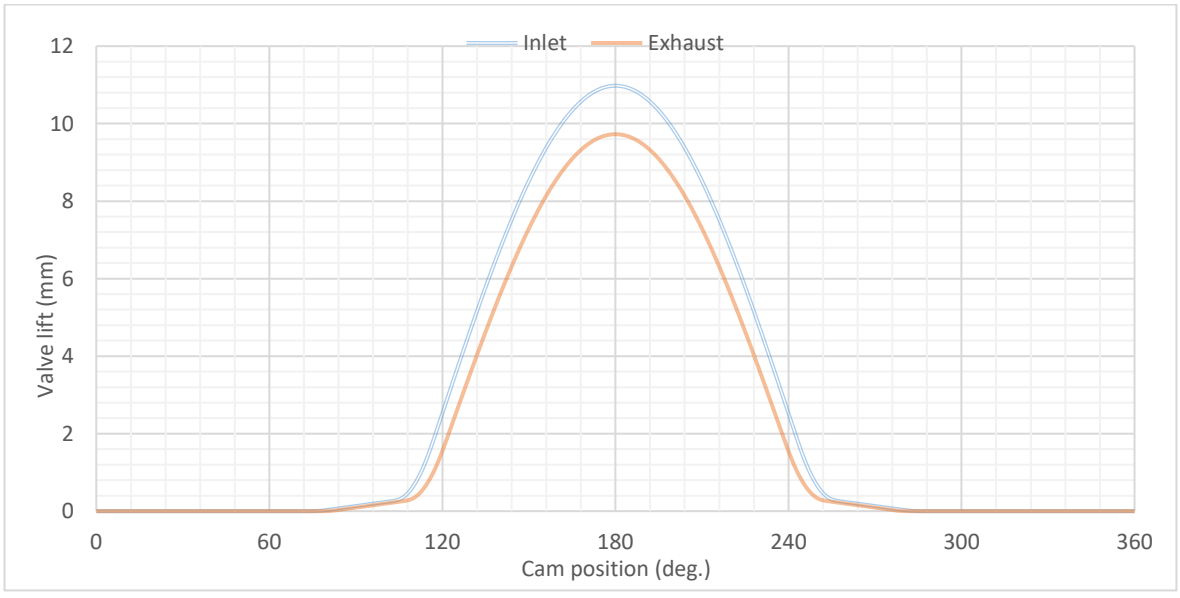

Figure 35: V-Twin Measured Camshaft Lift Profiles

The cam cap top face and sprocket carrier external cylindrical face were identified as the most suitable for camshaft alignment. Viewed directly from above, the increased diameter of the camshaft at the sprocket carrier gave greater rotational accuracy during alignment, and provides the least invasive method of inspection. The position allows for a pointer to be temporarily attached during inspection to minimise parallax error.

The angle between the centreline of peak cam lift and the normal to the cylinder head top was calculated through engine timing specifications, allowing aligning marks to be laser etched on each shaft and the adjacent caps. Multiple marks are etched on the cam caps, allowing different valve timings to be tested without recalculation. With the respective piston at top dead centre of the compression stroke, the camshaft can be rotated freely to align the reference with the desired timing mark on the cam cap, when viewed normal to the top face of the cylinder head (Figure 36).

Figure 36: Cam Cap Etching

This arrangement allows for visualisation of misalignment in the event of a change in chain tension or rotational displacement between the camshaft and affixed sprockets. The compounded tolerance of the equipment used and camshaft chain tension has been considered in piston clash analysis by Douglas [56] to provide the safe operating range of valve timings, whilst providing suitable valve duration and overlap for motorsport applications (Section 2.2.5) (Figure 37).

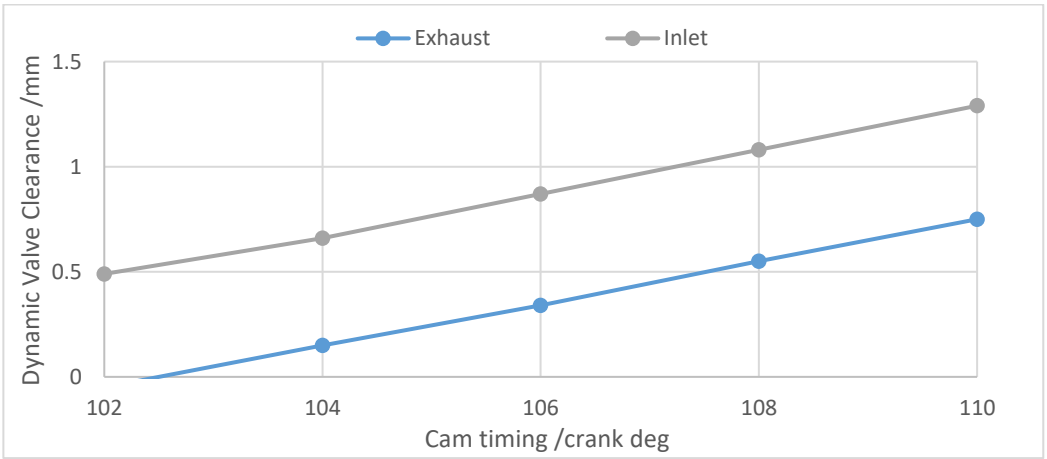

Figure 37: Valve to Piston Dynamic Clearance [56]

A jig is used to replicate the bearing load on the end of the half speed stack, to prevent deflection of the shaft during tensioning and chain failure through over tensioning (Figure 38).

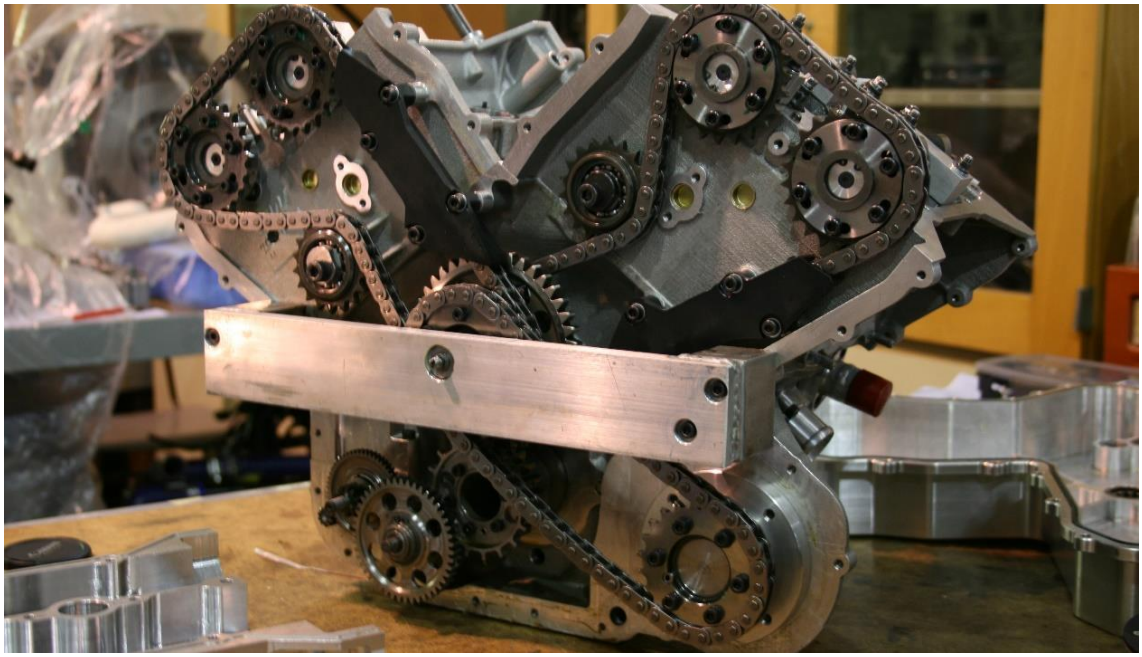

Figure 38: Use of half speed stack support Jig during camshaft timing procedure

3.1.2 | Pump Stack Chain Tensioner

To prevent excessive movement in the pump stack chain and to normalise chain loading, an adjustable tensioner was designed and manufactured. Acting on the non-driven side of the chain, the tensioner was designed within the confines of existing machining points and manufacturability targets.

Several designs were considered with respect to their reliability, ease of manufacturing, complexity, ease of installation and number of components, with descending importance. The selected design featured a torsion-sprung arm, mounted from an unused boss on the front cover (Figure 39). Whilst the pivot for the tensioner was designed in single shear, this allowed for the full assembly to be mounted inside the front engine cover: other designs hindered the removal of such panels and increased the complexity of installation procedures. The contour of the arm matched the measured deflection of the chain once tensioned by hand, to promote uniform wear of the arm and prevent the chain from catching protruding geometry.

As the V-Twin engine uses a dry sump lubrication system (Section 2.2.6), and there are no oil jets primarily at the tensioner, the solution needed to comprise of a self-lubricating material or suffice with the minimal lubrication and cooling effect of the oil sprayed on the half speed stack.

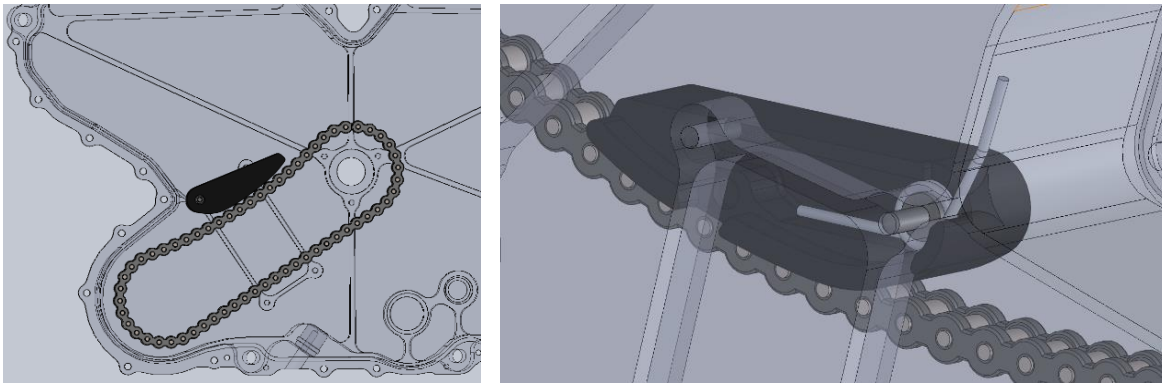

Figure 39: Representation of final pump stack chain tensioner, in the context of the front engine cover

To contain any failure in the event of excessive temperature, wear or opposed crankshaft direction, the tensioner incorporated additional material to collide with the front casing supports at maximum travel (Figure 40). This allows for a safe wall thickness between the leg of the torsion spring and the surface of the tensioner arm, minimising the risk of the spring braking through the arm and damaging the chain. The installation of the front cover is also aided, whereby the tensioner arm must be fully raised and temporarily locked with an external pin for the system to pass over the non-tensioned chain. The external hole to release the tensioner is tapped, allowing the containment of the crankcase gases with a cap-head bolt.

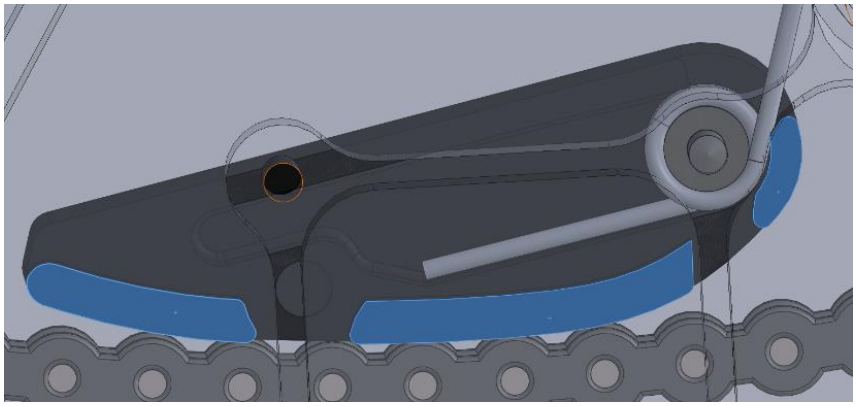

Figure 40: Chain Tensioner Fail-safe Ribs (blue) clash with casing pocket before system failure

To reduce complexity as well as improve the accuracy and finish of the resulting component, the milled tensioner arm was designed such that all machining passes could be performed from one face. Simulated machining time was reduced by 30% compared to initial designs through removing the pocketing of the front face of the arm, to the detriment of component mass.

3.1.3 | External Ancillary Systems

Coolant System

Designed to minimise the propensity of knock and prevent component failure, the cooling system utilises a heat exchanger to reject heat from the cylinder block (Sections 2.2.5, 2.3.2). The configuration allows for the cell to be connected to a series of radiators mounted external to the building, to maximise heat rejection and provide sufficient capacity for all test beds to be run simultaneously.

To provide sufficient coolant flow within the engine circuit of the system, an electric water pump was installed by the author. Controlled through the electronic control unit, this provides a consistent flow rate once the engine has exceeded a specified rotational speed, minimising the load on the battery when cranking. Whilst in many installations the pump is activated through measured coolant temperature, this is not feasible in the V-Twin installation and could cause overheating. The position of the coolant temperature sensor relative to the engine block, coupled with the absence of a crank driven pump would result in significant temperature discrepancy before activating: the stagnant coolant must conduct energy between the block and sensor before any rise in temperature is recorded, causing delay.

A thermostat is included in the cooling system to allow for progressive engine warm-up in the presence of excessive heat rejection or flow rate.

Lubrication System

Similarly to the coolant pump, the dry sump scavenge and pressure pumps are external ancillaries. Driven from the half-speed output shaft for the future pump stack, the twin stage oil pump rotates in the opposing direction to the crankshaft and required significant testing and development to meet system requirements.

Exhaust System

The exhaust system has been completed to conform to both financial and geometric constraints within the cell. Continuing from work completed by previous students, an Akrapovic silencer from the formula student team was refurbished and swaged to provide an air tight transition fit to the end of the main exhaust header. The ceramic-coated system is mounted in isolation to the rig and extraction system, to improve system longevity and minimise heat rejection to the surrounding auxiliary components.

Runner lengths for the separate and combined headers were measured at 770mm and 520mm respectively, providing resonance effects within the torque curve around 10000 and 13000 rev/min and repeating at lower speeds with diminishing effect (Section 2.2.3). These compliment the tuned lengths in the intake system in anticipation of a broader torque curve.

3.1.4 | Rig Design and Implementation

To accommodate for geometry difference between the V-Twin and the previously installed KTM engine, the dynamometer rig was remanufactured. The setup allows for the engine and frame to be safely hoisted out of the cell, providing a support stand for bench work (Figure 41). Rig design prioritised ease of manufacture, stiffness, reliability and adjustability.

Figure 41: *Engine unit with external oil pump fitted to rig for cell installation*

With the engine crankshaft coupled directly to the dynamometer, the propshaft is misaligned by 1° to properly operate the universal joints, and has been guarded to contain failure and minimise risk to operators.

Vertical alignment was calculated using a height gauge, sampling at known intervals along the portion of the propshaft with uniform diameter, whilst horizontal alignment was measured using a straight edge perpendicular to the dynamometer connecting face (Figure B3).

Without a clutch between the crankshaft and the propshaft, additional load is placed on the starter motor when cranking; the crank and cam sensors are not speed dependant therefore the slower rotational speed when cranking does not affect timing synchronisation.

3.1.5 | Drivetrain Resonance Analysis

It is often perceived that, under steady state use, the torque delivery of an engine is constant. However, torque is transmitted through the drivetrain in short duration pulses in relation to the configuration and firing order of the cylinders (Figure 42). When connected to a dynamometer specific engine speeds can cause a frequency input to the driveline that produces a harmonic; the amplitude of torque oscillation can be several times greater than the input.

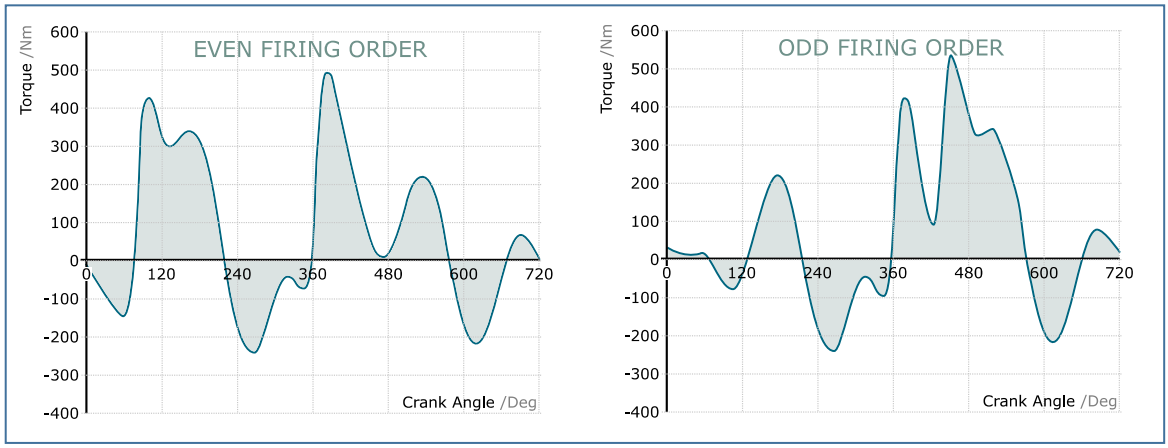

Figure 42: Instantaneous Torque Output of V-Twin Engine with respect to firing order. Adapted from [110]

In a conventional mass-spring system the resonant frequency is proportional to the specific stiffness of the system. An equivalent applies for rotation systems where natural frequency is related to the torsional stiffness of the system, in this case the propshaft, and the polar inertias of components within the system (Equation 4).

$$F_n = \frac{1}{2\pi}\sqrt{\frac{C\,(J_E + J_D)}{J_E \cdot J_D}} \qquad \textit{Equation 4 [101]}$$

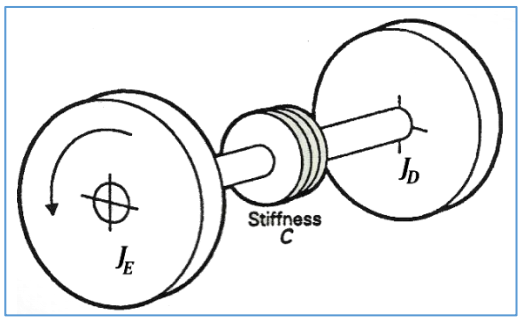

Figure 43: Categorisation of Torsional Oscillation in Two-Mass System [99]

As resonance may only occur at or below the natural frequency it is important to tune this to below idle speeds, where engine torque is minimal and can be passed quickly during the start procedure. The resonant torque experienced by the propshaft can lead to an increased wear rate for the propshaft and coupling: whilst it may not cause immediate damage, loading the drivetrain at resonance modal frequencies can cause the shaft to fail under high-cycle fatigue or thermal degradation of its rubber components.

The inertia of the dynamometer is specified by the manufacturer as 0.14 Kgm^2 [100], and the effect of the inertia of the propshaft is considered negligible. Engine inertia was calculated by the author through analysis of CAD models as $4.8x10^{-3}$ Kgm^2 (Table C2). As the wear of the propshaft was unknown, physical testing was required to calculate torsional stiffness to suitable accuracy.

Propshaft Torsional Testing

To determine the torsional stiffness of the propshaft available for use, the shaft was fitted to a torsional test rig (Figure 44). The machine applies a rotational displacement to one of the propshaft flanges (pictured right), whilst measuring the torque experienced at the other.

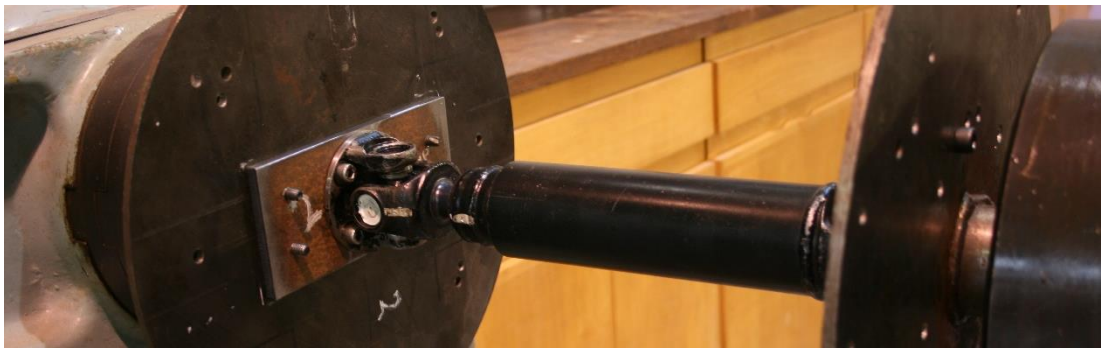

Figure 44: *Dyno Cell 4 Propshaft as fitted to Torsion Test Rig*

Rotation displacement was applied using a motor, clutch and gearbox arrangement, allowing a displacement strain of 2 degrees per minute to be applied. To minimise the error obtained from stiction of the load measurement system, rotational displacement was constantly applied until a torque was observed equal to the anticipated maximum average engine torque at WOT of 100Nm (Figure 45). The time per each measurable division of the load cell was recorded and interpreted using several methods to verify the calculated stiffness (Table C1).

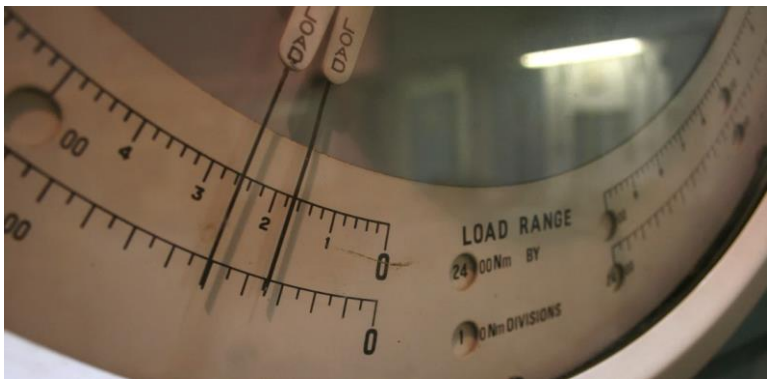

Figure 45: *Torsional Load Measurement*

As the equipment was unable to determine propshaft position at which zero torque was applied, this was identified by hand as the point at which maximum play could be felt in the system. In addition, the first 10Nm increment of loading was omitted from the output results due to the error associated with the clearance between the propshaft flanges and the retaining bolts.

The construction of the propshaft incorporates a rubber coupling between the internal and external tubes of the body; the viscoelastic properties of which were anticipated to provide hysteresis (Figure A3). The accuracy of the equipment when removing load from the propshaft was deemed insufficient to contribute to stiffness calculations, but gave an indication of hysteresis (Figure 46).

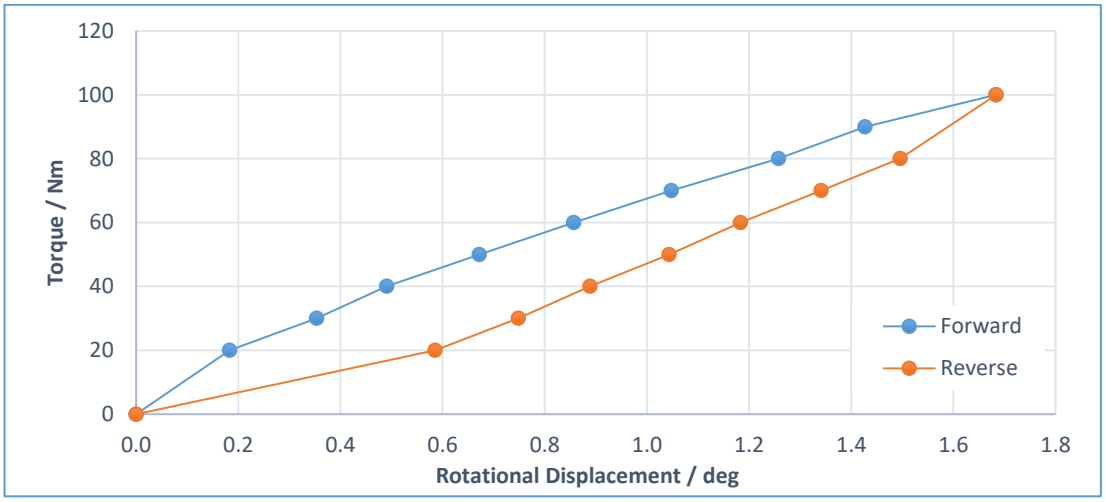

Figure 46: Hysteresis Loop of Propshaft

Linear regression of the valid data provides a torsional stiffness of 53.38Nm/deg (3058 Nm/Rad), with an R^2 value of 99.13% (Figure 47).

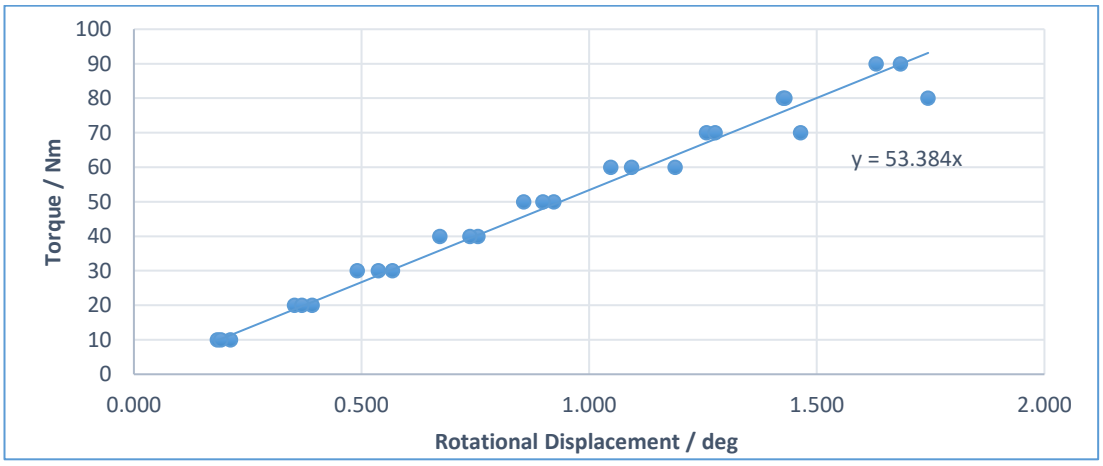

Figure 47: Linear Estimation of Propshaft Stiffness, Calculated through cumulative FWD data

Resonant Frequency Calculation

The previously calculated arguments can be substituted in Equation 4 to give a natural frequency of the drivetrain of 128Hz. Assuming an ideal case, whereby the two-cylinder firings are evenly distributed across the 720-degree cycle, natural frequency will occur at an engine speed of 7240 rev/min. However, in a Vee configuration the firing order is influenced by the bank angle (75 degrees), resulting in separations between torque pulses of 435 and 285 degrees. This yields primary and secondary resonant speeds of 8749 and 5732 rev/min respectively: their combined effect is represented in Figure 48, where the scale of torsional amplitude is arbitrary.

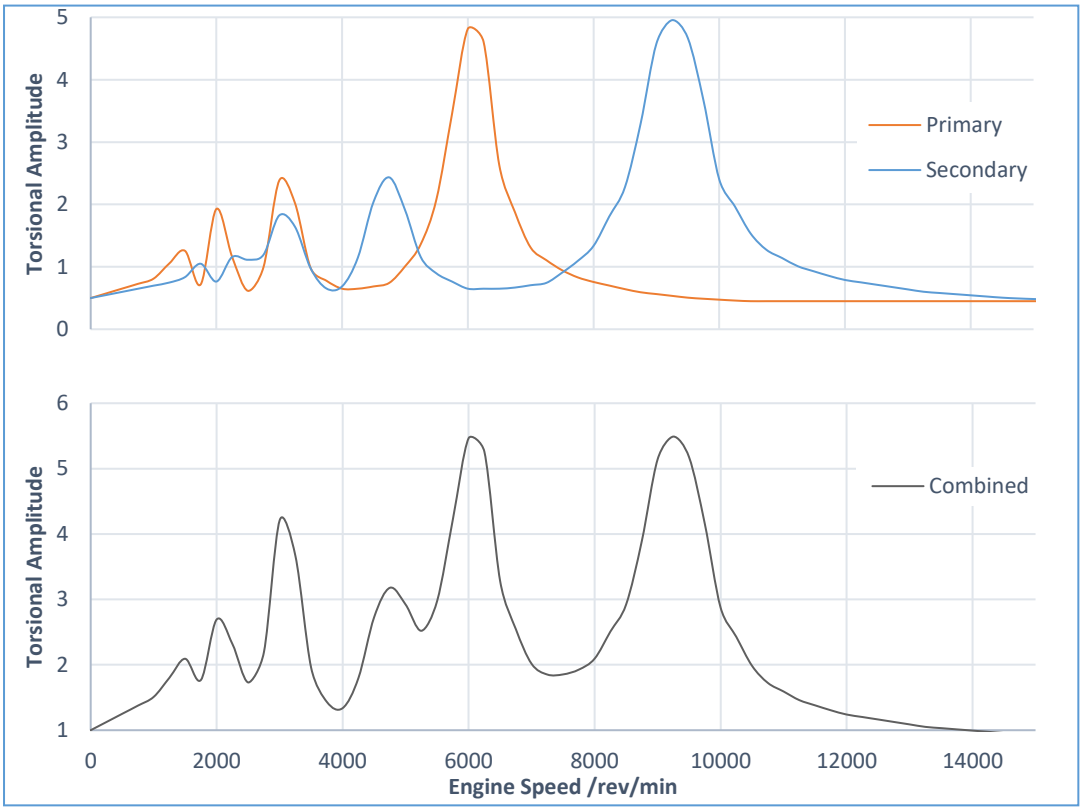

Figure 48: Modified torsional amplitude traces assuming multiple resonant speeds through firing offset

Summary

The relationship between engine and dynamometer inertias and the stiffness of the connecting medium result in a maximum safe operating speed around 4000 rev/min. This particular speed has been identified as a safe operating point regardless of interpretation method of torsional resonance calculation, in conjunction with anticipated engine torque and the propshaft rated speed. In addition duration at high load sites shall be minimied to prevent heat build-up in the driveshaft.

Through interpretation of Equation 4, Figure 49 indicates that a combination of modifications to the system are required in order to sufficiently tune resonance outside of operating regions.

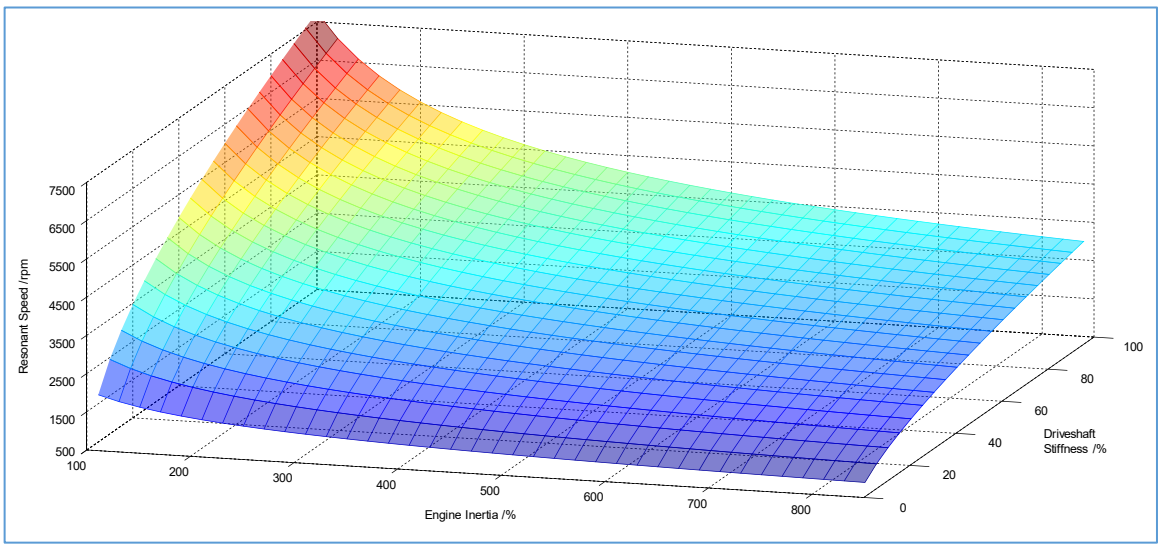

Figure 49: Sensitivity of Engine Inertia and Driveshaft Stiffness on Resonant Speeds

Solutions were investigated but these could not be implemented with the resources available to the project (Appendix D). A quill shaft coupling is recommended, in conjunction with an engine mounting solution that isolates the engine and dynamometer equally from the floor of the cell.

3.1.6 | Summary of Mechanical Systems Developments

To facilitate the correct operation of the v-twin powertrain within the test cell, significant work has been conducted to complete the mechanical development of the engine and the auxiliary components. A system for valvetrain timing has been designed and implemented, allowing the camshaft timing to be set away from valve lift to minimise load during setup, as well as providing quick visual identification of any misalignment during service.

A pump stack chain tensioner was designed and manufactured. Designed within geometry and manufacturing constraints, this incorporated failsafe features to prevent damage during service. The design was optimised for machinability, milled in a 2.5D operation to reduce datum errors and machining time. The lubricant and cooling systems were interfaced with the test cell equipment to facilitate suitable regulation, and an exhaust system was completed around test cell requirements.

A rig was designed and manufactured in order to accurately and securely install the V-Twin engine and ancillaries to the test cell. The direct coupling between the crankshaft and the dynamometer, and the disproportion between the engine and dynamometer inertias result in the potential for drivetrain resonance. After extensive analysis of the system and experimental investigation of the propshaft torsional stiffness, resonance was predicted above speeds of 4000rev/min. Whilst several alternative configurations have been assessed, the system remained in this configuration until the mechanical stability and potential of the engine can be proven below this resonant speed.

3.2 | Electronic Control System Development

3.2.1 | Engine Wiring Harness Design & Manufacture

Precedence was given in the design of the electrical system to both reliability and flexibility, to suitably fulfil the specifications of the required control system (Section 2.3). The main harness sections were constructed from motorsport grade components for mechanical resistance, durability, compatibility and minimal losses over large cable lengths (Figure 50).

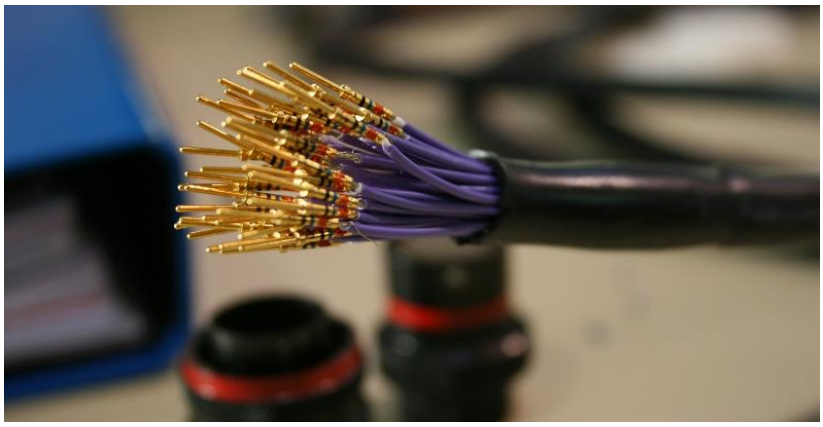

Figure 50: Wiring Harness Manufacture

Sensor and actuation connections were split into two separate harnesses, to minimise the probability of electrical interference on sensor output. Both featured break connections near the engine to simplify engine removal process, leaving overhead connectors designed to carry a suitable number of contacts for most bespoke engine configurations (Figure 51). This helps to reduce the cost of implementing a control system for future engine configurations within the cell, as only the harness immediate to the engine and devices would require manufacture.

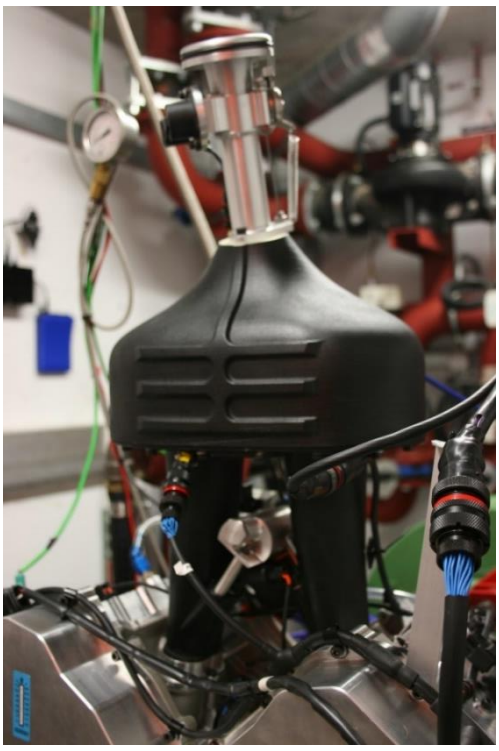

Figure 51: Completed installation of wiring harness on Plenum with sensor (left) and actuation legs.

3.2.2 | Dynamometer Cell Interface & Instrumentation

A junction box was created in order to interface the engine harness and dynamometer cell ancillaries to the ECU (Figure 52). To create a universal system to reduce installation time of any other bespoke engine to the cell, the system has been designed to operate with Link (Vi-PEC) and MoTeC control units, and as such incorporates two external lambda controllers. These can be bypassed in order to allow control units with on-board lambda control to manage these directly to better represent vehicle installation. Installed on the cell's walls, the ECU and junction box are isolated from vibration and heat, in order to maximise component life and system reliability.

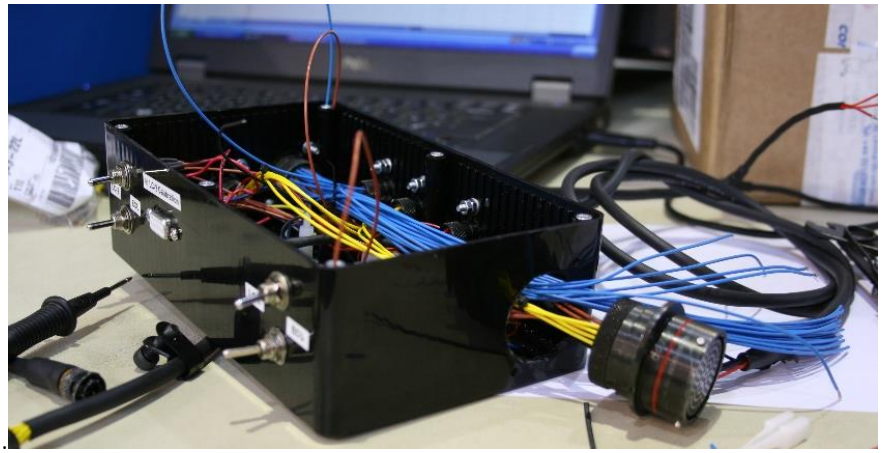

Figure 52: Engine Control Junction Box Manufacture

Furthermore, the 12v supply cell to the dynamometer ancillaries, ECU and starter motor has been replaced and incorporates a permanent charging system. This helps to maintain battery voltage during cranking procedures, providing sufficient voltage to the coils, ECU and injectors to prevent malfunction or misfiring during this high drain situation. Safety within the cell is also improved through the minimisation of trailing wires and reduced risk of electrical fire from the grounding or shorting of temporary charging wires (Figure 53 and Figure 54).

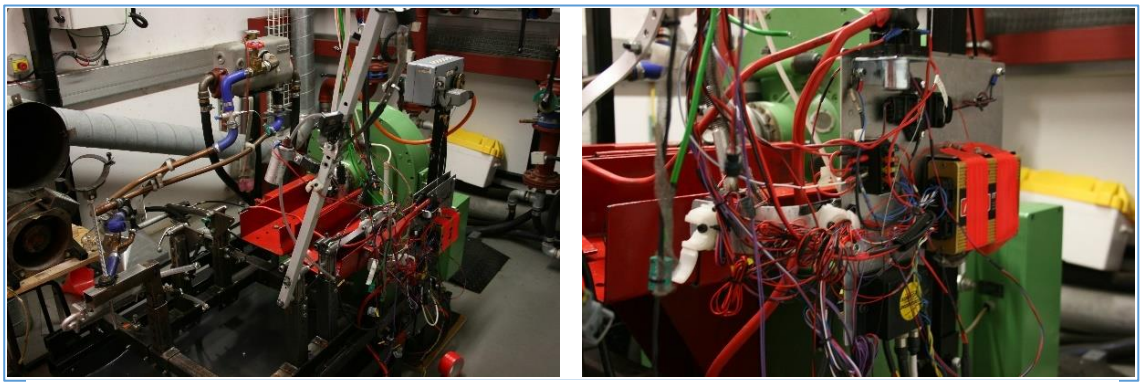

Figure 53: Previous KTM Rig and Wiring Harness

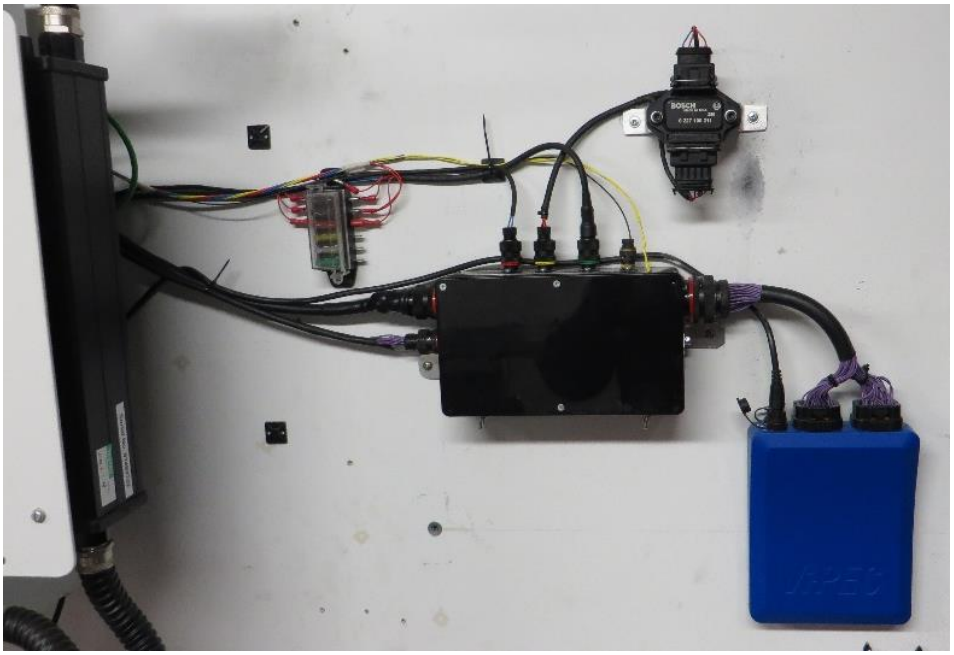

Figure 54: Completed installation of (from left to right): system fuses, universal junction box, ignition amplifier and ECU

The fuel system within the cell has been serviced to better contain the fuel vapour, and incorporates an adjustable pressure regulator to deliver gauge pressure between 100 and 800kPa, suitable for the PFI configuration implemented (Section 2.3.1). Whilst the system does not currently include gravimetric fuel measurement, injector characterisation was undertaken across suitable operating pressures in order to estimate through post processing the quantity of fuel injected per cycle (see Section 4.1).

Figure 55: Variable fuel pressure regulation through adjusting spring preload to open tank return

4 | Base Calibration

This section discusses the base calibration work completed by the author to fulfil the project objectives. Using theoretical background from the literature review, distinct workstreams were identified in order to populate the main calibratable parameters in the ECU for first fire (Figure 56). The following sections of the chapter document the work undertaken to achieve this.

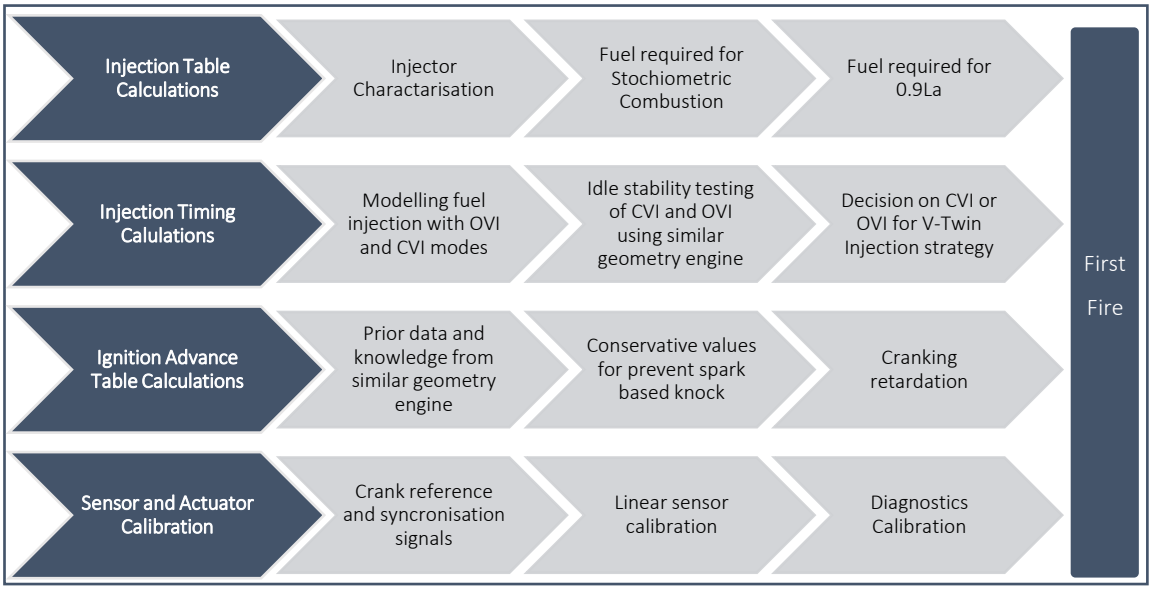

Figure 56: *Identified workstreams for population of main ECU parameters*

4.1 | Fuel Injection Table Calculations

Injector testing was conducted to approximate the base fuel table, and to provide the basis of BSFC and thermal efficiency calculations (Figure 57). The effects of fuel pressure and requested pulse width were recorded on the quantity of fuel injected, with 5000 pulses per test to minimise the error due to balance resolution, drift, and particles lost to atmosphere. At each pressure, the peak and hold current settings for the injector were swept to aid validation of the obtained results. A fuel pressure of 450kPa gave good balance between sensitivity at low pulse widths to minimised duty cycle at maximum engine speed (Figure 58).

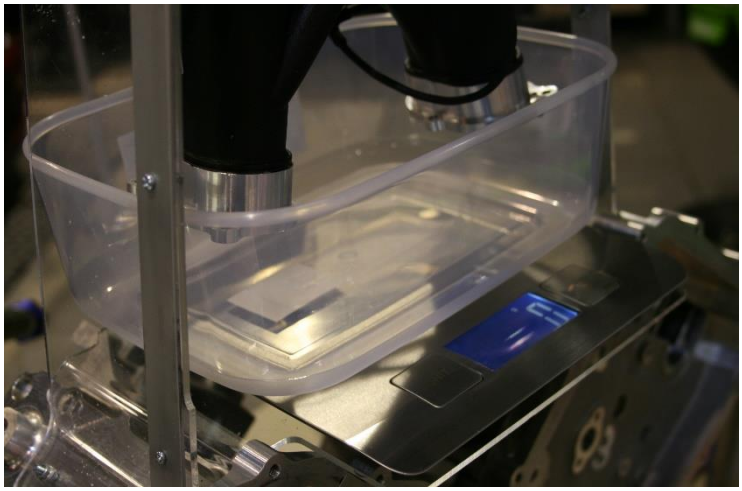

Figure 57: *Injection Test Rig (Cover Removed for clarity)*

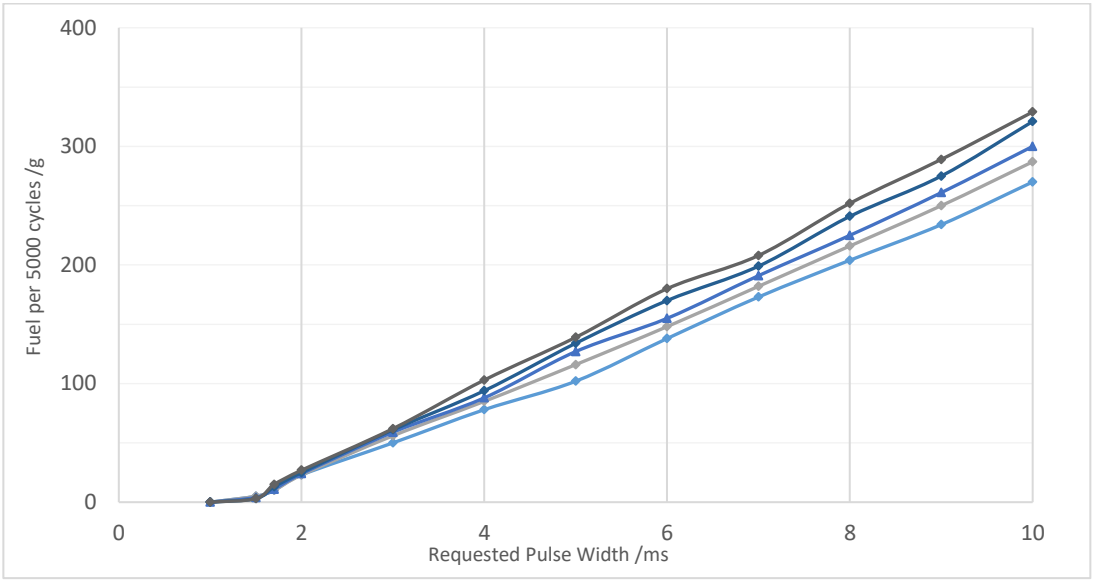

Figure 58: Injector Testing Results at Various Fuel Pressure

To create an approximated base fuel map for the system, throttle linearity curves based on experimental studies by Little [101] and Percival [102] were combined with the predicted volumetric efficiency based on resonance and torque output calculations by Larsson and Douglas [35] (Figure 59).

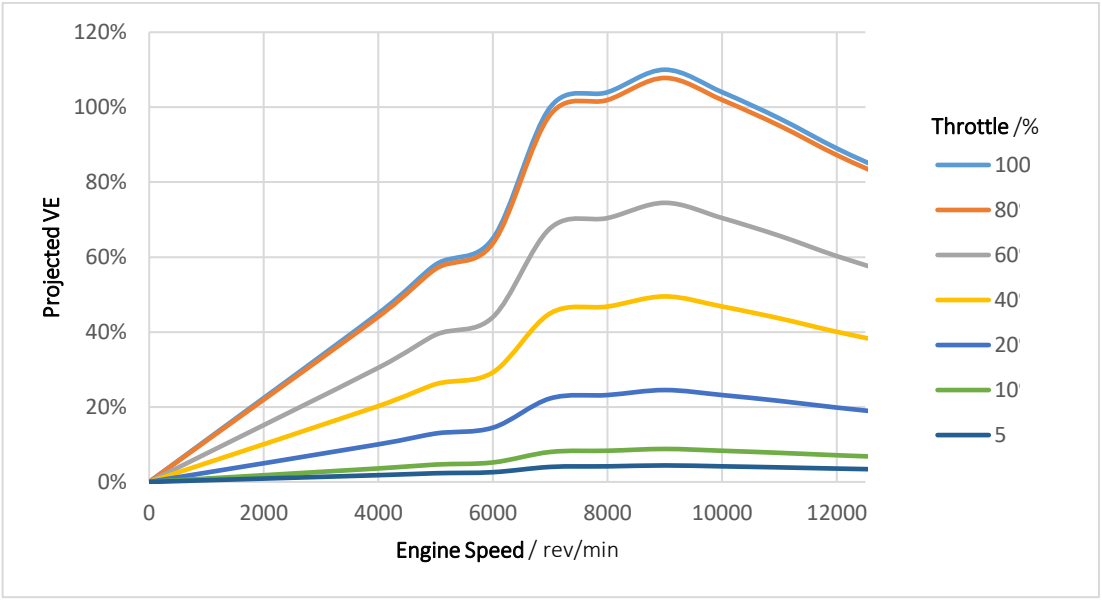

Figure 59: Projected volumetric efficiency map using torque and throttle linearity estimations

To give overhead for port and chamber wetting, a target air/fuel ratio of 13.2:1 (0.9La) was used when calculating the quantity of fuel to inject per cycle, and the corresponding pulse width through interpolation of experimental data. Targeting rich combustion allowed manifold wall wetting or mass flow to be greater than calculated without risking component damage through excessive combustion temperatures (Section 2.3.1). Fuel quantity was to be adjusted in initial engine runs at idle, allowing adjacent sites to be trimmed to suit.

4.1.2 | Injection Timing Calculations

Experimental investigation was conducted to determine the sensitivity of a KTM 570cc single-cylinder engine to injection timing strategies. Comparing an open valve injection time strategy (red) to CVI used in previous formula student configurations (blue), significant improvements in idle speed stability and fuel efficiency can be noted (Figure 60) (Figure 61). This is primarily due to predictable, and hence more controllable, fuel delivery, allowing the idle throttle angle and engine speed to be reduced without the risk of engine stall (Sections 2.1; 2.3.1).

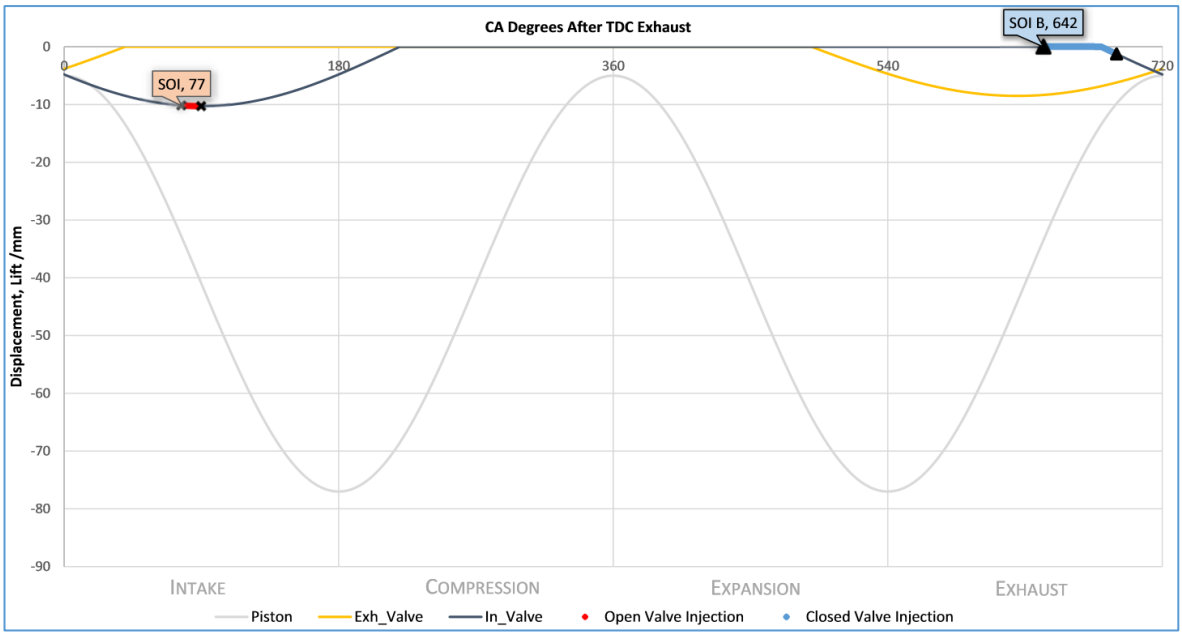

Figure 60: Comparison of Injection Timing Strategies with KTM 570EXC single-cylinder engine at idle conditions

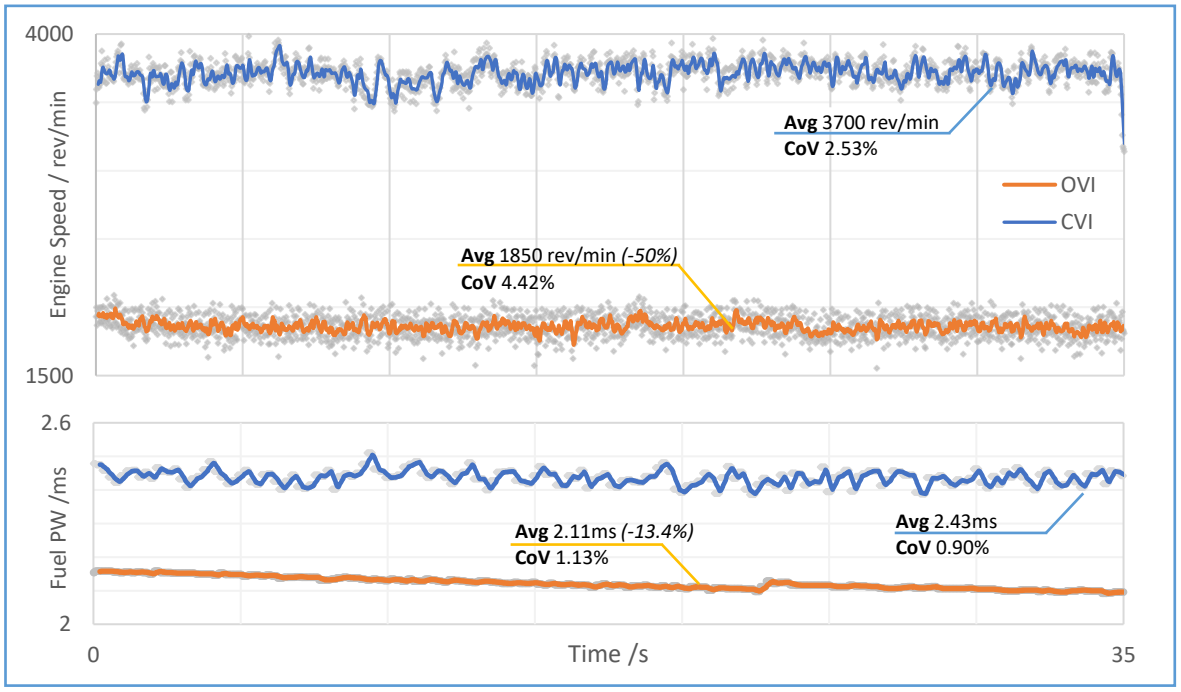

Figure 61: Effect of OVI (Orange) on KTM operating conditions compared to 2015 Competition Data (Blue)

Interpretation of the fuel table developed in section 4.1.1 shows a maximum injector duty cycle of 50% at high speed and load (Figure 62).

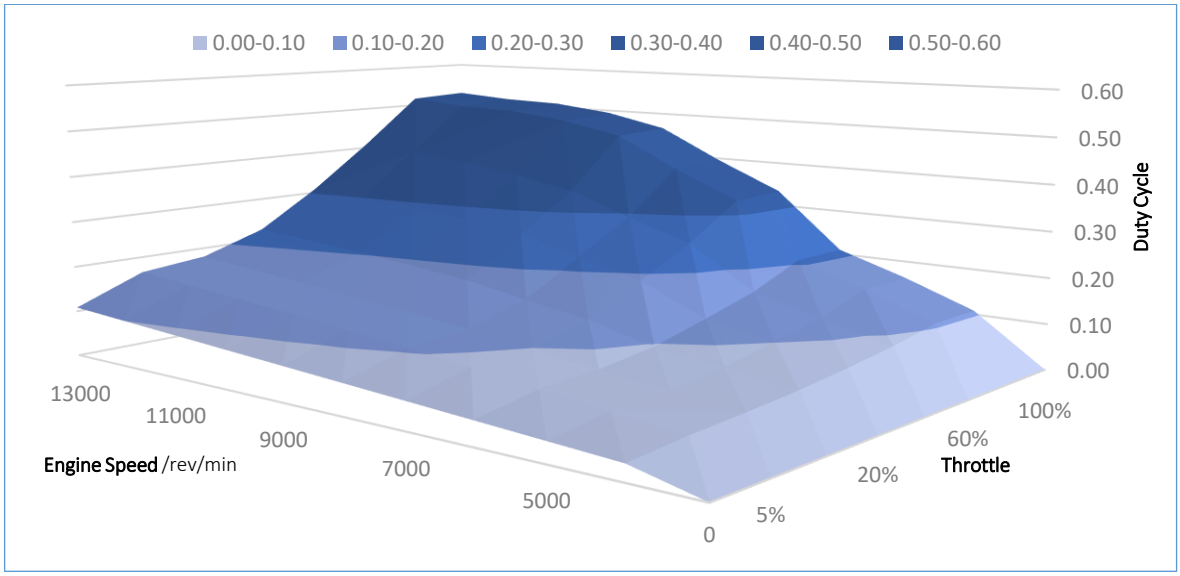

Figure 62: Plot of projected injector duty cycle across engine speed and load sites

Whilst the advantages of OVI and CVI strategies were discussed in sections 2.2.5 and 2.3.1, Figure 63 shows that under high speed and load conditions a combination of CVI and OVI would occur (Red). As such, the injection strategy focuses on the idle and part load conditions, where the injection event occurs within a small window of crank angle (Blue).

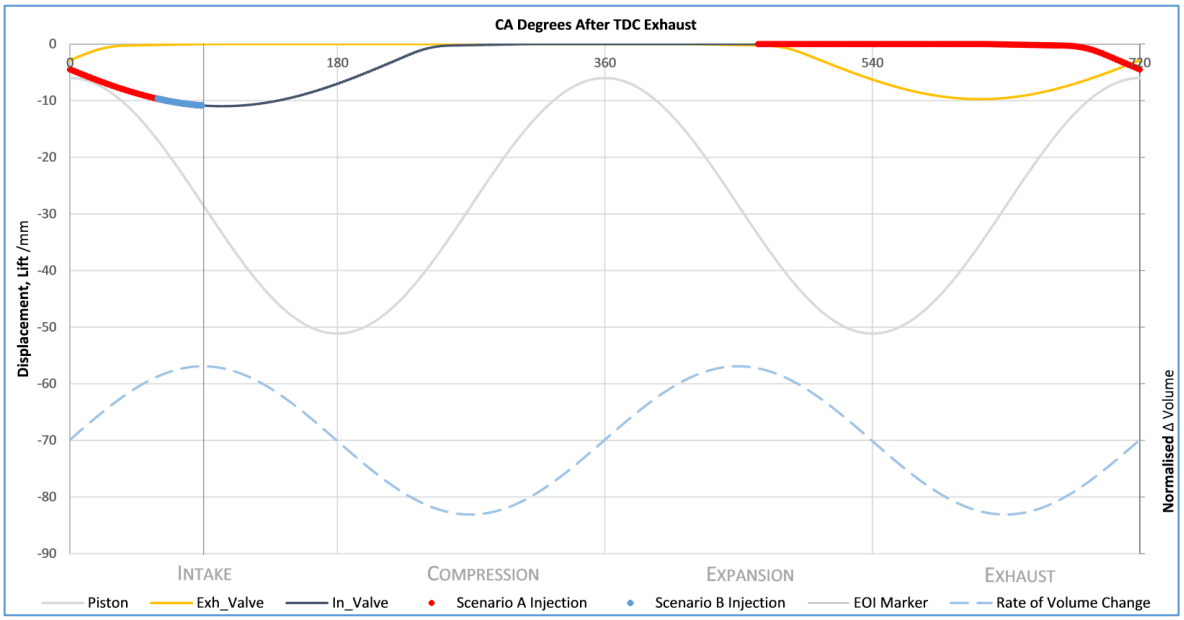

Figure 63: Comparison of Injection Duration at 4000rev/min, 20%TP (Blue) and 12000rev/min, WOT (Red), using OVI

Section 2.3.1 notes that the optimum injection timing is heavily influenced by the characteristics of the injector, airpath and targeting: the OVI strategy implemented is to be reviewed once stable engine operation is achieved.

4.1.3 | Ignition Advance Table Calculations

To facilitate engine firing and minimise the probability of knock (Section 2.3.3), base values for ignition timing were intentionally conservative for the large bore and over square geometry of the engine (Section 2.1.1) (Figure 64). In the absence of cylinder pressure transducers to allow for the accurate determination of the 50% mass fraction burned point, ignition timing was based on prior knowledge of the 100mm bore KTM 570 EXC engine (Section 2.2.5). Values were to be increased during testing to keep exhaust gas temperatures within component limits (Table 4).

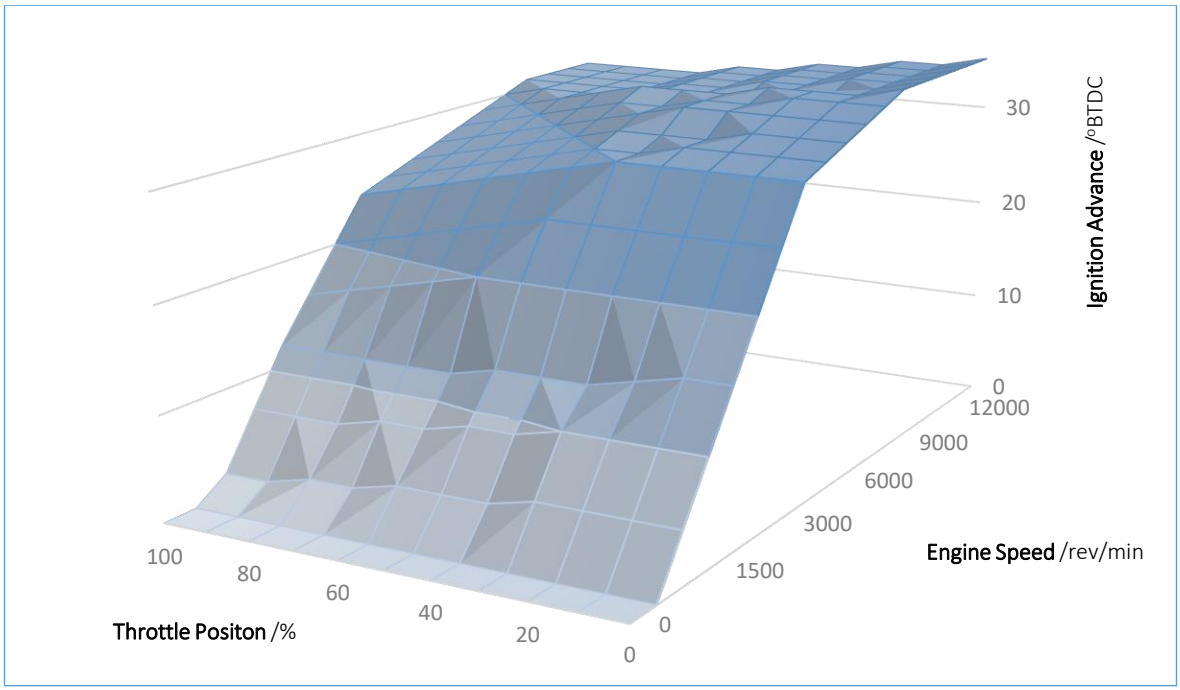

Figure 64: Conservative base ignition timing map used to promote firing

At cranking speed (<500 rev/min), the ignition is retarded to occur at or after TDC to promote the correct crank rotation direction whilst minimising load on the starter motor. With a linear trend to ignition advance with engine speed, values are intended to be retarded at idle conditions to reduce engine speeds and give headroom for short term ignition trim during pull-away conditions, improving the engine response to abrupt changes in load demand.

Section 2.3.2 discusses how the ignition advance should be reduced as the load is increased, due to the relationship between flame speed and volumetric efficiency. As the characteristics of the throttle and air path are unknown, the decay of ignition advance with throttle angle is adjusted during dynamometer testing. The relationship will differ with engine speed as the throttle is oversized for low engine speeds.

4.1.4 | Sensor Calibration

To determine engine speed and position, two Hall Effect triggers are used on the V-Twin engine. These provide a clear signal at low engine speeds, however require large notch widths [103]. An evenly spaced trigger wheel is mounted to the crankshaft for calculation of engine speed; a notch removed from the LH Intake cam is used to identify TDC position and stoke of the LH cylinder (Figure 65). The corresponding position of the RH cylinder can be inferred through mechanical geometry.

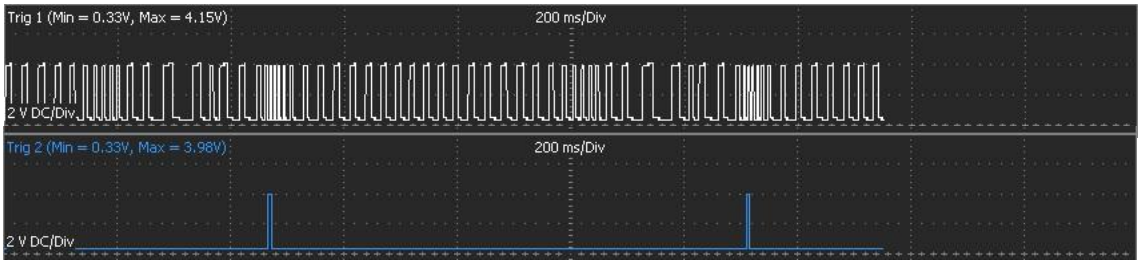

Figure 65: Ref/Sync capture of crank trigger (white) and cam trigger (blue) during cranking

Sensors used to monitor pressures and temperatures within their linear region were calibrated at the extremities of anticipated operated range. Calibration values were determined through correlation with a mechanical gauge or known points (such as ambient air temperature and pressure). A third point, midpoint of the operating limits, was used to validate the calibration and to check for proper interpolation of each channel. Lambda sensors were calibrated through performing basic setting of the sensors and control module with the sensors placed in free air. External lambda controllers were programmed to provide a 0-5V analogue input for the ECU. These sensors were also used as inputs to the fault detection systems of the ECU and the dyno control system (Table 1).

Table 1: Engine parameter operating tolerance during initial calibration and cold start conditions

Parameter	Severity	Target	Diag Lo	Diag Hi	Comments
Engine Coolant Temperature /°c	High	70	</IAT	80	Check for gradual temperature increase. *See Section 2.2.5*
Exhaust Gas Temperature /°c	High	800	500	1000	
Ignition Advance /°BTDC	High	30	20	35	Idle values. Controlled by failsafe in ECU. *See Sections 2.3.2; 2.3.3*
Lambda	High	0.8 λ	0.9 λ	0.92 λ	High λ raises flame speed and temperature. *See Section 2.3.1*
Oil Pressure	High	3 bar	2bar	4bar	Allow lower pressure during cranking. *See Sections 2.3.3*
Engine Speed /rev/min	Med	2000	1000	4000	Limited due to drivetrain resonance; controlled by ECU. *See Sections 2.2.1; 3.1.5*
Load Speed /rev/min	Med	4000	4000	4000	Cold values during calibration. Used as fail safe for rev limit.
Load Torque	Med	0%	--	--	No load torque during start-up calibration. *See Sections 3.1.5*
Throttle Position	Med	17.5%	10%	20%	Start-up values specified
Battery Voltage	Low	13v	11.5v	14.5v	Expect 11v during cranking
Fuel Pressure /bar	Low	4.5	4.4	4.6	Tight tolerance to minimise effect on fuel injection quantity. *See Sections 2.3.1; 3.2.1*

4.2 | Bedding-in, Diagnostics and Steady-State Tuning

Two logging systems were used in order to quantify the characteristics and behaviour of the engine, allowing for iterative development of the control system. The ECU provided an internal logging feature at 10ms, whilst the dynamometer control software provided data from the test procedure and dynamometer parameters, as well as the K-Type thermocouple interface for exhaust gas temperature measurements (Table C3). Rotation speed, battery voltage and coolant temperature measurements were used to synchronise data, allowing data from both sources to be analysed simultaneously.

4.2.1 | System Diagnostics and First Fire-Up

After safety tests on each subsystem, engine firing and calibration could commence. A default throttle position was established through providing a 1mm diameter aperture at the midpoint of the butterfly opening. This was deemed sufficient air to test for combustion, although additional throttle angle was anticipated for start-up to overcome the increased system inertia through the direct coupling to the dynamometer.

During initial testing, a discrepancy was observed in exhaust gas temperature between the cylinders (Figure 66), although the recorded data could not be used solely to diagnose the cause without speculation.

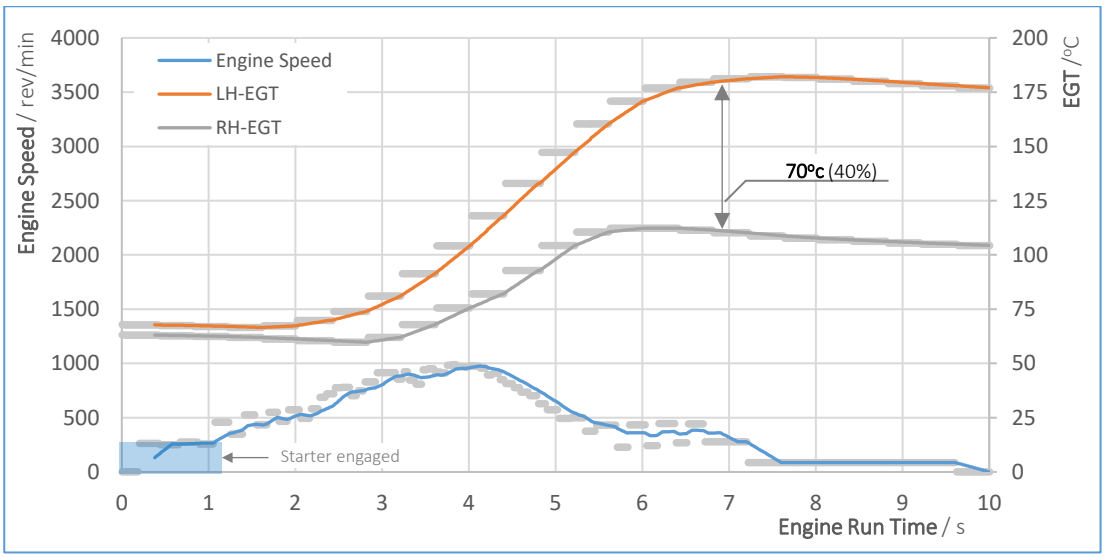

Figure 66: First start-up and cylinder temperature discrepancy {EN-10}

The engine was tested for compression in both cylinders, in order to further diagnose any differences in combustion conditions and to validate engine health (Table 2). This also gave the potential to calculate the dynamic compression ratio: whilst this may change at operating speeds due to the change in time duration of overlap and the energy of exhaust gas, this provides useful information relating to start-up procedure and required quantities of fuel.

Table 2: Cylinder Compression Test Measurements

CYLINDER PRESSURE (PSI/BAR)	CYL-1 (LH)	CYL-2 (RH)
TEST 1	172/ 11.86	175 / 12.07
TEST 2	173 / 11.93	176 / 12.13
AVERAGE	172.5 / 11.89	175.5 / 12.10
ENG AVERAGE	174 / 12.00	
CYL DIFFERENCE	± 1.5 / 0.10 (0.86%)	

Further investigation with a timing light indicated the right-hand cylinder bank was firing too late in the cycle. To counter this, an individual cylinder correction was incrementally added to a value of 2 degrees to note the effect on EGT and operating parameters. Given the conservative ignition advance angles set, the effect of this offset could be safely quantified (Figure 67).

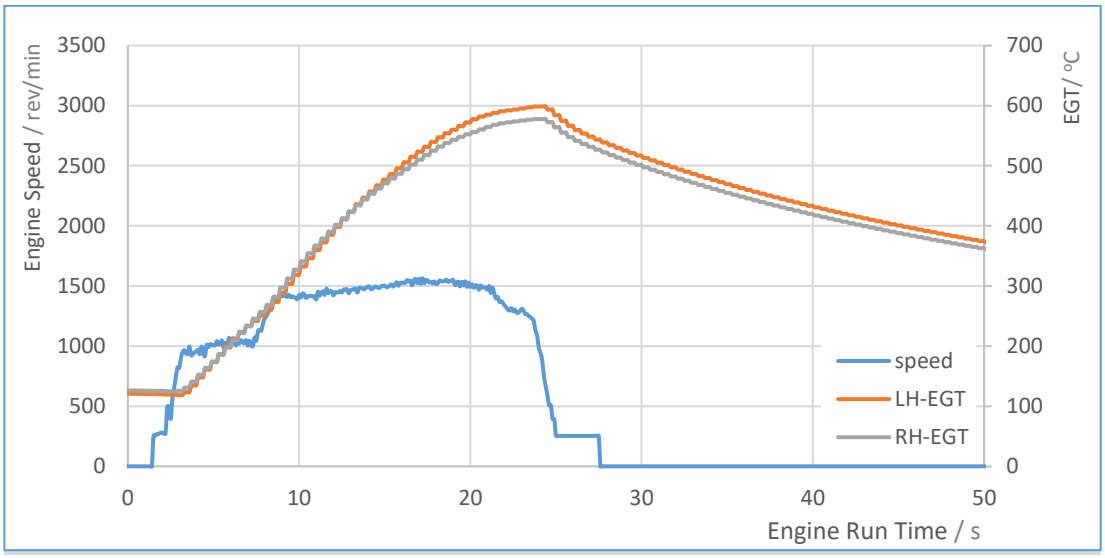

Figure 67: Exhaust Gas Temperature discrepancy with 2deg cylinder correction, even firing

4.2.2 | Calibration of Fuel Enrichment Strategies

The ECU allows for the implementation of several fuel enrichment strategies for cold start operation [104]: each aim to compensate for the reduction of combustion efficiency in a specific start-up phase to promote engine stability and response (Figure 68). Whilst some enrichment strategies have been disabled as they are disadvantageous for test cell operation, relevant parameters have been adjusted through dynamometer testing to achieve a suitable calibration.

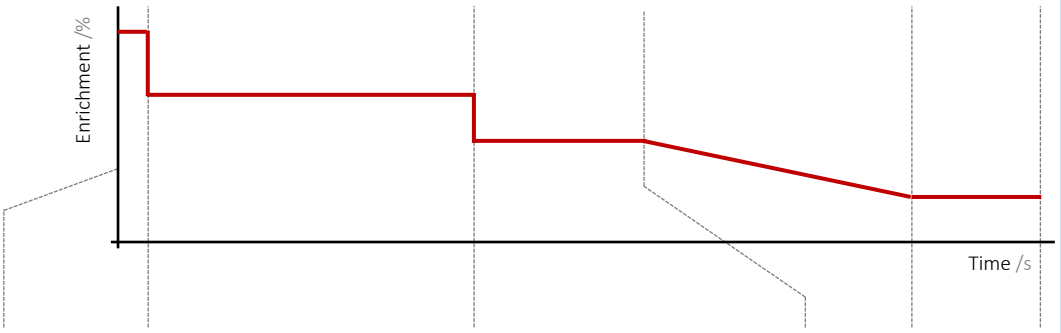

	First Crank Enrich /%	Cranking Enrichment		Post Start Enrichment		Decay Time /s	Warm Up Enrich/%
		Value /%	Hold Time /s	Value /%	Hold Time /s		
EN-30	40	90	1.7	0	0	0	10
EN-33	40	80	0.6	24	3.3	2.5	10
EN-37	40	100	1.2	38	1.3	2.5	10

Figure 68: Description of fuel enrichment strategies used at 20°c coolant temperature

The effect of each parameter on lambda stability during cold start is displayed in Figure 69. Throttle position and remaining engine management parameters were maintained to create a fair test. Note that in a vehicle installation any stability complaints would be exaggerated as the package would not benefit from the increased inertia experience through the direct coupling to the dynamometer.

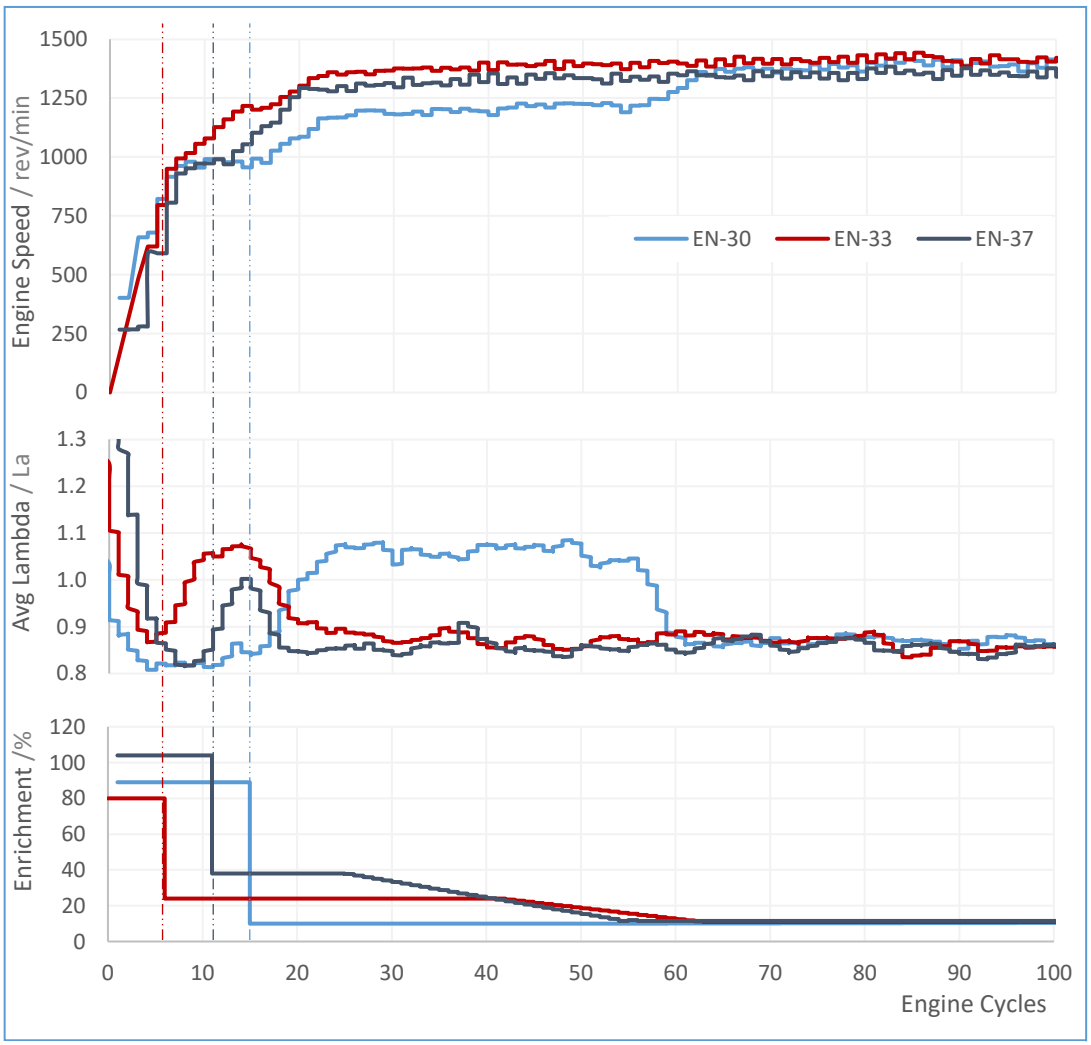

Figure 69: Effect of fuel enrichment and average lambda on engine speed rise during cold start-up

The default fuel enrichment strategy, shown in the EN-30 trace, can be seen to promote excessively lean combustion during the start-up phase. EN-33 and EN-37 provided acceptable lambda stability during the start-up phases, although the engine could not be run up to operating temperature to assess the suitability of the warm-up enrichment phase. Further testing will be conducted when the base map is complete, which can incorporate any offset from the enrichment table when the air/fuel mixture is appropriate at operating temperatures.

4.2.3 | Cooling System Diagnostics

The functionality and effectiveness of the coolant system was tested at 1500 rev/min idle: the configuration was varied across several runs, with the engine allowed to cool to ambient before the next. The rate of coolant temperature rise per run was comparatively assessed according to theoretical understanding. Operating during the warm-up phase at a constant speed and load, a constant temperature gradient was anticipated, after coolant flow was experienced at the temperature sensor (Figure 70).

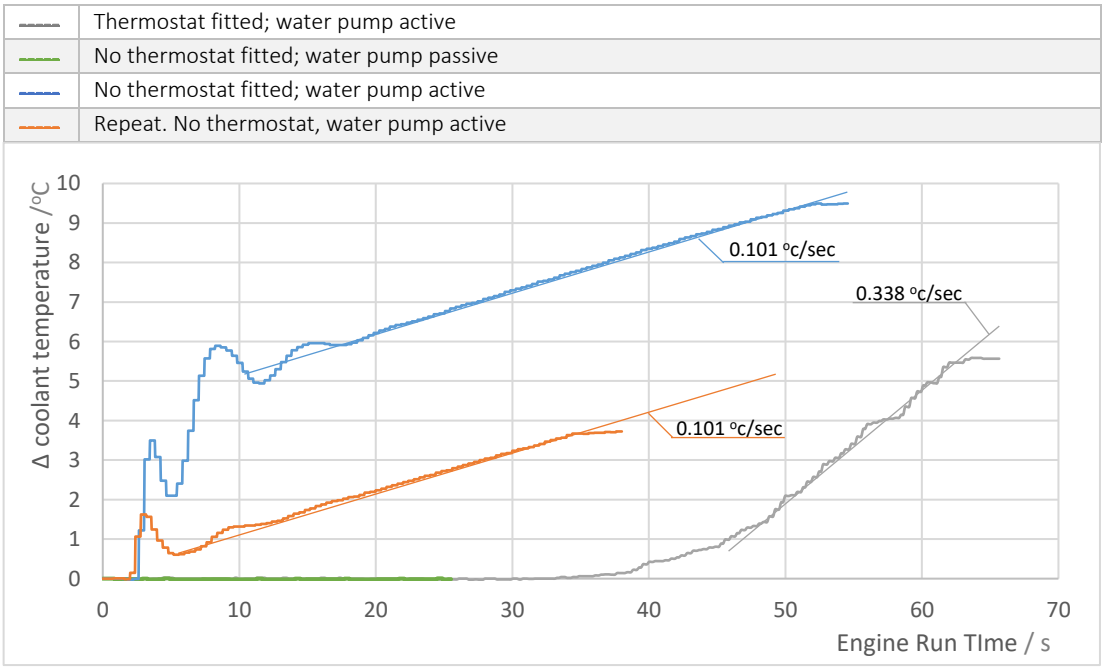

Figure 70: Coolant system configuration vs coolant temperature gradient

Due to the diameter of the locating boss, the coolant temperature sensor could only be fitted upstream of the thermostat. As no other coolant or block temperature sensors were available, the engine temperature could not be effectively measured during warm-up when a thermostat was installed. The thermostat was bypassed in subsequent testing due to the risk of measuring coolant temperature after the thermostat: in the event of thermostat failure, sufficient fluid flow may still be prevented when the coolant is over the threshold temperature, leading to engine overheating and component damage. A new boss allowing the coolant temperature sensor to be installed upstream of the thermostat is recommended.

Due to concerns of propshaft integrity, the engine was not run for a sufficiently long period of time to identify the equilibrium temperature of the cooling system. However, the heat exchanger system had been noted to maintain coolant temperatures on similar displacement engines below temperatures of 60°c when required.

4.2.4 | Steady State Idle Mapping and Bedding In

After verifying the integrity of the engine, ancillaries and control system, the engine speed and run time could be steadily increased (Figure 71). The quantity of air ingested by the engine each cycle varies significantly at low speeds given the valve timing and intake manifold configurations. As such, significant steps in calibration could only be achieved through steadily increasing engine speed up to stable idle conditions. The increased engine speed also correlates with typical bedding in procedures, whereby the load and speed are gradually altered to correctly seat critical components.

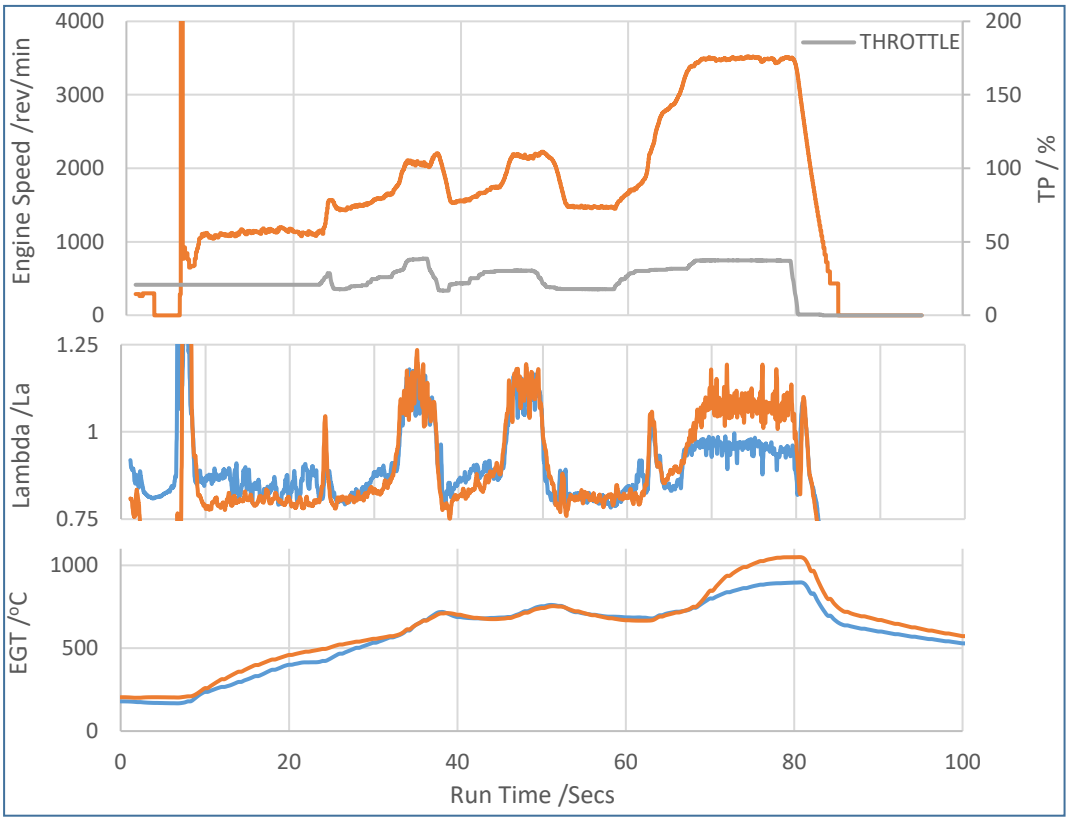

Figure 71: Trace from Base Map up to 3500 rev/min, 37% throttle.

The test was ceased once the exhaust gas temperature of the right-hand cylinder exceeded the threshold value set in Table 1. Ignition angle was increased by 10% to note the effect on the excessive exhaust gas temperatures and lambda recorded in the previous run. Whilst the measurement system did not include a knock sensor, for a target lambda of 0.9, knock was not anticipated above exhaust gas temperatures of 750-800°C [23]. Additional advance was added incrementally, to minimise cylinder head and combustion chamber exposure to excessive heat. Additional benefit was noted when comparing the stability of engine parameters between the two ignition angles (Figure 72).

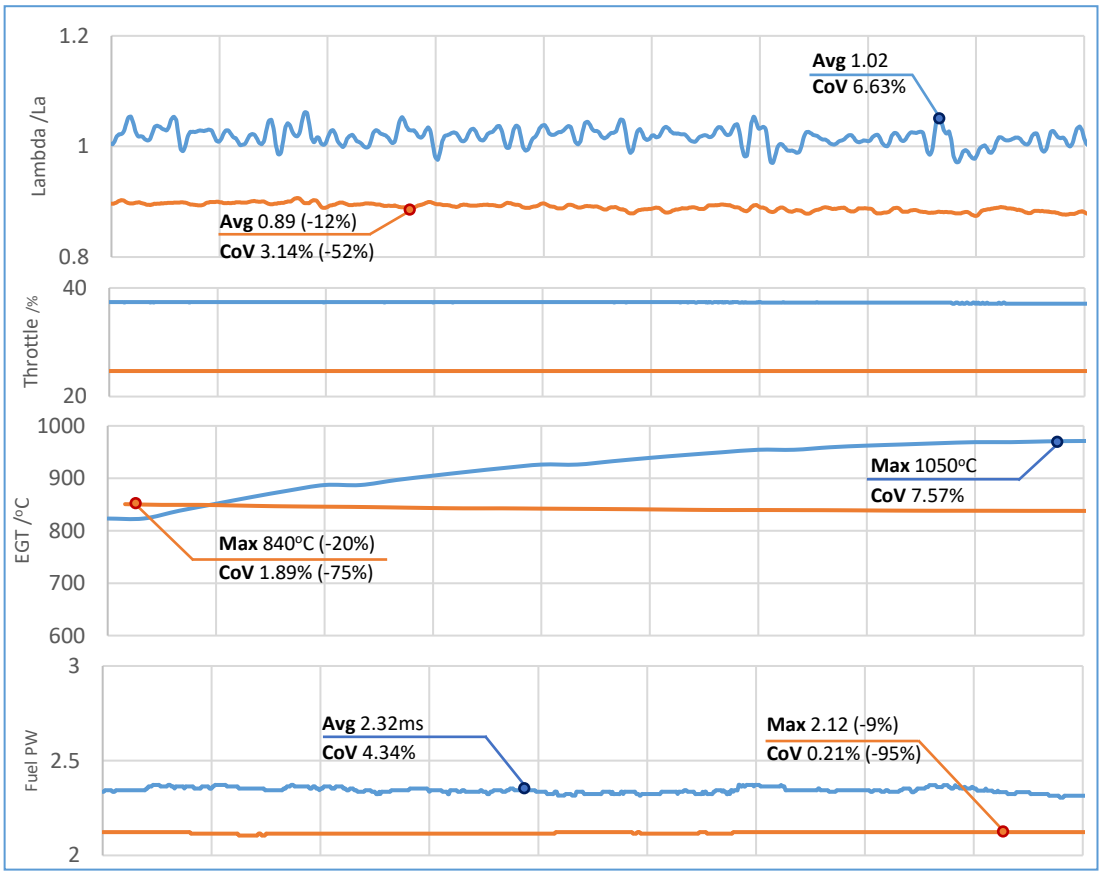

Figure 72: Effect of ignition angle on parameter stability over a 10 second time period at 3500 rev/min

4.3 | Summary of Base Calibration Work

To validate the mechanical operation of the engine and auxiliary systems, and to adjust the base calibration values and strategies, a series of low load diagnostic tests were conducted. The data from each test was critically analysed in order to iteratively optimise the mechanical and electronic subsystems with minimal risk to components.

Analysis of the first fire attempts highlighted a difference between the exhaust gas temperatures of the two cylinders, which after compression tests and timing strobe investigation, was rectified by an individual cylinder offset of ignition advance.

Within the safe operating limits defined, the control system was further calibrated in tandem with bedding-in and stabilisation procedures, primarily focussing on the fuel enrichment strategies to minimise flare and undershoot during start events. Diagnostics were performed on the cooling system, testing circuit configurations to ensure the system is allowed to heat up at a controlled rate for component protection and minimised wear.

Ignition advance was adjusted to maintain EGT within the defined component limits, with notable effect at 3500 rev/min idle on required throttle angle and fuel injection quantity. These adjustments were extrapolated to surrounding sites in order to provide safe transition in the following stages of dynamometer testing.

5 | Motoring Dynamometer Results and Discussion

This section discusses the data collected from steady state testing at speeds below the drivetrain resonant speed. Steady state testing was employed in order to negate the effect of transient actuation and excessive PID control events, as well as the sporadic relationship between dynamometer throttle demand and output.

For each requested dynamometer speed, the engine speed was increased through manual actuation of the throttle, until a control torque was observed *(Point A,* Figure 73). The throttle position was held in the centre of each load site to provide clear data for analysis and adjustment of fuel and ignition tables. The throttle was increased and the procedure repeated for the subsequent sites *(Points B, C)*, until wide open throttle *(Point D)*. Critical engine health indicators (Table 1) were carefully observed during the process to minimise the risk of component damage or failure during operation.

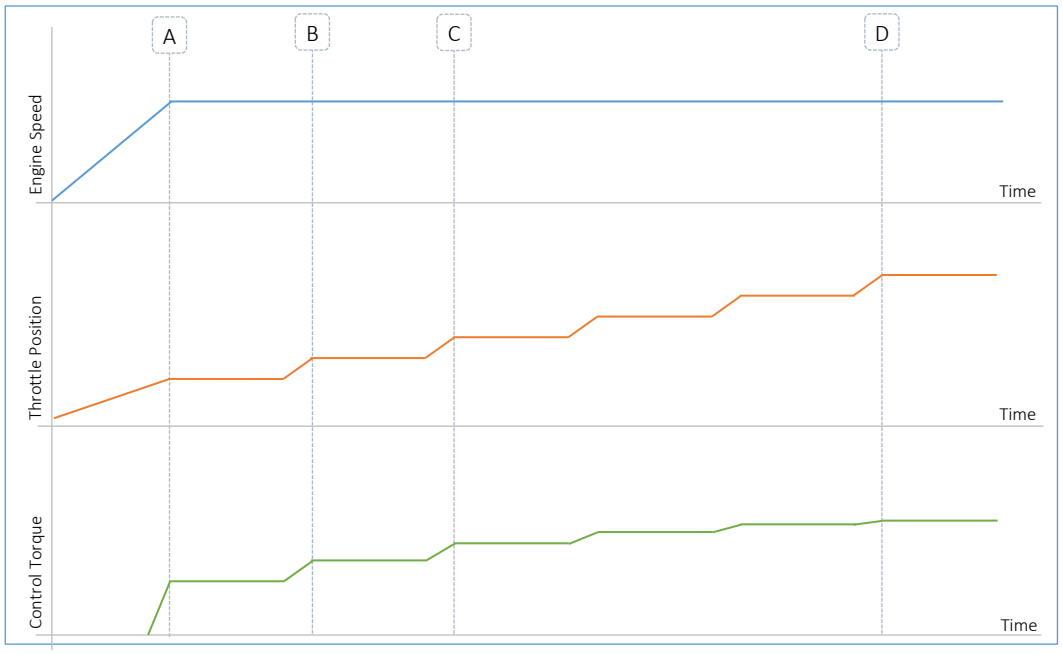

Figure 73: Depiction of steady state, constant speed testing conducted to collect load data

Due to the concern of propshaft integrity, each test run was limited to a maximum of three minutes, minimising the heat accumulation in the elastomer components. Subsequent tests were not conducted due to the concern of degradation of the shaft with respect to operating speeds, loads and duration accumulated (see 3.1.5 | Drivetrain Resonance , pg. 32).

The dynamometer losses were noted to be significant compared to other engine configurations tested by the author with the designated eddy-current dynamometer. Powertrain packages typically tested comprise an internal gearbox, reducing the rotational speed and increasing the torque observed at the dynamometer. In such cases, the dynamometer losses are a negligible percentage

of the observed torque at the propshaft. In addition, the direction of dynamometer rotation when motored by the v-twin engine is counter clockwise and opposes that conventionally experienced.

As such, the torque output from the dynamometer traces was manipulated to consider the difference between the observed torque and the zero offset at rest with the dynamometer coolant pump active. Observed power was recalculated as a function of the corrected torque and engine speed.

5.1 | Lambda Stability Analysis

Figure 74 presents a summary of the load and speed sites entered through the course of load testing, whilst demonstrating the air-to-fuel ratios were within acceptable range for safe operation. This also provides an indication of calibration maturity, as less explored sites have not benefited from iterative fuelling and spark adjustments.

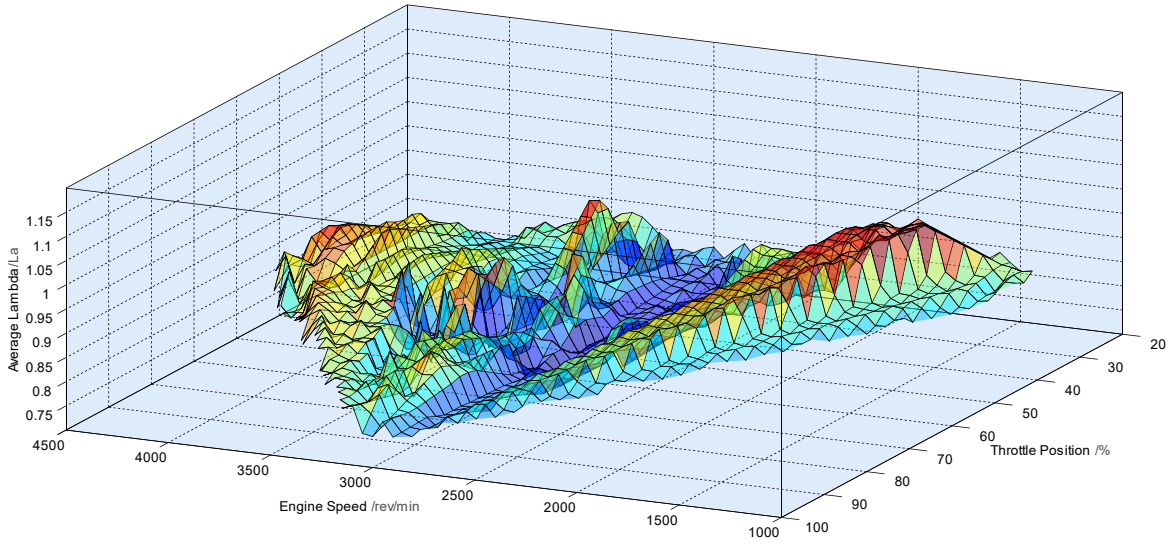

Figure 74: Map of average lambda recorded during dynamometer runs with respect to engine speed and throttle opening

The air/fuel ratio was conservatively rich to minimise component temperature and to provide factor of safety in the event of cylinder-to-cylinder or cyclic variance. Data is collected using the base map, and no adjustment of calibration was possible during the runs. Ignition advance was equally conservative, to minimise the likelihood of knock in previously unentered load/speed sites. Observing the MBT and Air fuel ratio diagrams (Figure 26), it is plausible for the difference between simulated and predicted values to be reduced.

Lambda and EGT on cylinder 2 (RH Bank) are notably higher than that of cylinder 1. With correct TDC identification achieved in the base calibration, this may be a result of variance in injector or ignition coil characteristics or a difference in the quantity, turbulence, dilution or homogeneity of intake charge between cylinders. Further testing at higher engine speeds could help to identify these causes, although a small variation between the requirements of each bank should be noted as expected (Figure 74).

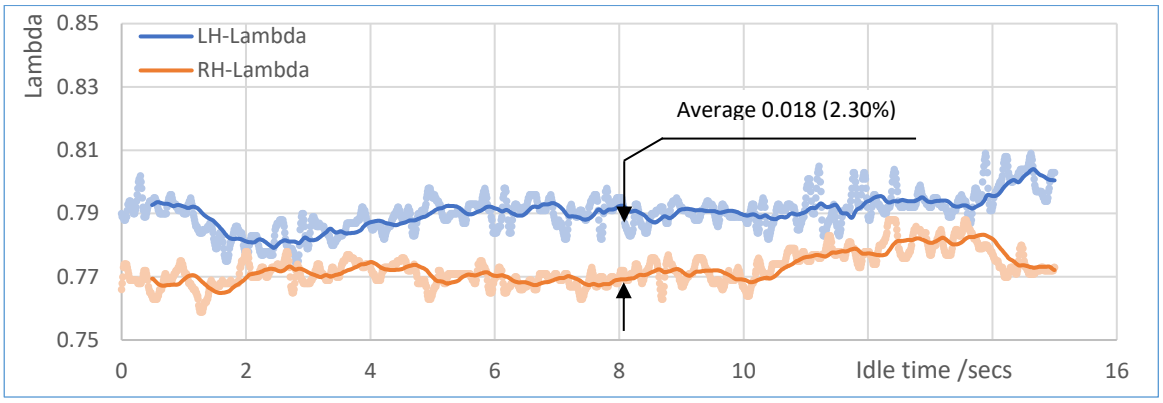

Figure 75: Cylinder to Cylinder discrepancy in measured lambda at 3600 rev/min idle.

Due to torque fluctuations, primarily through low cranktrain inertia, firing order and driveshaft flexure, variance between requested and instantaneous dynamometer speed was noted. Output from Lambda and exhaust gas temperature sensors may be used to understand the combustion stability, and any contribution this has on dynamometer speed variance.

5.2 | Idle Stability Analysis

Figure 76 documents the stability of key parameters when the minimum throttle demand is set for the engine to maintain each desired setpoint. Tabulated data can be found in Appendix C.

The PID control of the dynamometer speed control was not calibrated for such a high speed, low inertia engine and as such strong fluctuations in the control torque caused an increased speed variance at 3600 rev/min compared to 3000 rev/min. This variation is unlikely to be due to combustion stability as the oscillation of Lambda is small and fluctuation in the test cell throttle control is observed.

Whilst there are no sensors available to directly quantify the phenomenon, it was hypothesised that the cycle-to-cycle variation of intake charge would be more pronounced at low engine speeds due to intake and valvetrain optimisations for high speed operation. This is supported by the improved lambda stability at the highest speed of the tested range.

Variation in exhaust gas temperature for the 3600 rev/min case is likely due to the fluctuation in ignition advance as the ECU interpolates from adjacent speed sites. In the 3000 rev/min case, adjacent speed sites had same ignition advance values, resulting in zero variance. As engine run time was limited for driveshaft protection, it is likely the EGT had not reached equilibrium when the log was started.

The spread of variation in Fuel and Oil pressure may be due to the changing relationship between sampling rate and engine speed or a change in supply voltage. This is supported by the observation that their variation both follow the same pattern with engine speed.

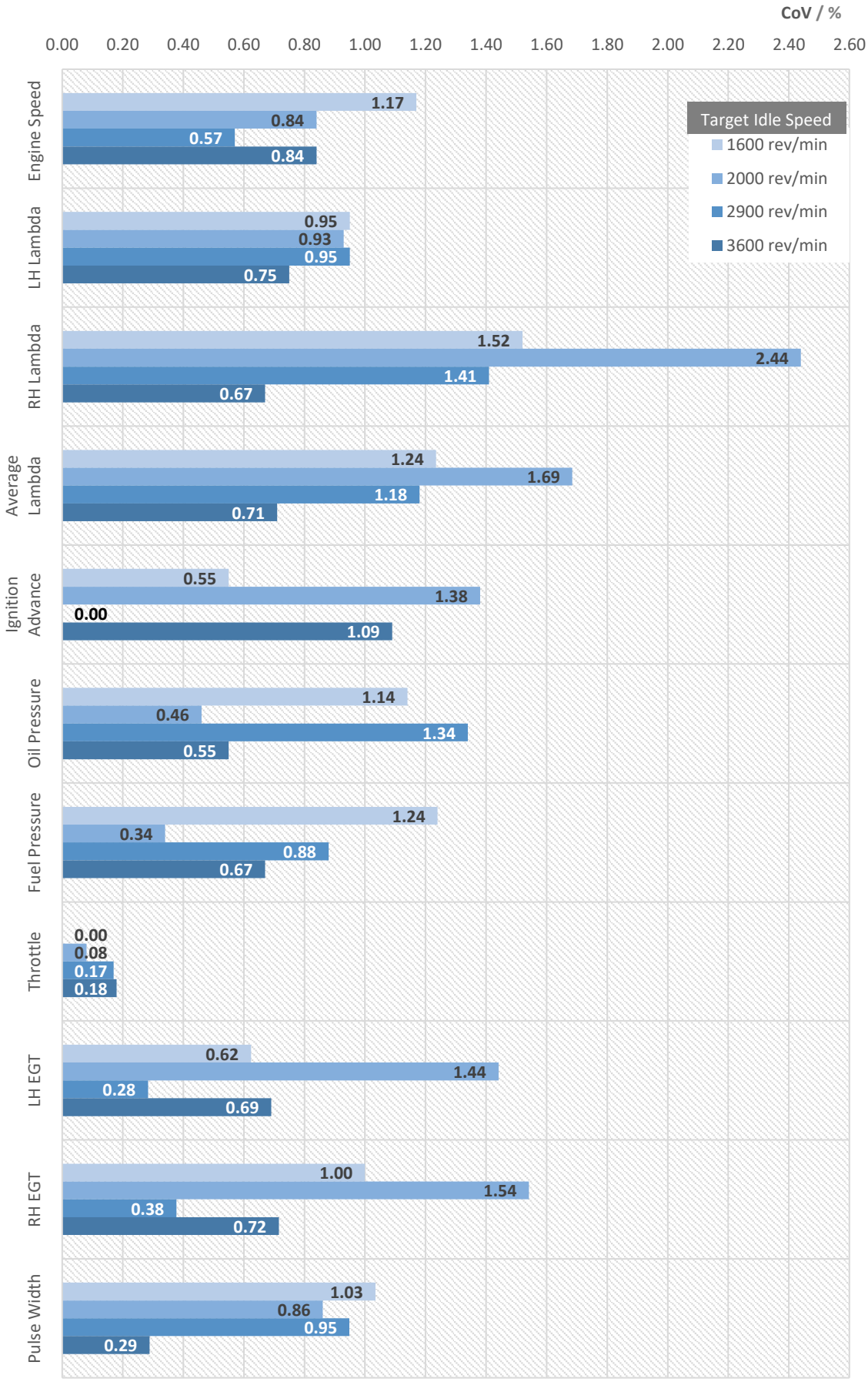

Figure 76: Comparison of engine parameters at idle conditions

5.2 | Throttle Linearity Analysis

Figure 77 displays the compiled dynamometer data in order for the base map to be analysed and iteratively improved. Error bars, where included, denote the cylinder values that constitute the average trend.

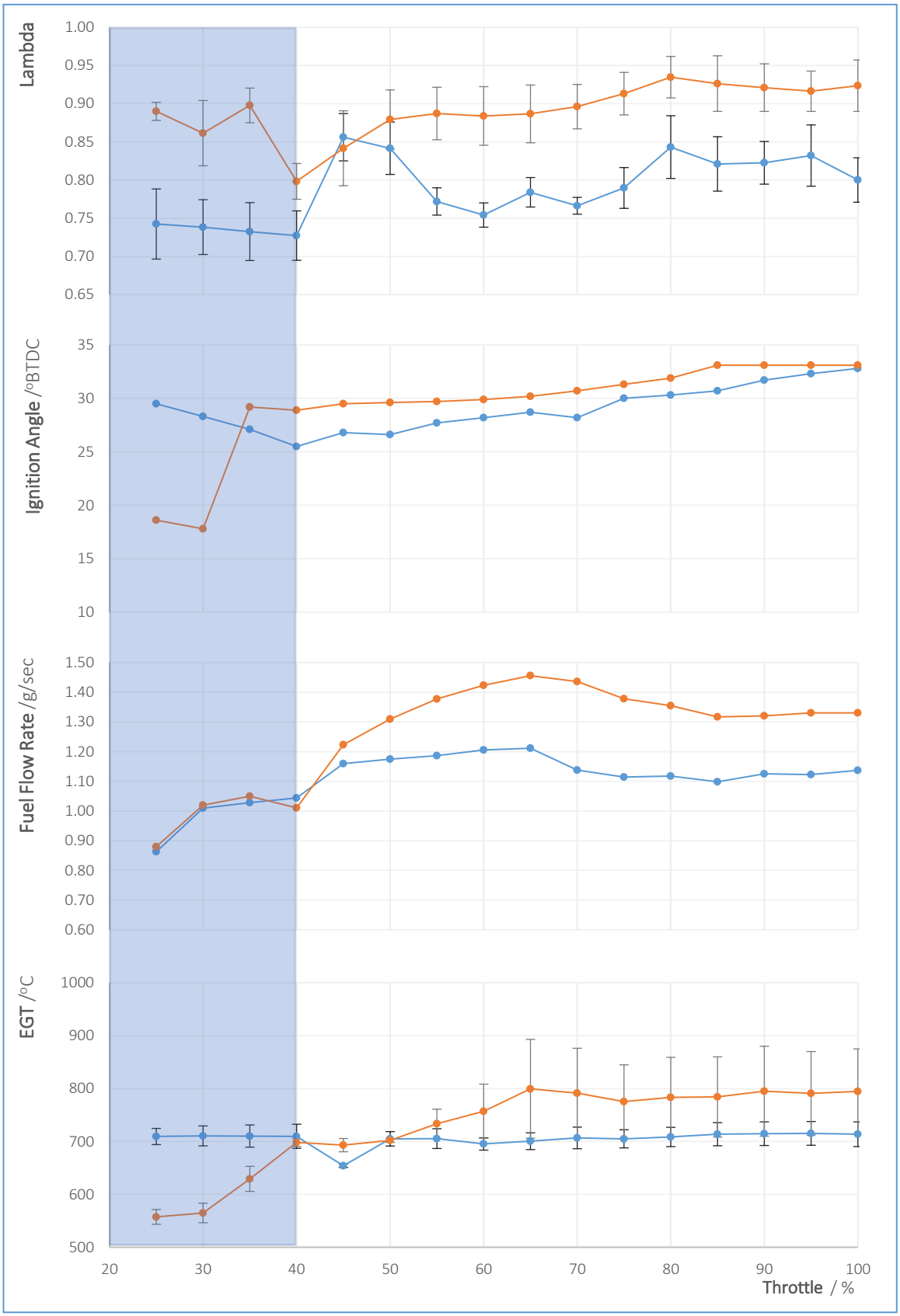

Figure 77: Engine ECU measured parameters (base map) at 3000rev/min (blue) and 3500rev/min (orange)

The average air-to-fuel ratio is significantly leaner in the 3500rev/min speed case, with greater disparity between cylinder than observed in the 3000rev/min run. This approaches stoichiometric conditions in one cylinder as the test approaches wide open throttle. The difference between the two cylinders is likely the result of tolerances in the valve timing, variation in the required trigger offset, plenum flow preference or variances between coils, spark plugs or injectors.

It should be noted that, as the air-fuel ratio is calculated using wideband oxygen sensors, a lean measurement can be obtained when partial combustion occurs and there is unburnt air/fuel mixture in the exhaust product.

Increasing the ignition angle could improve the combustion stability in conditions where the ignition is currently excessively retarded from MBT, to the benefit of Lambda measurements, EGT, power and efficiencies. Given that, for a set air-to-fuel ratio, the flame speed is related to the cylinder air density, future adjustments to the base map could allow for more advance at part throttle, as the sites with the greatest volumetric efficiency (approaching wide open throttle) should have the least advance (pg 19).

Whilst EGT is constant through the 3000rev/min speed case, this approaches the maximum permissible temperature in the 3500rev/min case (Figure 77). In particular, this displays the relationship with air-fuel ratio as described on page 16: as lambda approaches 1 (stoichiometric combustion), the exhaust gas and cylinder head temperatures rise, both to the detriment of power output.

Exhaust gas temperature measurements may be loosely proportional to rate of exhaust energy input (i.e. engine power output), however the lower exhaust gas temperatures at the start of the run are likely to be linked to the minimal time between engine start-up and the 3500 rev/min load sweep. Additionally, EGT is stable across all load sites in the 3000rev/min speed case, where the probability of this theoretical occurrence is more likely. Whilst the compression has previously been measured (Table 7), the negligible difference noted between the EGT of both banks in Figure 77 may be more important when operating at higher speeds or loads.

Figure 78 displays the performance related measurements and calculations obtained from the same dynamometer runs as Figure 77.

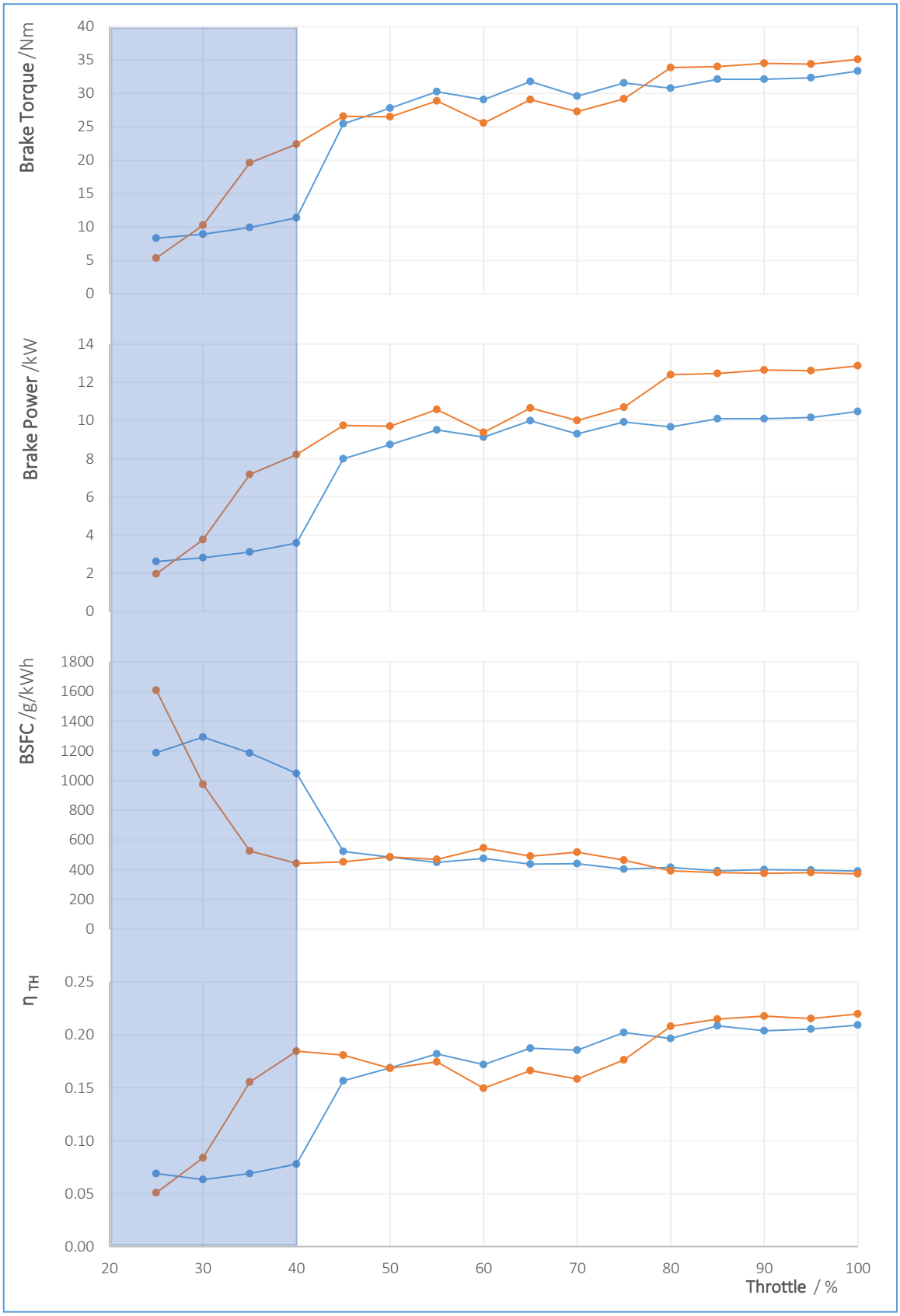

***Figure 78**: Observed performance of V-Twin (base map) at 3000rev/min (blue) and 3500rev/min (orange)*

Brake Torque, thermal efficiency and BSFC are comparable for all throttle positions exceeding 65% opening (at 3000 rev/min) or 70% opening at 3500 rev/min. At low engine speeds the plenum pressure can be maintained at partial throttle angle. As such, fluctuations are due to the gradual adjustment of fuel table and ignition advance values, where the design point of the intake system is achieved at an earlier-than-predicted throttle opening angle. Moreover, these fluctuations can be removed in subsequent testing and calibration runs. The effect of this phenomenon cannot be generalised for all engine speeds in this manor: at high engine speeds the throttle plate is likely to regulate intake flow until opened to at least 85%.

The similarity between the torque observed at 3000 and 3500 rev/min is also contributed by the minimal difference between ignition angles at these two sites, further presenting this as an important area for future calibration.

Torque output with respect to throttle position is noted to be non-linear; a characteristic that is influenced by operating engine speed. This highlights the requirement for electronic throttle actuation in vehicle application, to provide a progressive relationship between the pedal demand and engine output during transient operation. Figure 79 depicts a hypothetical relationship between pedal position (torque demand) and throttle position based on the collated dynamometer data to achieve linear torque response; this relationship is likely to change significantly through the operating speed range requiring a 2D lookup table or similar implementation method.

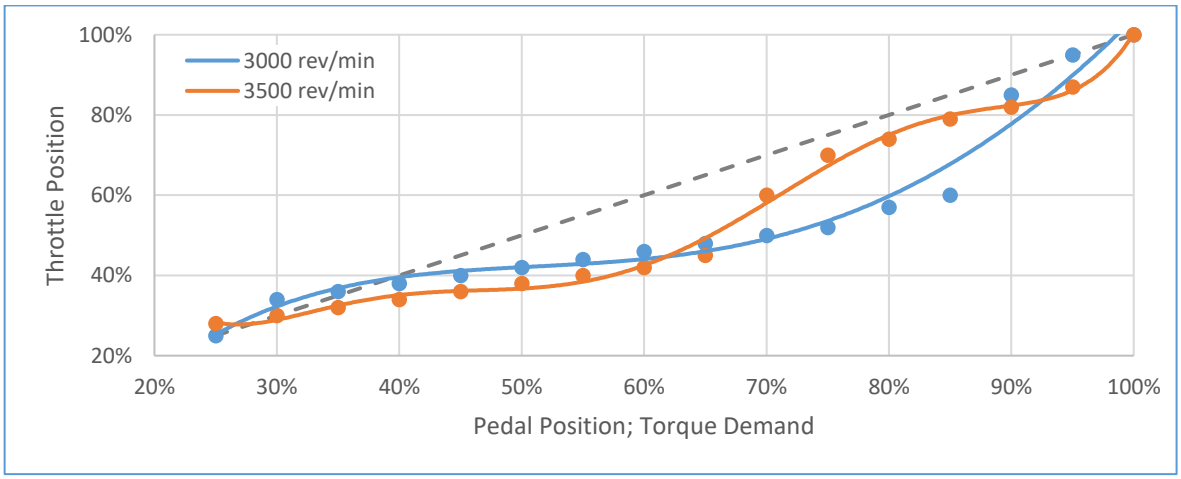

Figure 79: Required relationship between pedal and throttle positions at differing speeds to achieve linear torque response

5.4 | Comparison of Performance Variables with 1D Analysis

The observed torque output (and resulting power) from 3000 and 3500 rev/min load cases were comparable to GT-Power predictions constructed during the design process of the engine [35]. Measured output from the engine dynamometer indicated approximately 14-17 percent lower performance than anticipated in simulation at wide open throttle (Table 3, Figure 80).

Table 3: Comparison of predicted and observed WOT performance

		Predicted	Observed	% Difference
Torque /Nm	3000 rev/min	40.14	33.30	-17.0%
	3500 rev/min	41.25	35.10	-14.9%
Power /kW	3000 rev/min	12.61	10.48	-17.0%
	3500 rev/min	15.12	12.87	-14.9%

The test engine was configured with the minimum valve overlap to minimise risk of valvetrain clash, as such the runs equally served as a demonstration of the potential of the engine. Reduced valve overlap may account for performance within tested sites; margins in air/fuel ratio and ignition advance may also improve thermal efficiency and torque output when the calibration is iterated

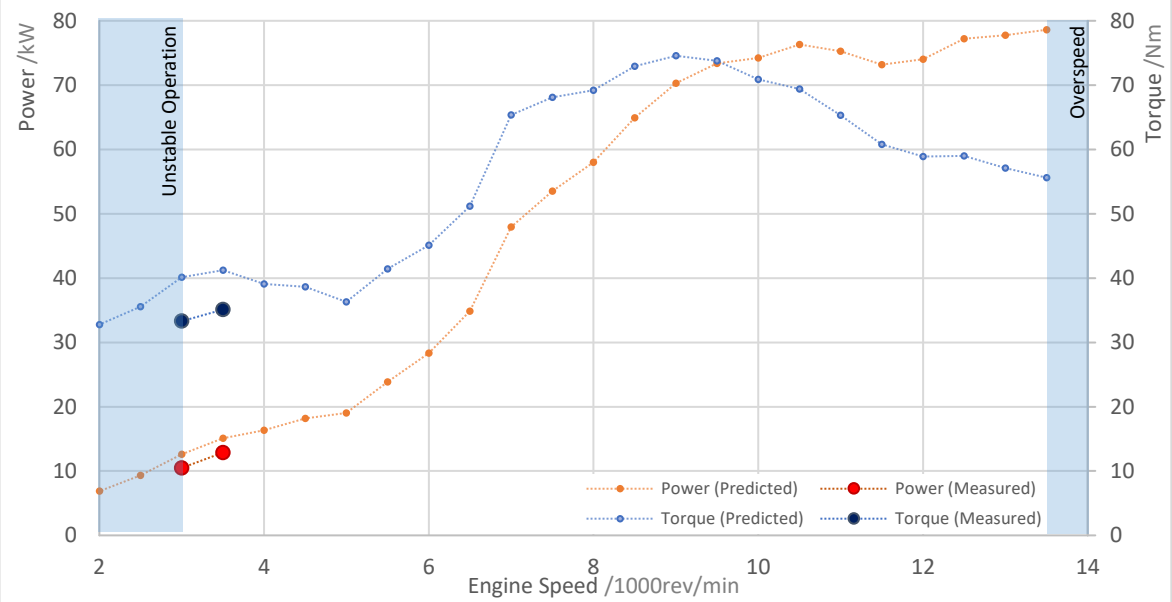

Figure 80: Comparison between GT-Power predictions and recorded dynamometer values

Simplifications in the design of auxiliary components, such as exhaust, silencer and auxiliary drive units, do not appear to be of significant detriment to engine performance under the operated conditions. Fuel pressure stability is deemed acceptable due to the minimal changes in flow rate characteristics and ballistic region limits with respect to fuel pressure (Figure 58)

6 | Conclusions

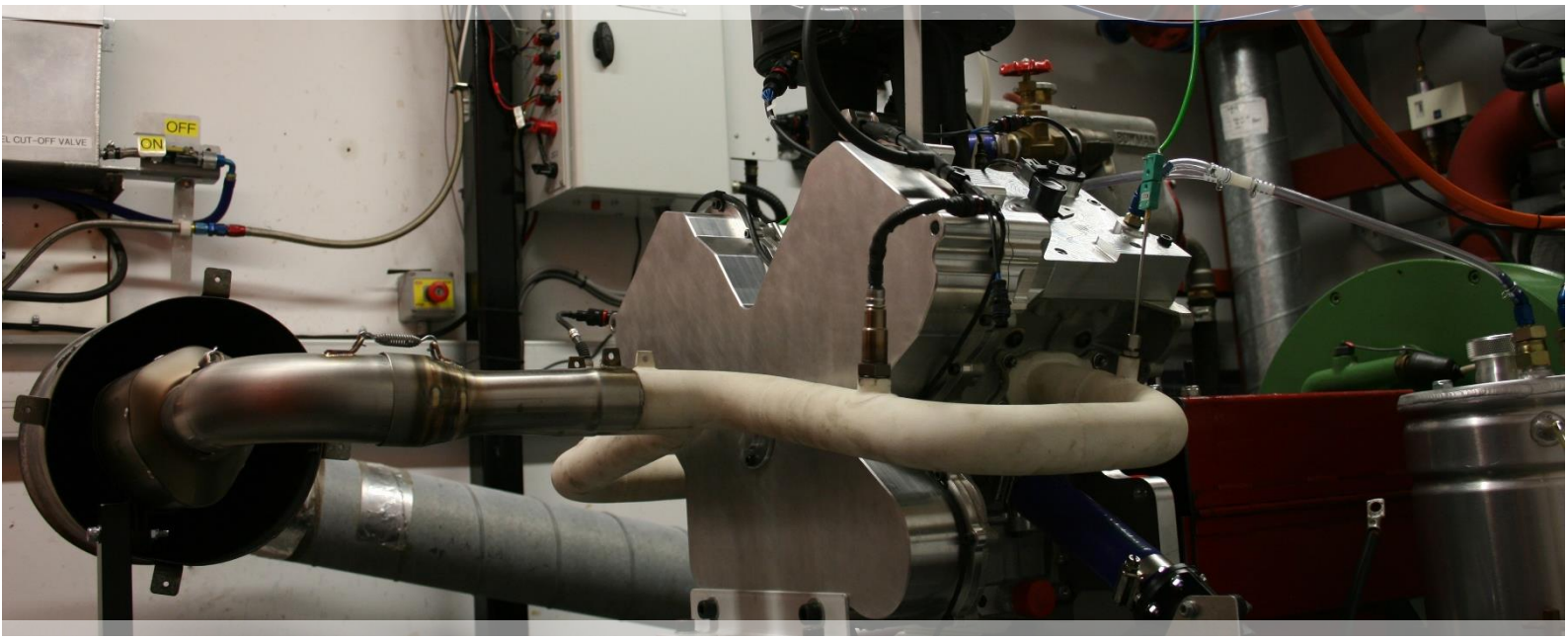

Figure 81: Engine and ancillaries operating on dynamometer test cell, Sept 2016

The aim of the project was to derive and validate a base calibration for the v-twin engine, using research to understand the notable design considerations of the engine and their influence on calibration and control strategy.

Whilst the base calibration allowed for successful first fire and idle operation, more testing is required for a full validation process. However, this requires resource investment in the test cell setup and drivetrain configuration to achieve this safely.

During drivetrain resonance calculations it was established that the speed limit could not exceed 4000 rev/min to maintain propshaft integrity, which severely limited the proportion of speed and load sites that could be validated. This is also below the optimal operating speeds for the engine, providing cycle to cycle variation in mass flow.

Mechanical development of the engine prior to first fire was completed, most notably a procedure for assessing valvetrain timing and the design and manufacture of a pump stack chain tensioner. A bespoke wiring harness and control system was designed and manufactured for the engine and test cell. Following the system calibration, diagnostics and bedding in phase, steady-state load testing was conducted at 3000 and 3500 rev/min, with deviation of WOT torque output of 14 and 19% respectively from GT-Power predictions.

Analysis has been conducted within the scope of the available sensors and hardware to assess the combustion stability and cylinder-to-cylinder balance, which have again showed promising results. Despite operation of the engine below the anticipated range of such high overlap camshafts, the engine produced displayed a maximum thermal efficiency of 22% and minimum BSFC of 372 g/kWh.

During testing it was difficult to isolate the variances caused by engine calibration and the aggressive PID control of the dynamometer control torque. Calibration of the test cell control system or the implementation of a gearbox would improve the validity of test data. With the concern of drivetrain integrity, subsequent calibration was not conducted. Whilst the completed testing proved the suitability of the base calibration in the explored sites, further testing and iterative adjustments to fuel quantity and ignition angle could reduce the variation noted.

Recommendations for future developments on the V-Twin project have been included at the end of the report, with particular focus on the integrity and resulting safety of the driveline and auxiliary systems.

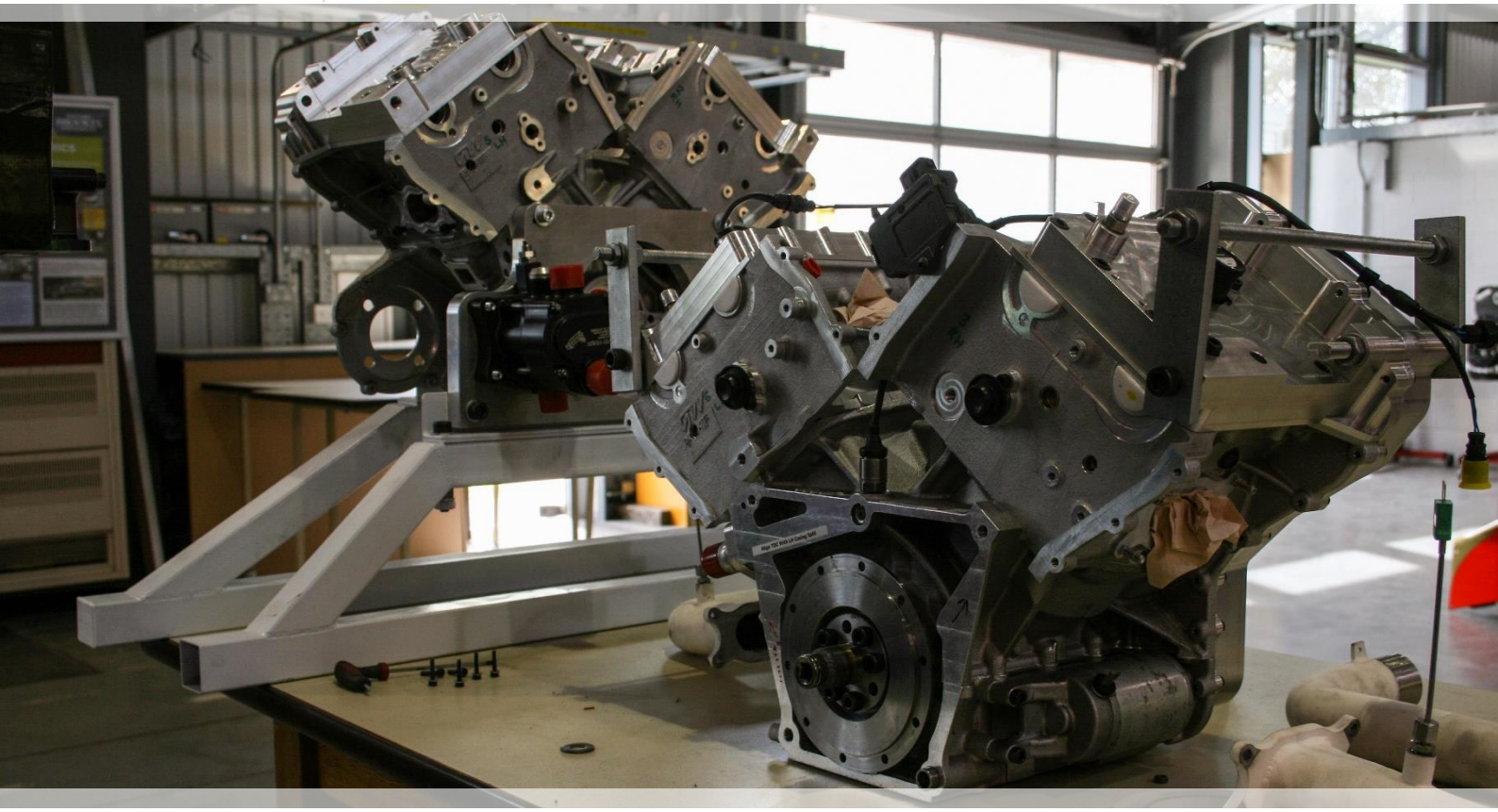

Figure 82: V-Twin engine and mock-up during rig installation

The work completed during this research provides a platform on which further testing and development can be conducted. To that end, this section discusses potential areas of future work around the project, recommended based on their feasibility, required resource investment and the anticipated quality and merit of experimental findings.

During the course of bedding in and low speed engine testing, it can be seen from Figure B1 that the engine has been operated for a combined 1.5 hours. As such, it is recommended for the rocker covers and engine front cover to be removed, such that the condition of internal components can be visually inspected. The engravings added to the camshafts and retaining caps during this project can be used to assess the condition of the chains and to ensure correct valve timing is maintained. A borescope can be used to indicate the condition of the cylinders and oil galleries as appropriate, however it is strongly recommended that no further disassembly is conducted, to minimise wear on permanently stressed components and to reduce risk of contamination.

Through the implementation of pressure transducers and a crank resolved encoder, the spark timing and, to some extent injection timing, may be adjusted to improve efficiency and reduce component temperatures. It is important to complete the base calibration of the engine to a sufficient level before installation of the spark plug based transducers as to not cause premature wear to the bespoke sensors.

Caution must be used when calibrating a knock sensor to minimise noise from the rig and ancillary components, and should only be installed to provide redundancy in the event advance is inadvertently excessive. Closed loop lambda control can be employed once the fuel table is suitably calibrated under steady state conditions, compensating for changes in fuel temperature, dilution and injector deposit build-up.

An external coolant heater should be implemented, to minimise wall and chamber wetting in extreme cold-start operations. Many auxiliaries within the powertrain were intended to provide an adequate and resource effective solution for test cell operation. However, these should be redeveloped to minimise parasitic loads and to accommodate vehicle packaging requirements.

Tuning of the dynamometer PID system would allow for more accurate steady state testing, improving the stability of the measured parameters of control torque, power, and BSFC through reduced 'hunting'. Its importance is exacerbated as the engine torque output is significantly lower than the dynamometer capability, when connected without a gearbox or torque converter.

Electronic throttle actuation may be implemented in future development to provide the required control of torque delivery of the engine in vehicle installations. However, its implementation would be similarly beneficial in test cell applications, allowing for predictable, repeatable throttle actuation difficult to achieve with the current mechanical system.

To improve the accuracy of measuring the instantaneous fuel flow during testing, and the thermal efficiency and BSFC as a result, the fuel flow metering apparatus could be installed. Presently, fuel flow is estimated using the requested pulse width, as logged by the ECU or connected computer, which is combined with the injector flow test results to give the fuel quantity injected. This, however, is subject to errors due to discrepancies in logging time (affecting the validity of measured values) and the cumulative accuracy of the calculation steps. In addition, the injector characteristics are subject to supply voltage, dwell, fuel pressure, cleanliness and age, hence fuel flow metering presents a much more accurate solution.

References

[1] D. Cheng, *Formula Student Photograph,* 2014.

[2] IMechE, Class 1 Formula Student Rules, London: IMechE, 2016.

[3] F. Bengolea and S. Samuel, "Technology Choices for Optimizing the Performance of Racing Vehicles," *SAE Papers,* 2016.

[4] S. Okunishi, K. Izumi, T. Tokinoya, T. Kubori and K. Yoshida, "Technical Development of Power Train of the F-SAEJ Championship Car Originally Devleloped by Osaka University Formula Student Team," *SAE Papers,* 2011.

[5] M. E. Biancolini, "Engine/Vehicle Matching for a FSAE Race Car," *SAE Papers,* 2007.

[6] M. Bassett, J. Hall, T. Cains and M. Underwood, "Dynamic Downsizing Gasoline Demonstrator," *SAE Papers,* 2017.

[7] D. Hancock, N. Fraser, M. Jeremy and R. Sykes, "A New 3 Cylinder 1.2l Advanced Downsizing Technology Demonstrator Engine," *SAE Papers,* 2008.

[8] R. G. Sykes, "Tickford Five Valve Per Cylinder Technology for Optimised Performance and Combustio," *SAE Papers,* 1995.

[9] B. Jawad, A. Dragoiu, L. Dyar, K. Zellner and C. Riedel, "Intake Design for Maximum Performance," *SAE Papers,* 2003.

[10] N. Takahashi, "Downsizing as Evolution of High Thermal Efficiency Gasoline Engine," *Honda R&D Technical Review,* 2015.

[11] G. M. Bianchi, G. Cantore, E. Mattarelli, G. Guerrini and F. Papetti, "The Influence of Stroke-to-Bore Ratio and Combustion Chamber Design on Formula One Engines Performance," in *Design of Racing and High-Performance Engines*, Warrandale, PA, Society of Automotive Engineers, 1998, pp. 495-509.

[12] C. R. Morgan and P. W. Kirklin, "The Effects of Engine Variables and Exhaust Gas Recirculation on Emissions, Fuel Economy and Knock," *SAE Papers,* 1977.

[13] M. Gurty and J. Heywood, "An Investigation of Gasoline Engine Knock Limited Performance and the Effects of Hydrogen Enhancement," *SAE Papers,* 2006.

[14] A. Ayala, M. D. Gerty and J. B. Heywood, "Effects of Combustion Phasing, Relative Air-Fuel Ratio, Compression Ratio, and Load on SI Engine Efficiency," *SAE Papers,* 2006.

[15] S. Bogomolov, V. Dolecek, J. Macek, A. Mikulec and O. Vitek, "Combining Thermodynamics and Design Optimization for finding ICE Downsizing limits," *SAE Papers,* 2014.

[16] F. Westin and H. Ångström, "Optimisation of Turbocharged Engines' Transient Response with Application on a Formula SAE / Student engine," *SAE Papers,* 2005.

[17] T. Fukuoka, K. Fujimoto, Y. Hongo and S. Kajiwara, "Tuning for FSAE Engine with a Supercharger," *SAE Papers,* 2015.

[18] A. J. Feneley, A. Pesiridis and A. M. Andwari, "Variable Geometry Turbocharger Technologies for Exhaust Energy Recovery and Boosting - A Review," *Renewable and Sustainable Energy Reviews,* 2016.

[19] Aeristech, "Electric Superchargers (eSuperchargers)," 2015. [Online]. Available: http://www.aeristech.co.uk/electric-supercharger/. [Accessed 12 December 2016].

[20] H. Holloway, "The scalable technology that could save the combustion engine," Autocar, 6 February 2017. [Online]. Available: https://www.autocar.co.uk/car-news/industry/scalable-technology-could-save-combustion-engine. [Accessed 12 February 2017].

[21] MAHLE Powertrain, "MAHLE eSupercharged Downsizing Engine," May 2016. [Online]. Available: http://www.mahle-powertrain.com/media/mahle-powertrain/experience/mahle-advanced-downsizing-engine/mahle-esupercharged-downsizing-engine-final-non-print.pdf. [Accessed 20 December 2016].

[22] N. Okanishi and K. Miyake, "Study on Crankcase Supercharging," *SAE Papers,* 2002.

[23] G. Goddard, *V-Twin and Formula 1 Design Concepts [Interview],* 2015.

[24] FSAE, Formula SAE rules, Society of Automotive Engineers, 2016.

[25] L. J. Hamilton and J. E. Lee, "The Effects of Intake Plenum Volume on the Performance of a Small Normally Aspirated Restricted Engine," *SAE Papers,* 2008.

[26] E. Mattarelli and C. A. Rinaldini, "Development of a High Performance Engine for a Formula SAE Racer," *SAE Papers,* 2012.

[27] Formula Student Germany, "FSC Autocross Event Results," 2013. [Online]. Available: http://www.formulastudent.de/uploads/media/.

[28] H. Hemholtz, "On the Theory of Pipes," in *On the Sensations of Tone as a Physiological Basis for the Theory of Music*, London, Longmans, Green and Co, 1895, pp. 388-398.

[29] G. Goddard, *'Organ Tuning' Intake Resonance Calculation,* 2012.

[30] A. J. Torregrosa, A. Broatch and R. Payri, "On the Influence of Manifold Geometry on Exhaust Noise," *SAE Papers,* 1999.

[31] R. Jameson and P. Hodgins, "Improvement of the Torque Characteristics of a Small, High-Speed Engine Through the Design of Hemholtz-Tuned Manifolding," *SAE Papers,* 1990.

[32] Y. Cui, W. Pan, J. H. Leylek, R. G. Sommer and S. K. Jain, “Cylinder-to-Cylinder Variation of Losses in Intake Regions of IC Engines,” *SAE Papers,* 1998.

[33] B. Jawad, K. Yee, S. Arslan and L. Liu, “Improving Engine Performance Through Intake Design,” *SAE Papers,* 2013.

[34] M. Claywell and D. Horkeheimer, “Improvement of Intake Restrictor Performance for a Formula SAE Race Car through 1D & Coupled 1D/3D Analysis Methods,” *SAE Papers,* 2006.

[35] C. E. Douglas and F. Larsson, “V-Twin Plenum Design and Output Modelling,” 2010.

[36] R. J. Primus, “A Second Law Approach to Exhaust System Optimisation,” *SAE Papers,* 1984.

[37] M. Lakshmikantha, “Optimisation of Exhaust Systems,” *SAE Papers,* 2002.

[38] R. Wade and J. C. Hsieh, “Exhaust Manifold Durability Subject to Splash Quenching,” *SAE Papers,* 2015.

[39] J. Taylor, R. McKee, G. McCullough, G. Cunningham and C. McCartan, “Computer Simulation and Optimisation of an Intake Camshaft for a Restricted 600cc FourStroke Engine,” *SAE Papers,* 2006.

[40] S. McClintock, J. Walkingshaw, C. McCartan and G. McCullough, “Camshaft Design for an Inlet-Restricted FSAE Engine,” *SAE Papers,* 2008.

[41] H. Sandquist, J. Wallesten, K. Enwald and S. Stromberg, “Influence of Valve Overlap Strategies on Residual Gas Fraction and Combustion in a Spark-Ignition Engine at Idle,” *SAE Papers,* 1997.

[42] J. M. Brady, “A Simple High Efficiency S.I. Engine Design,” *SAE Papers,* 2003.

[43] J. Taylor, N. Fraser, R. Dingelstadt and H. Hoffmann, “Benefits of Late Intake Valve Timing Strategies Afforded Through the Use of Intake Cam In Cam Applied to a Gasoline Turbocharged Downsized Engine,” *SAE Papers,* 2011.

[44] C. E. Newman, R. A. Stein, C. C. Warren and G. C. Davis, “The Effects of Load Control with Port Throttling at Idle - Measurements and Analyses,” *SAE Papers,* 1989.

[45] T. Baker and C. J. Nightingale, “Port Throttling and Port Deactivation Applied to a 4-Valve SI Engine,” *SAE Papers,* 1996.

[46] K. Nakano, Y. Wada, M. Jono and S. Narihiro, “New In-Line 4-Cylinder Gasoline Direct Injection Turbocharged Downsizing Engine,” *Honda R&D Technical Review,* 2016.

[47] T. Sahirasuna, H. Saito and T. Nomura, “Research on Combustion Improvement Techniques by Intake Valve Offset and Squish Effect,” *Honda R&D Technical Review,* 2013.

[48] R. D. Rabbitt, “Fundamentals of Reciprocating Engine Airflow Part I: Valve Discharge and Combustion Chamber Effects,” *SAE Papers,* 1994.

[49] Prokart Engine Parts, *Honda GX390 Cylinder Head.*

[50] Vespa, *Vespa 3 Valve Cylinder Head.*

[51] Performance Trends, *YZ450F Cylinder Heads.*

[52] K. Aoi, K. Nomura and H. Matsuzaka, “Optimization of Multi-Valve, Four Cycle Engine Design - The Benefit of Five-Valve Technology,” *SAE Papers,* 860032.

[53] D. Corrigan, G. McCullough and G. Cunningham, “Evaluation of the Suitability of a Single-Cylinder Engine for Use in FSAE,” *SAE Papers,* 2006.

[54] S. Kim and S. Kim, “Effects of Swirl and Spark Plug Shape on Combustion Characteristic in a High Speed Single-Shot Visualized SI Engine,” *SAE Papers,* 1995.

[55] A. Cairns and C. G. Sheppard, “Cyclically Resolved Simultaneous Flame and Flow Imaging in a SI Engine,” *SAE Papers,* 2000.

[56] C. E. Douglas, “Valvetrain Clash Analysis,” 2010.

[57] D. Child and M. Banyai, *Piston Representation in V-Twin Camshaft Timing Spreadsheet,* 2009.

[58] P. Mandloi, S. Shrivastava, C. Patil and S. Kottalgi, “Simulation driven design of Engine Cylinder Head,” *SAE Papers,* 2015.

[59] A. Graham Bell, Four Stroke Performance Tuning, 3rd ed., Somerset: Haynes Publishing, 2006.

[60] A. Schilling, Automotive Engine Lubrication, Worchester: Scientific Publications, 1972.

[61] Machinery Lubrication, “A Balanced Approach to Lubrication Effectiveness,” 11 2010. [Online]. [Accessed 22 December 2016].

[62] C. Atkinson, “Fuel Efficiency Optimization using Transient Engine Calibration,” *SAE Papers,* 2014.

[63] A. Hundere, “New Approaches to Electronic Throttle Control,” *F/A by EGT (Mixture Control by Exhaust Gas Temperature),* 1965.

[64] X. Tang, J. R. Asik, G. M. Meyer and R. G. Samson, “Optimal A/F Ratio Estimation Model (Synthetic UEGO) for SI Engine Cold Transient AFR Feedback Control,” *SAE Papers,* 1998.

[65] D. Tang, M. Chang and M. C. Sultan, “Predictive Engine Spark Timing Control,” *SAE Papers,* 1994.

[66] S. Yamamoto, S. Matsumoto, T. Ueda, T. Kodama, Y. Honda and K. Wakabayashi, “A Study on Intake and Exhaust System of Turbocharged Engine under Regulations of Formula SAE,” *SAE Papers,* 2007.

[67] F. Zhao, M. Lai and D. L. Harrington, “A review of Mixture Preparation and Combustion Control Strategies for Spark-Ignited Direct Injection Gasoline Engines,” *SAE Papers,* 1997.

[68] MAHLE Powertrain, “MAHLE Jet Ignition,” [Online]. Available: http://www.mahle-powertrain.com/en/experience/mahle-jet-ignition/. [Accessed 12 November 2016].

[69] S. Ashley, “Attacking GDI Engine Particulate Emissions,” 23 December 2014. [Online]. [Accessed 18 November 2016].

[70] M. Yumoto, K. Goto, S. Kato and M. Iida, “Influence of Injection and Flame Propagation on Combustion in Motorcycle Engine – Investigation by Visualisation Technique,” *SAE Papers,* 2011.

[71] E. Corti and C. Forte, “Idle Stalling Phenomena in High Performance Spark Ignition PFI Engines: an Experimental Analysis,” *SAE Papers,* 2011.

[72] C. Brehm, J. H. Whitelaw, L. Sassi and C. Vafidis, “Air and Fuel Characteristics in the Intake Port of a SI Engine,” *SAE Papers,* 1999.

[73] S. Chappuis, B. Cousyn, M. Posylkin, F. Vannobel and J. H. Whitelaw, “Effects of injection timing on performance and droplet characteristics of a sixteen-valve four cylinder engine,” *Experiments in Fluids,* pp. 336-344, 1997.

[74] D. Whitelaw, “Droplet atomisation of Newtonian and non-Newtonian fluids incluidng automotive fuels,” *Imperial College of Science, Technology and Medicine, London,* 1997.

[75] J. E. Pakkala and J. B. Burl, “Fuel Evaporation Parameter Identification During SI Cold Start,” *SAE Papers,* 2001.

[76] F. T. Scafati, F. Pirozzi, S. Cannavacciuolo, L. Allocca and A. Montanaro, “Real Time Control of GDI Fuel Injection during Ballistic Operation Mode,” *SAE Papers,* 2015.

[77] X. Ding, J. Wang and Y. Z. Liu, “A Study of Calibration of Electronic-controlled Injector Employed in High Pressure Common Rail System,” *SAE Papers,* 2008.

[78] Y. Nishimura and K. Ishii, “Engine Idle Stability Analysis and Control,” *SAE Papers,* 1986.

[79] L. Eriksson, “Spark Advance for Optimal Efficiency,” *SAE Papers,* 1999.

[80] L. Eriksson and I. Andersson, “An Analytic Model for Cylinder Pressure in a Four Stroke SI Engine,” *SAE Papers,* 2002-01-0371.

[81] P. Yoon, S. Park, M. Sunwoo, I. Ohm and K. Yoon, “Closed-Loop Control of Spark Advance and Air-Fuel Ratio in SI Engines Using Cylinder Pressure,” *SAE Papers,* 2000.

[82] R. Stone, Introduction to Internal Combustion Engines, 4th ed., Basingstoke: Palgrave Macmillan, 2012.

[83] L. C. Yang, A. Hamada and K. Ohtsubo, “Engine Valve Temperature Simulation,” *SAE Papers,* 2000.

[84] J. Heywood, Internal Combustion Engine Fundamentals, 3rd ed., New York; London: McGraw-Hill, 1988.

[85] W. R. Leppard, “Individual-Cylinder Knock Occurrence and Intensity in Multicylinder Engines,” *SAE Papers,* 1982.

[86] K. Burgdorf and I. Denbratt, “A Contribution to Knock Statistics,” *SAE Papers,* 1998.

[87] W. Huber, B. Lieberoth-Leden, W. Maisch and A. Reppich, “New Approaches to Electronic Throttle Control,” *SAE Papers,* 1991.

[88] M. Costin, R. Schaller, M. Maiorana, J. Purcell, R. Simon, P. Bauerle and J. Stockbridge, “An Architecture for Electronic Throttle Control Systems,” *SAE Papers,* 2003.

[89] J. Wengert, D. Rommel and R. Krzok, “Electronic Throttle Control for Motorcycles,” *SAE Papers,* 2007.

[90] S. Jiang, M. H. Smith and J. Kitchen, “Optimisation of PID Control for Engine Electronic Throttle System using Iterative Feedback Tuning,” *SAE Papers,* 2009.

[91] J. M. Galante-Fox, D. E. Jarvis, R. D. Garrick and A. J. Chen, “Throttle Icing: Understanding the Icing Mechanism and Effects of Various Throttle Features,” *SAE Papers,* 2008.

[92] E. Hashimoto, T. Ishiguro, Y. Yasui and S. Akazaki, “High Reliability Electronic Throttle System Design,” *SAE Papers,* 2003.

[93] A. Pechlaner and B. Steurich, “Electronic Throttle Control with Contactless Position Sensor and Smart Power Full-Bridge,” *SAE Papers,* 2001.

[94] R. Royo, J. Corberá, L. Azara and E. Marcheguet, “The New “Torque Strategy” for the Control of the Spark Ignition Engine. Development of a Motorized Butterfly Valve Through Experimental Techniques and Computation Modelling,” *SAE Papers,* 2001.

[95] B. Badreddine, A. Zaremba, J. Sun and F. Lin, “Active Damping of Engine Idle Speed Oscillation by Applying Adaptive Pid Control,” *SAE Papers,* 2001.

[96] H. B. Pacejka, Tyre and Vehicle Dynamics, 2nd ed., Amsterdam; London: Butterworth-Heinemann, 2006.

[97] D. D. Hoffman, “The Corvette Acceleration Slip Regulation (ASR) Application with Preloaded Limited Slip Differential,” *SAE Papers,* 1992.

[98] W. F. Milliken and D. L. Milliken, Race Car Vehicle Dynamics, Warrandale, PA: Society of Automotive Engineers, 1995.

[99] M. Plint and A. Martyr, Engine Testing: Theory and Practice, 2nd ed., Warrandale, PA: Society of Automotive Engineers, 1999.

[100] Schenck, Technical Specifications - Eddy Current Dynamometer - W Series, 2001.

[101] L. Little, *Design, Development, Configuration and Engine Testing of a KTM Engine for use on the ISIS XI Class 1 Car,* Dissertation: Oxford Brookes University, 2011.

[102] M. Percival, *Dynamometer testing, development and design work of the KTM 530 EXC 2011 Oxford Brookes Formula Student engine,* Dissertation: Oxford Brookes University, 2011.

[103] Honeywell, "GT101 Hall Effect Datasheet," 1991. [Online]. Available: http://sensing.honeywell.com/1gt101dc-hall-effect-gear-tooth-sensor-88720-sep91-install.pdf. [Accessed 04 April 2016].

[104] Link ECU, *Start/Warmup Enrichment Graph.*

[105] FSAE, " FSAE Lincoln Site Map," 28 03 2014. [Online]. Available: http://www.fsae.com. [Accessed 25 07 2020].

[106] Bailey Morris, Dynamometer Driveshaft 14AS-20 Specification.

[107] Vibracoustic, "Powertrain Products: Centering devices, Isolators & Dampers," 2016. [Online]. Available: https://www.vibracoustic.com/products/passenger-cars/powertrain/centering-devices-isolators-dampers . [Accessed 16 Sept 2016].

[108] Antivibration Methods, Load/Deflection Graph of Rubber Isolators.

[109] CCA, "Torsionally Soft Couplings: Quill Shafts," [Online]. Available: http://couplingcorp.com/products/torsionallysoft-couplings/quill-shaft/. [Accessed 16 Sept 2016].

[110] G. Goddard, "Cosworth BD4 and DA2 Cam Profiles," 2010.

[111] P. Smith, J. Heywood and W. Cheng, "Effects of Compression Ratio on Spark-Ignited Engine Efficiency," *SAE Papers,* 2014.

[112] J. Banerjee and J. McPhee, "Volumetric Tire Models for Longitudinal Vehicle Dynamics Simulations," *SAE Papers,* 2016.

[113] G. Cathcart and C. Zavier, "Fundamental Characteristics of an Air-Assisted Direct Injection Combustion System as Applied to 4-Stroke Automotive Gasoline Engines," *SAE Papers,* 2000.

[114] R. F. Duckworth and L. Barker, "A Comparative Study of Variable Camshaft Phasing and Port Throttling for Performance and Emissions," *SAE Papers,* 1996.

[115] S. M. Dues, J. M. Adams and G. A. Shinkle, "Combustion Knock Sensing: Sensor Selection and Application Issue," *SAE Papers,* 1990.

[116] C. Hallum, "Understanding Race Tyres," *SAE Papers,* 1998.

[117] B. Jawad and S. Arsian, "Cylinder Head Intake Flow Analysis," *SAE Papers,* 2013.

[118] J. Mayo, "The Effect of Engine Design Parameters on Combustion Rate in Spark-Ignition Engines," *SAE Papers,* 1975.

[119] P. J. Shayler and L. Alger, "Experimental Investigations of Intake and Exhaust Valve Timing Effects on Charge Dilution by Residuals, Fuel Consumption and Emissions at Part Load," *SAE Papers,* 2007.

[120] A. Smith, S. Rajauria and S. Agarwal, "Development of Cylinder Block and Cylinder Head for Four Valve/Cylinder OHV Engine for Future High Performance and Durability Needs," *SAE Papers,* 2013.

[121] A. Sorniotti and M. Velardocchia, "Enhanced Tire Brush Model for Vehicle Dynamics Simulation," *SAE Papers,* 2008.

[122] Zircotec, "Description of Motorsport Applications and Ceramic Exhaust Coatings," [Online]. Available: www.zircotec.com. [Accessed 21 Dec 2015].

[123] MAHLE Powertrain, *Torsional Vibration in Driveshafts.*

[124] Dynamometer World, "Consultancy Services," [Online]. Available: https://www.dynamometer-world.com/index.php/dyno-data/consultancy-services.html.

[125] DSG Group, "Bespoke Engineering," 2012. [Online]. Available: http://www.dsgroup.uk.com/bespoke-engineering.

[126] P. Han-rui, P. Mei-chun, Z. Lin-li and D. Xu-bing, "An Optimisation Design of Throttle Body for EFI Motorcycle Engine," *SAE Papers,* 2008.

[127] O. Stenlåås, O. Erlandsson, R. Egnell, B. Johansson, E. Alm, M. Alaküla and F. Mauss, "The Effect of Unconventional Piston Movement on SI Engine Combustion and Emissions," *SAE Papers,* 2005.

[128] J. Hoard and L. Rehagen, "Relating Subjective Idle Quality to Engine Combustion," *SAE Papers,* 1997.

Appendices

Appendix A – Ancillary Components and Regulations

Formula Student Dynamic Competitions

Table A1: *Definition of Dynamic Competitions in Formula Student Events. Adapted from [24]*

Event Type	Objective / Description	Length	Available Points
Acceleration	Evaluates vehicle acceleration in a straight line on flat pavement.	75m	100
Skidpad	To measure vehicle cornering ability on a flat surface while making a constant-radius turn	-- Figure A1	75
Autocross	To evaluate vehicle manoeuvrability and handling qualities on a tight course without the hindrance of competing cars. The autocross course will combine the performance features of acceleration, braking, and cornering into one event	~800m Figure A2	125
Endurance	To evaluate the overall performance, durability and reliability of the vehicle	22,000m Figure A2	275
Efficiency	Measured in conjunction with the endurance event, the efficiency under competition conditions is important in most vehicle competitions and also shows how well the vehicle has been tuned for the competition.	-- Figure A2	125

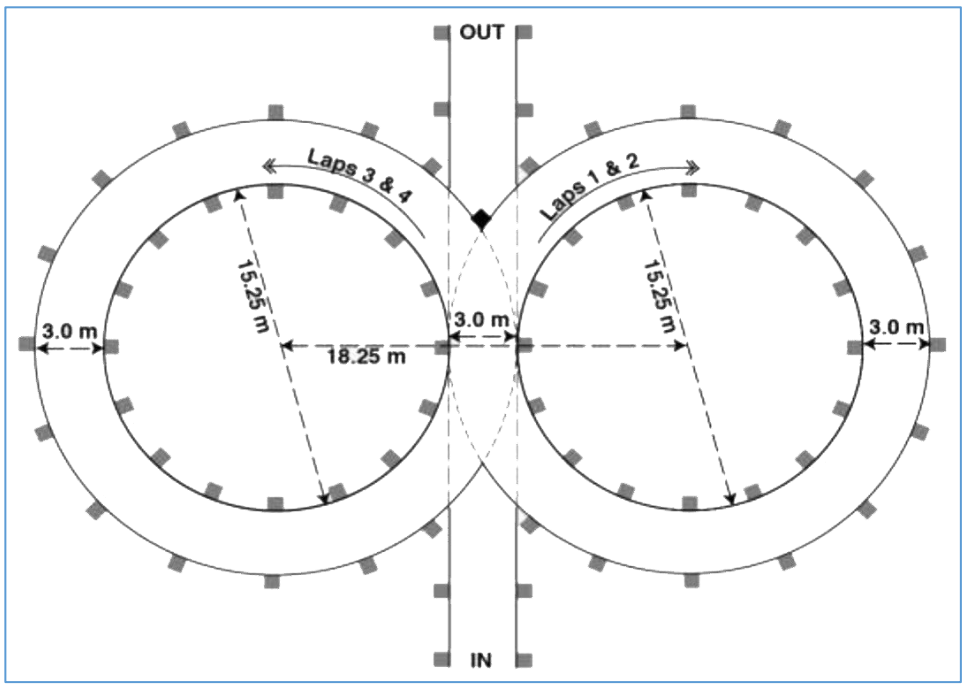

Figure A1*: Formula Student Skidpad Layout [24]*

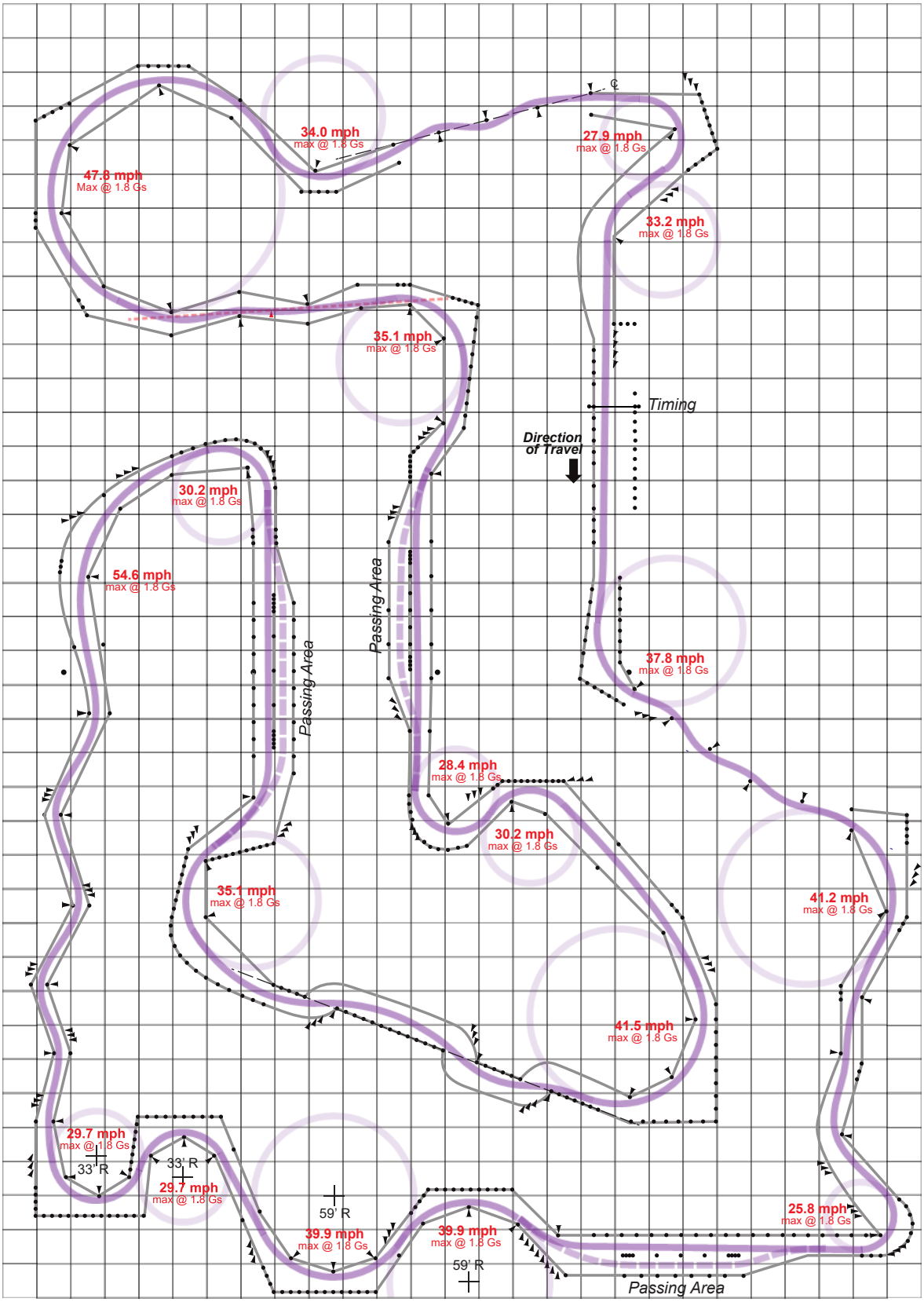

Figure A2: Typical Formula Student Autocross / Endurance Layout [105]

Propshaft

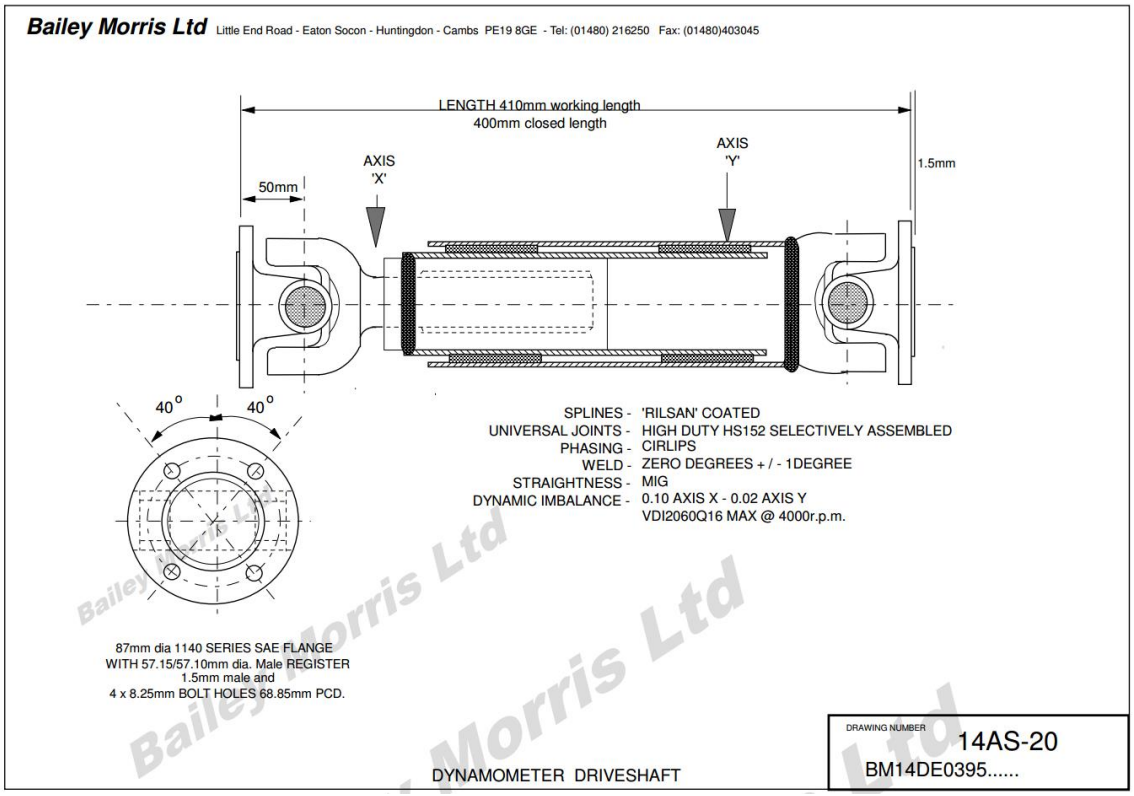

Figure A3: Dynamometer Cell 4 Propshaft [106]

Dynamometer

		W 40	W 70	W 130	W 230	W 700
Power	[kW]	40	70	130	230	700
Rated torque	[Nm]	75	150	400	750	4000
Minimal speed for rated torque	[rpm]	2000	1350	1250	620	400
Maximal speed	[rpm]	17000	13000	10000	7500	4000
Minimal speed for maximal power	[rpm]	5093	4457	3104	2928	1671
Moment of inertia	[kgm²]	0,01	0,035	0,14	0,53	7,9
Maximal share of mass to be coupled at n_{max}	[kg]	0,5	1,0	2,0	4,5	26,0
Maximum exciting current	[A]	1,8	3,6	6,1	6,1	10,0
Weight	[kg]	125	170	270	472	1810
Color pendulum body		RAL 7032				
Color frame		RAL 7022				
Operating temperature	[°C]	0...+70 without cooling water addition –25...+70 with antifreezer and power reduction of 10-20%				
Transporting and storage temperature	[°C]	–50...+85				
Cooling water supply	[m³/h]	see chapter "Cooling Water Supply"				
Torque / Speed Measuring System						
Measuring accuracy speed	[rpm]	± 1, not lower than 0.025 % of rating				
Measuring accuracy torque	[%]	0.2 , referring to rating				
Control accuracy speed*	[rpm]	± 10				
Control accuracy torque*	[%]	± 1 , referring to rating				

* referring to the system eddy-current dyno, power supply unit, test stand controller

Figure A4: W130 Eddy-Current Dynamometer Specification [100]

Appendix B – Engine Records

OBR V-Twin ECU Configurations

OBR[ ]_VTWIN_0012

Chassis Year (Blank if N/A) — Integer

VTWIN: Oxford Brookes Churchill V-Twin
K-570: KTM EXC 530 (570cc)
K-510: KTM EXC 530 (510cc)

V-Twin Engine Dynamometer Configurations			Failsafes			Base Tables			Sensors					Triggers			
Filename	Description	Date Created	RPM	P_Oil	ECT	Fuel	Ign	P-Start	P_Oil	P_Fuel	ECT	TP	MAP	Crank	Cam	Offset	Cyl2 adv
OBR_VTWIN_000	Original Base map for calibration of sensors. Set basic engine geometries and reduced number of active tables	16/05/2016	✗	✗	✗	✗	✗	✗	✗	✗	✗	✗	✗	✗	✗	✗	✗
OBR_VTWIN_001	Set Advance limit to 30deg to prevent damage to engine incase of incorrect entry. Set RPM limiter type.	16/05/2016	✓	✗	✗	✗	✗	✗	✗	✗	✗	✗	✗	✗	✗	✗	✗
OBR_VTWIN_002	Added Pullup resistors for crank (Trig1) and cam (Trig2) hall effect sensors.	31/05/2016	✓	✗	✗	✗	✗	✗	✗	✗	✗	✗	✗	✗	✗	✗	✗
OBR_VTWIN_003	Setup and calibration of ECT, Oil Presure, IAT and External Lambda Controllers.	20/06/2016	✓	✗	✗	✗	✗	✗	✗	✗	✗	✗	✗	✗	✗	✗	✗
OBR_VTWIN_004	Corrected number of teeth on trigger 1 wheel settings. Coolant Pump added as engine thermo fan 1. Hall effect trigger edges defined.TP set	22/06/2016	✓	✗	✗	✗	✗	✗	✓	✓	✓	✗	✗	✓	✓	✗	✗
OBR_VTWIN_005	Set trigger 2 TDC offset based mechanically from CA between timing notch and TDC	11/07/2016	✓	✗	✗	✗	✗	✗	✓	✓	✓	✓	✗	✓	✓	✗	✗
OBR_VTWIN_006	Set Ign advance to zero across all sites in order to use timing light. Ajusted Offset to match Strobe at TDC	19/07/2016	✓	✗	✗	✗	✗	✗	✓	✓	✓	✓	✗	✓	✓	✓	✗
OBR_VTWIN_007	Added Ignition advance map at 75% of maximum. Set Zero degree advance at first firing sites to prevent engine damage. Accr enrichment off	28/07/2016	✓	✓	✓	✓	✓	✓	✓	✓	✓	✓	✗	✓	✓	✓	✗
OBR_VTWIN_008	Post Start Enrichment added. RPM filtering added and Ignition Adv set to zero for timing light on Cyl2. Individual Cyl trim set on Cyl2	31/07/2016	✓	✓	✓	✓	✗	✓	✓	✓	✓	✓	✗	✓	✓	✓	✓
OBR_VTWIN_009	Custom TDC positions set for odd firing order (0, 75). Cam sensor offset to 115deg.	31/07/2016	✓	✓	✓	✓	✓	✓	✓	✓	✓	✓	✗	✓	✓	✗	✗
OBR_VTWIN_010	More Ivel added to cranking regions. Cam sensor offset to 113 deg.	01/08/2016	✓	✓	✓	✓	✓	✓	✓	✓	✓	✓	✗	✓	✓	✓	✓
OBR_VTWIN_011	Custom TDC positions set for even firing (0deg, 435 deg)	19/08/2016	✓	✓	✓	✓	✓	✓	✓	✓	✓	✓	✗	✓	✓	✓	✗
OBR_VTWIN_012	increased fuelling around 1000rpm sites. Restored individual cylinder ign trim to cyl2	21/08/2016	✓	✓	✓	✓	✓	✓	✓	✓	✓	✓	✗	✓	✓	✓	✓
OBR_VTWIN_013	increased fuelling around 1000rpm sites. Restored individual cylinder ign trim to cyl3	22/08/2016	✓	✓	✓	✓	✓	✓	✓	✓	✓	✓	✗	✓	✓	✓	✓
OBR_VTWIN_014	increased fuelling around 1000rpm sites. Restored individual cylinder ign trim to cyl4	23/08/2016	✓	✓	✓	✓	✓	✓	✓	✓	✓	✓	✗	✓	✓	✓	✓
OBR_VTWIN_015	increased fuelling around 1000rpm sites. Restored individual cylinder ign trim to cyl5	24/08/2016	✓	✓	✓	✓	✓	✓	✓	✓	✓	✓	✗	✓	✓	✓	✓
OBR_VTWIN_016	increased fuelling around 1000rpm sites. Restored individual cylinder ign trim to cyl6	25/08/2016	✓	✓	✓	✓	✓	✓	✓	✓	✓	✓	✗	✓	✓	✓	✓
OBR_VTWIN_017	Based on 016 - reduced crank hold and post start decay time	30/08/2016	✓	✓	✓	✓	✓	✓	✓	✓	✓	✓	✗	✓	✓	✓	✓
OBR_VTWIN_018	Based on 017 - Increased Post start and reduced hold times	31/08/2016	✓	✓	✓	✓	✓	✓	✓	✓	✓	✓	✗	✓	✓	✓	✓
OBR_VTWIN_019	Based on 018 - increased fuel sites above 1000rpm by 5%	31/08/2016	✓	✓	✓	✓	✓	✓	✓	✓	✓	✓	✗	✓	✓	✓	✓
OBR_VTWIN_022	Based on 017 - Increased 1000-2000rpm advance and OVT injection timing	31/08/2016	✓	✓	✓	✓	✓	✓	✓	✓	✓	✓	✗	✓	✓	✓	✓
OBR_VTWIN_021	Based on 020 - Adjusted fuel at 20% TP	01/09/2016	✓	✓	✓	✓	✓	✓	✓	✓	✓	✓	✗	✓	✓	✓	✓
OBR_VTWIN_022	Based on 021 - Recalibrated engine coolant temperature sensor	01/09/2016	✓	✓	✓	✓	✓	✓	✓	✓	✓	✓	✗	✓	✓	✓	✓
OBR_VTWIN_023	Based on 022 - Fuel table adjusted by ECU to match recorded lambda. Post start hold time reduced to note effect on engine startup	02/09/2016	✓	✓	✓	✓	✓	✓	✓	✓	✓	✓	✗	✓	✓	✓	✓
OBR_VTWIN_024	Based on 022 - Increased ignition at 40kPa, 2000rpm to note effect on engine pick-up and EGT	02/09/2016	✓	✓	✓	✓	✓	✓	✓	✓	✓	✓	✗	✓	✓	✓	✓
OBR_VTWIN_025	Based on 024 - Increased fuelling at 2000rpm, 40% throttle to improve pickup	02/09/2016	✓	✓	✓	✓	✓	✓	✓	✓	✓	✓	✗	✓	✓	✓	✓
OBR_VTWIN_026	Based on 025 - Increased fuelling at 3000rpm and 4000rpm sites to increase pickup. Recalibrated ECT Sensor	02/09/2016	✓	✓	✓	✓	✓	✓	✓	✓	✓	✓	✗	✓	✓	✓	✓
OBR_VTWIN_027	Based on 026 - Increased ignition advance for all sites up to 5000rpm to match NMK values. Leaned mixture at 2000-4000rpm to accommodate for improved combustion efficiency	10/09/2016	✓	✓	✓	✓	✓	✓	✓	✓	✓	✓	✗	✓	✓	✓	✓
OBR_VTWIN_028	Based on 027 - Increased Maximum Advance Limit to allow for full advance at higher speeds	10/09/2016	✓	✓	✓	✓	✓	✓	✓	✓	✓	✓	✗	✓	✓	✓	✓
OBR_VTWIN_029	Based on 028 - added further load points to provide smoother throttle transition	10/09/2016	✓	✓	✓	✓	✓	✓	✓	✓	✓	✓	✗	✓	✓	✓	✓
OBR_VTWIN_030	Based on 029 - MAP sensor calibration and logging. Added NMK ignition to all sites	19/09/2016	✓	✓	✓	✓	✓	✓	✓	✓	✓	✓	✓	✓	✓	✓	✓
OBR_VTWIN_031	Based on 030 - Increased number of load and speed sites in fuel table	22/09/2016	✓	✓	✓	✓	✓	✓	✓	✓	✓	✓	✓	✓	✓	✓	✓
OBR_VTWIN_032	Based on 031 - Replaced and recalibrated MAP sensor, smoothed Ivel table for mid/high load operation	07/01/2017	✓	✓	✓	✓	✓	✓	✓	✓	✓	✓	✓	✓	✓	✓	✓

Figure B1: *V-Twin ECU Configuration History*

V-Twin Engine Testing Record

EN-10_21-08-16_Startup5

Integer — Short Date — Description

CH: Chassis Dynamometer **TT**: Track Test
EN: Engine Dynamometer

Engine Dynamometer Testing - Startup and idle conditions

Run ID	Date	Time	Source	Description	Run Time /s	Logged Data
EN-01	30/07/2016	17:06	ECU	Cranking	5	EN-01_30-07-16_ECU_Cranking1
EN-02	30/07/2016	17:08	ECU	Cranking	10	EN-02_30-07-16_ECU_Cranking2
EN-03	01/08/2016	01:36	PC	Startup and 600rpm idle	20	EN-03_01-08-16_PC_Startup-OddFire
EN-05	01/08/2016	13:25	PC	cranking	5	EN-05_01-08-16_PC_Cranking1
EN-06	01/08/2016	13:28	ECU	Startup		EN-06_01-08-16_ECU_Startup-OilPress
EN-07	19/08/2016	19:41	PC	Startup	5	EN-07_19-08-16_PC_Startup
EN-08	21/08/2016	21:07	PC	Startup and 600rpm idle	15	EN-08_21-08-16_PC_Startup-600Idle
EN-09	21/08/2016	21:07	ECU	""		EN-09_22-08-16_ECU_Startup-600Idle
EN-10	22/08/2016	18:18	CADET			EN-10_22-08-16_CADET_Startup-600Idle
EN-11	22/08/2016	20:03	PC	Startup and 1500rpm idle	45	EN-11_22-08-16_PC_Startup-1500Idle
EN-12	22/08/2016	20:06	PC	Startup and 1600rpm idle	25	EN-12_22-08-16_PC_Startup-1600Idle
EN-13	22/08/2016	22:08	CADET	""		EN-13_22-08-16_CADET_Startup-1600Idle
EN-14	22/08/2016	20:09	ECU	""		EN-14_22-08-16_ECU_Startup-1600Idle
EN-15	26/08/2016	19:37	PC	Startup and 1500rpm idle	70	EN-15_26-08-16_PC_Startup-1500Lambda
EN-16	26/08/2016	19:39	ECU	""		EN-16_26-08-16_ECU_Startup-1500Lambda
EN-17	26/08/2016	20:10	CADET	""		EN-17_27-08-16_CADET_Startup-1500Lambda
EN-18	27/08/2016	15:24	ECU	Startup and 1500rpm idle	90	EN-18_27-08-16_ECU_Startup-1500Water
EN-19	27/08/2016	15:39	CADET	""		EN-19_27-08-16_CADET_Startup-1500Water
EN-20	27/08/2016	15:58	PC	Startup and Crankcase Pressure Testing	60	EN-20_27-08-16_PC_Startup-Crankcase
EN-21	27/08/2016	16:12	ECU	""		EN-21_27-08-16_ECU_Startup-Crankcase
EN-22	28/08/2016	17:54	PC	Water Pump, Thermostat and inj timing testing	120	EN-22_28-08-16_PC_Startup-ThermostatInj
EN-23	28/08/2016	17:54	ECU	""		EN-23_28-08-16_ECU_Startup-ThermostatInj
EN-24	28/08/2016	18:08	CADET	""		EN-24_28-08-16_CADET_Startup-ThermostatInj
EN-25	29/08/2016	23:55	ECU	Fuel Enrichment Calibration	55	EN-25_29-08-16_ECU_Startup-EnrichmentData
EN-26	29/08/2016	23:57	ECU	Effect Of Inj timing	45	EN-26_29-08-16_ECU_Startup-InjData
EN-27	29/08/2016	23:57	PC	Both EN-25 and EN-26 Runs		EN-27_29-08-16_PC_Startup-EnrInjData
EN-28	29/08/2016	23:59	CADET	Both EN-25 and EN-26 Runs		EN-28_29-08-16_CADET_Startup-EnrInjData
EN-29	31/08/2016	11:36	ECU	Startup and Header Smoke Identification	70	EN-29_31-08-16_ECU_Startup-1500
EN-30	31/08/2016	11:44	ECU	""	70	EN-30_31-08-16_ECU_Startup-1500
EN-31	31/08/2016	11:44	PC	""		EN-31_31-08-16_PC_Startup-1500
EN-32	31/08/2016	11:51	CADET	""		EN-32_31-08-16_CADET_Startup-1500
EN-33	31/08/2016	11:52	ECU	Cranking and Post Start Configurations	140	EN-33_31-08-16_ECU_Startup-EnrichCal1
EN-34	31/08/2016	11:52	PC	""		EN-34_31-08-16_PC_Startup-EnrichCal1
EN-35	31/08/2016	11:59	CADET	""		EN-35_31-08-16_CADET_Startup-EnrichCal1
EN-36	31/08/2016	16:04	ECU	Cranking and Post Start Configurations 2	220	EN-36_31-08-16_ECU_Startup-EnrichCal2
EN-37	31/08/2016	16:04	PC	"" map18		EN-37_31-08-16_PC_Startup-EnrichCal2
EN-38	31/08/2016	16:10	CADET	""		EN-38_31-08-16_CADET_Startup-EnrichCal2
EN-39	31/08/2016	22:15	ECU	Map 19		EN-39_31-08-16_ECU_Startup-EnrichCal3
EN-40	31/08/2016	22:17	ECU	Map 19 Hot Start		EN-40_31-08-16_ECU_Startup-FuelTrim1
EN-41	31/08/2016	22:17	PC	Map 19 Both Runs	420	EN-41_31-08-16_PC_Startup-FuelTrim1
EN-42	31/08/2016	22:23	ECU	Map 17 Advance and Ignition Changes		EN-42_31-08-16_ECU_Startup-AdvOV11
EN-43	31/08/2016	22:23	PC	Map 17 Advance and Ignition Changes	150	EN-43_31-08-16_PC_Startup-AdvOV11
EN-44	31/08/2016	22:29	ECU	Map 20 Transient. 2.5deg cyl correction		EN-44_31-08-16_ECU_Startup-CylTrim1
EN-45	31/08/2016	22:29	PC	Map 20 Transient	160	EN-45_31-08-16_PC_Startup-CylTrim1
EN-46	31/08/2016	22:35	CADET	EN-39 to EN-45		EN-46_31-08-16_ECU_Startup-FuelIgnTrim
EN-47	01/09/2016	13:40	PC	Warmup and Throttle Increase 2500rpm idle		EN-47_01-09-16_PC_Startup-2500
EN-48	01/09/2016	13:46	ECU	""	260	EN-48_01-09-16_ECU_Startup-2500
EN-49	01/09/2016	13:51	CADET	""		EN-49_01-09-16_CADET_Startup-2500
EN-50	01/09/2016	16:21	ECU	Warmup and 300rpm testing	230	EN-50_01-09-16_ECU_Startup-3000
EN-51	01/09/2016	16:21	PC	""		EN-51_01-09-16_PC_Startup-3000
EN-52	01/09/2016	16:46	CADET	""		EN-52_01-09-16_CADET_Startup-3000
EN-53	02/09/2016	09:48	ECU	Warmup and Fuel Calibration	195	EN-53_02-09-16_ECU_Startup
EN-54	02/09/2016	09:48	PC	""		EN-54_02-09-16_PC_Startup
EN-55	02/09/2016	09:57	CADET	""		EN-55_02-09-16_CADET_Startup
EN-56	02/09/2016	12:51	ECU	Warmup. Problems with LH cylinder combustion	180	EN-56_02-09-16_ECU_Startup2
EN-57	02/09/2016	12:52	PC	""		EN-57_02-09-16_PC_Startup2
EN-58	02/09/2016	12:57	CADET	""		EN-58_02-09-16_CADET_Startup2
EN-59	02/09/2016	14:47	ECU	Switch back to map 17. Cleaned Spark Plug	240	EN-59_02-09-16_ECU_Startup3
EN-60	02/09/2016	14:48	PC	""		EN-60_02-09-16_PC_Startup3
EN-61	02/09/2016	14:54	PC	Warmup and mapping to 3500rpm. High EGT		EN-61_02-09-16_PC_Startup-3500
EN-62	02/09/2016	15:30	ECU	""	140	EN-62_02-09-16_ECU_Startup-3500
EN-63	02/09/2016	19:22	CADET	EN-59 to EN-63		EN-63_02-09-16_CADET_Startup-3500
EN-64	04/09/2016	15:05	ECU	Oil Pump Configuration Testing	75	EN-64_04-09-16_ECU_Startup1
EN-65	04/09/2016	15:05	PC	""		EN-65_04-09-16_PC_Startup1
EN-66	04/09/2016	15:12	CADET	""		EN-66_04-09-16_CADET_Startup1
EN-67	08/09/2016	22:16	ECU	Startup and Cylinder Diagnostics 1	240	EN-67_08-09-16_ECU_Startup1
EN-68	09/09/2016	18:42	ECU	Startup and Cylinder Diagnostics 2	190	EN-68_09-09-16_ECU_Startup1

Engine Dynamometer Testing - Base Calibration

Run ID	Date	Time	Source	Description	Run Time /s	Logged Data
EN-69	10/09/2016	13:22	ECU	Startup and IGN advance mapping 3000rpm	260	EN-69_10-09-16_ECU_Startup-IGN-G
EN-70	10/09/2016	13:41	PC	""		EN-70_10-09-16_PC_Startup-IGN-G
EN-71	10/09/2016	13:46	CADET	""		EN-71_10-09-16_CADET_Startup-IGN-G
EN-72	10/09/2016	14:09	ECU	3500rpm fuel mapping	130	EN-72_10-09-16_ECU_Startup-3500-G
EN-73	10/09/2016	14:09	PC	""		EN-73_10-09-16_PC_Startup-3500-G
EN-74	10/09/2016	14:52	ECU	4000rpm fuel mapping	180	EN-74_10-09-16_ECU_Startup-4000-G
EN-75	10/09/2016	14:52	PC	""		EN-75_10-09-16_PC_Startup-4000-G
EN-76	10/09/2016	15:14	CADET	EN-72 to EN-75		EN-76_10-09-16_CADET_3500-4000-G
EN-77	13/09/2016	21:07	ECU	3500rpm warmup	180	EN-77_13-09-16_ECU_Startup-3500-C
EN-78	13/09/2016	21:25	CADET	3500rpm warmup		EN-78_13-09-16_CADET_Startup-3500-C
EN-79	22/09/2016	21:00	PC	MAP Sensor Calibration 1	135	EN-79_22-09-16_PC_Startup1
EN-80	22/09/2016	21:01	ECU	""		EN-80_22-09-16_ECU_Startup1
EN-81	22/09/2016	21:20	CADET	""		EN-81_22-09-16_CADET_Startup1
EN-82	22/09/2016	21:34	ECU	MAP Sensor Calibration 2	120	EN-82_22-09-16_ECU_Startup2
EN-83	22/09/2016	21:35	PC	""		EN-83_22-09-16_PC_Startup2
EN-84	22/09/2016	22:00	CADET	""		EN-84_22-09-16_CADET_Startup2
EN-85	24/09/2015	14:52	ECU	3000rpm warmup	360	EN-85_24-09-16_ECU_Startup1
EN-86	07/01/2017	15:47	PC	Cranking		EN-86_07-01-17_PC_Cranking
EN-87	08/01/2017	14:51	PC	Warmup1	45	EN-87_08-01-17_PC_Warmup1
EN-88	08/01/2017	15:51	ECU	""		EN-88_08-01-17_ECU_Warmup1
EN-89	08/01/2017	14:51	CADET	""		EN-89_08-01-17_CADET_Warmup1
EN-90	08/01/2017	15:15	ECU	Warmup2	120	EN-90_08-01-17_ECU_Warmup2
EN-91	08/01/2017	15:15	PC	""		EN-91_08-01-17_PC_Warmup2
EN-92	08/01/2017	15:15	CADET	""		EN-92_08-01-17_CADET_Warmup2
EN-93	08/01/2017	17:58	ECU	50%TP, 4000rpm loading	180	EN-93_08-01-17_ECU_Load-4000
EN-94	08/01/2017	17:58	PC	""		EN-94_08-01-17_PC_Load-4000
EN-95	08/01/2017	19:03	ECU	3000rpm to WOT	100	EN-95_08-01-17_ECU_Load-3000
EN-96	08/01/2017	19:03	PC	""		EN-96_08-01-17_PC_Load-3000
EN-97	08/01/2017	19:03	CADET	""		EN-97_08-01-17_CADET_Load-3000
EN-98	08/01/2017	19:53	PC	3500rpm to WOT	120	EN-98_08-01-17_PC_Load-3500
EN-99	08/01/2017	19:53	CADET	""		EN-99_08-01-17_CADET_Load-3500

Figure B2: *V-Twin dynamometer testing record*

V-Twin Propshaft Alignment

Date Tested: 01/09/2016

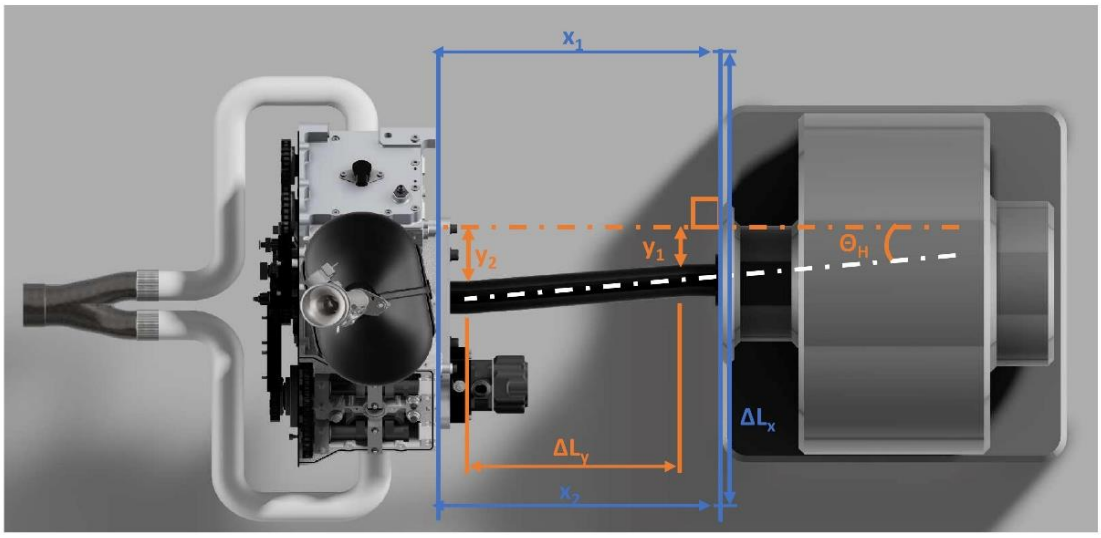

Original Alignment

HORIZONTAL DISPLACEMENT		
y1 /mm	y2 /mm	ΔLY /mm
4.38	10.51	170
Translation /mm		6.13
ΘH /Rad		0.036
ΘH /Deg		2.065

DYNO-ENGINE PARALLELISM		
x1 /mm	x2 /mm	ΔLX /mm
619	622	500
Translation /mm		3
Parallelism /Rad		**0.006**
Parallelism /Deg		**0.344**

Alignment Iterations

HORIZONTAL DISPLACEMENT				
y1 /mm	y2 /mm	ΔLY /mm	ΘH /Rad	ΘH /Deg
0	1.63	202	0.0081	0.462
0	1.2	208	0.0058	0.331
0	1.61	200	0.0080	0.461
0	1.3	195	0.0067	0.382
		Average	**0.0071**	**0.409**

DYNO-ENGINE PARALLELISM
Parallelism not adjusted

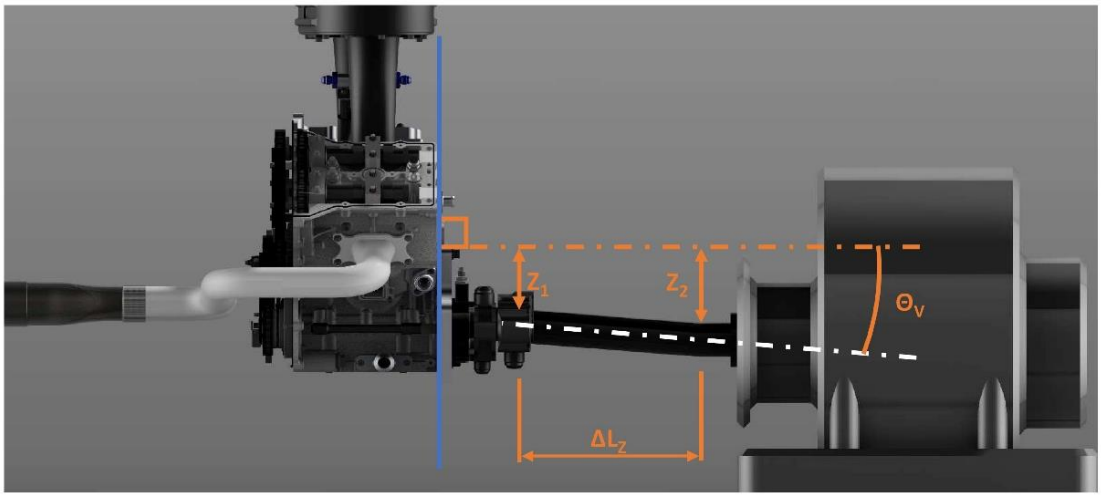

ORIGINAL VERTICAL DISPLACEMENT		
Z1 /mm	Z2 /mm	ΔLZ/mm
33.5	36.2	140
Translation		2.7
ΘV /Rad		0.019
ΘV /Deg		1.105

VERTICAL DISPLACEMENT -3MM SHIM		
Z1 /mm	Z2 /mm	ΔLZ/mm
33.5	33.2	140
Translation		-0.3
ΘV /Rad		**-0.002**
ΘV /Deg		**-0.123**

PROPSHAFT ANGLE SUMMARY			
ΘH /Deg	0.409	Paralleism /Deg	0.34
ΘV /Deg	-0.123		
Misalignment /Deg	0.532	*Misalignment allows appropriate cardan joint movement*	

Figure B3: Record of V-Twin Propshaft Alignment

Appendix C – Supplementary Data

Table C1: Incremental and Cumulative Propshaft Stiffness Calculations

	τ /Nm		Incremental / Instantaneous				Cumulative				
	act	Δ	T/s	Θ/deg	Stiffness /Nm/deg	Stiffness Error /%	T /s	Θ/deg	Stiffness /Nm/deg	Stiffness /Nm/rad	Stiffness Error /%
Run 1 - FWD	20	10	6.38	0.213	94.04	76.16	6.38	0.213	47.02	2694.2	-11.92
	30	20	5.37	0.179	55.87	4.65	11.75	0.392	51.06	2925.7	-4.35
	40	30	5.30	0.177	56.60	6.03	17.05	0.568	52.79	3024.4	-1.12
	50	40	5.63	0.188	53.29	-0.18	22.68	0.756	52.91	3031.5	-0.89
	60	50	5.00	0.167	60.00	12.39	27.68	0.923	54.19	3104.9	1.51
	70	60	8.00	0.267	37.50	-29.75	35.68	1.189	50.45	2890.5	-5.50
	80	70	8.25	0.275	36.36	-31.88	43.93	1.464	47.80	2738.9	-10.45
	90	80	8.41	0.280	35.67	-33.18	52.34	1.745	45.85	2627.2	-14.11
Run 2 - FWD	20	10	5.50	0.183	54.55	2.18	5.50	0.183	54.55	3125.2	2.18
	30	20	5.10	0.170	58.82	10.19	10.60	0.353	56.60	3243.2	6.03
	40	30	4.13	0.138	72.64	36.07	14.73	0.491	61.10	3500.8	14.45
	50	40	5.43	0.181	55.25	3.49	20.16	0.672	59.52	3410.5	11.50
	60	50	5.54	0.185	54.15	1.44	25.70	0.857	58.37	3344.1	9.33
	70	60	5.74	0.191	52.26	-2.10	31.44	1.048	57.25	3280.3	7.25
	80	70	6.29	0.210	47.69	-10.66	37.73	1.258	55.66	3189.0	4.26
	90	80	5.08	0.169	59.06	10.62	42.81	1.427	56.06	3212.1	5.02
	100	90	7.70	0.257	38.96	-27.02	50.51	1.684	53.45	3062.7	0.13
Run3 - REV	30	10	4.89	0.163	61.35	14.92	4.89	0.163	61.35	3515.1	14.92
	40	20	4.20	0.140	71.43	33.80	9.09	0.303	66.01	3781.9	23.65
	50	30	4.64	0.155	64.66	21.12	13.73	0.458	65.55	3755.7	22.79
	60	40	4.20	0.140	71.43	33.80	17.93	0.598	66.93	3834.6	25.37
	70	50	4.73	0.158	63.42	18.80	22.66	0.755	66.20	3792.7	24.01
	80	60	4.65	0.155	64.52	20.86	27.31	0.910	65.91	3776.4	23.46
	90	70	5.64	0.188	53.19	-0.36	32.95	1.098	63.73	3651.6	19.38
Run4 - FWD	20	10	5.73	0.191	52.36	-1.93	5.73	0.191	52.36	2999.8	-1.93
	30	20	5.34	0.178	56.18	5.24	11.07	0.369	54.20	3105.5	1.53
	40	30	5.04	0.168	59.52	11.50	16.11	0.537	55.87	3200.9	4.65
	50	40	6.05	0.202	49.59	-7.11	22.16	0.739	54.15	3102.7	1.44
	60	50	4.79	0.160	62.63	17.32	26.95	0.898	55.66	3189.0	4.26
	70	60	5.85	0.195	51.28	-3.94	32.80	1.093	54.88	3144.3	2.80
	80	70	5.50	0.183	54.55	2.18	38.30	1.277	54.83	3141.5	2.71
	90	80	4.61	0.154	65.08	21.90	42.91	1.430	55.93	3204.6	4.77
	100	90	6.00	0.200	50.00	-6.34	48.91	1.630	55.20	3162.9	3.41
								Average (Excl Rev)	**54.14**	**3102.1**	**(abs) 5.28**

Table C2: Considered Sub-Assemblies and Components in V-Twin Inertia Calculation

FS08-02-149: HALF SPEED GEAR ASSEMBLY						
Part #	**Description**	**Mass /g**	**J X-X**	**QTY**	**Σ J X-X**	
FS08-02-393	Sprocket, HS front	133.21	90282	2	180565	
FS08-02-054	HS Front Spacer	126.74	48626	1	48626	
FS08-02-395	Sprocket, HS rear	128.24	87409	1	87409	
FS08-02-051	NME HS Gear	418.55	561338	1	561338	
FS08-02-053	HS Rear Spacer	159.44	57652	1	57652	
FS08-02-057	10/32 Bolts Asm	15.89	5000	1	5000	
FS08-02-169	Shaft, Cam Drive	61.78	2362	1	2362	
FS08-02-146	Washer, HS Stack	5.86	241	1	241	
FS08-02-245	SKF Roller Bearing	11.06	873	1	873	
FS08-02-181	M6 K-Nut	1.39	18	1	18	
FS08-02-167	SKF Ball Bearing	22.57	3744	1	3744	
FS08-02-170	Circlip, 39mm	3.91	1318	1	1318	
	Total	**1221.85**	**858863**		**949146**	
FS08-02-055: CRANKSHAFT ASSEMBLY						
Part #	**Description**	**Mass /g**	**J X-X**	**QTY**	**Σ J X-X**	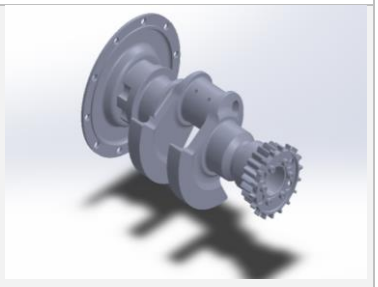
FS08-02-111	Crankshaft rev G	3068	2808300	1	2808300	
FS08-02-313	Flywheel 2009	400	506589	0	0	
FS08-02-617	Trigger Wheel	58.69	44389	1	44389	
FS08-02-628	Pinion Gear	214	114867	1	114867	
FS08-02-034	Bolts	132.9	563387	1	563387	
FS08-02-329	Bearing	15	1416	1	1416	
--	Prop Coupler	500	641700	1	641700	
	Total	**3987**	**4680648**		**4174059**	
RECIPROCATING MASS						
Part #	**Description**	**Mass /g**	**J X-X**	**QTY**	**Σ J X-X**	
FS08-02-121	Conrod	467	237681	1	237681	
FS08-02-114	Bearing Shell					
FS08-02-137	Bolts					
FS08-02-131	Piston	329	167578	1	167578	
FS08-02-112	Gudgeon Pin					
FS08-02-417	Rings					
	Total	**796**	**4038948**		**405259**	
SUMMARY						
Part #	**Description**		**J X-X (gmm²)**	**QTY**	**Σ J X-X (kgm²)**	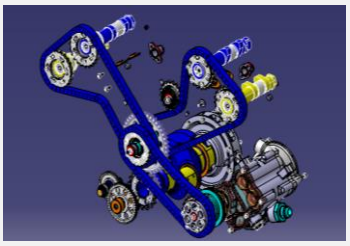
FS08-02-175	Pump Stack Main Assy		--	--	--	
FS08-02-502	Starter 1st Reduction Assy		--	--	--	
FS08-02-503	Starter 2nd Reduction Assy		--	--	--	
FS08-02-149	Half Speed Gear Assy		949146	1	9.4×10^{-4}	
FS08-02-002	Crankshaft Assy		4174059	1	4.2×10^{-3}	
--	Reciprocating Components		405259	1	4.0×10^{-4}	
				Total Engine Inertia	**5.5×10^{-3} Kgm²**	

Table C3: Available channels and data sources for logging

	ECU DATALOGGING (10MS)	CADET CHANNELS (50MS)
COMMON CHANNELS	Engine Speed / Dynamometer Speed	
	Battery Voltage	
	Engine Coolant Temperature	
UNIQUE CHANNELS	Dwell Time	Exhaust Thermocouple (Cyl 1)
	ECU Temperature	Exhaust Thermocouple (Cyl 2)
	Engine Speed ROC	Throttle Demand
	Fuel Pressure	Torque (Observed)
	Fuel QTY and Corrections	Power (Observed)
	Ignition Angle and Trims	-
	Injection Deadtime	-
	Injection Timing	-
	Injector Duty Cycle	-
	Lambda (Cyl 1)	-
	Lambda (Cyl 2)	-
	MAP	-
	MAP Limit	-
	Oil Pressure	-
	Output Voltages	-
	Engine Speed Limit Active	-
	Throttle (Butterfly) Position	-
	Trigger Status and Rotation Direction	-

Appendix D – Driveshaft Recommendations

Increased inertia of the engine through a larger flywheel. The engine inertia is currently significantly less than that of the dynamometer, hence their product can be doubled more easily through adding inertia to the engine side compared to modifying the dynamometer side of the system. However, the external oil pump and the propshaft guard prevent a large diameter flywheel to be added (Figure D1). This reduces the mass efficiency of any solution. Replacing the existing propshaft coupler, a suitable design adds 8.98×10^{-3} kgm^2 inertia (163%) and 1.62kg mass (31%) to the rotating components of the engine (Figure D2). With such a configuration, the average, primary and secondary resonant speeds reduce to 4605, 5565 and 3646 rev/min respectively.

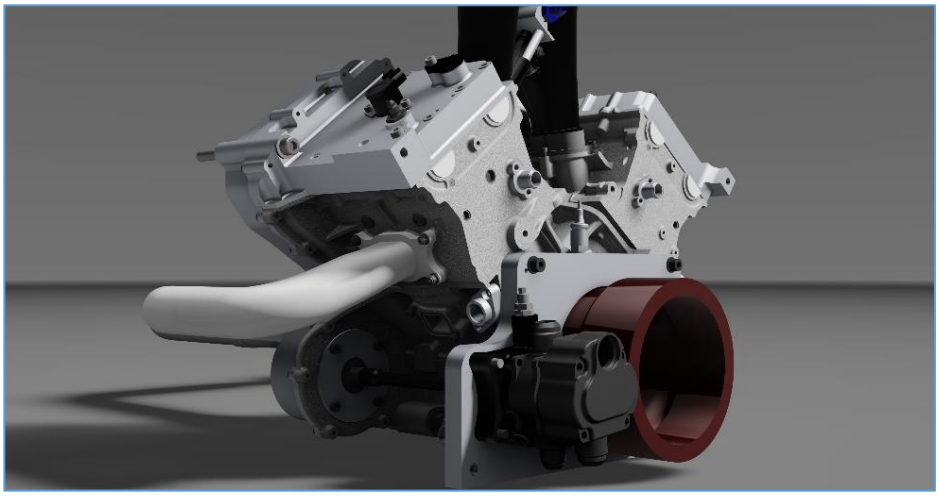

Figure D1: *Representation of permissible flywheel envelope for increased engine inertia*

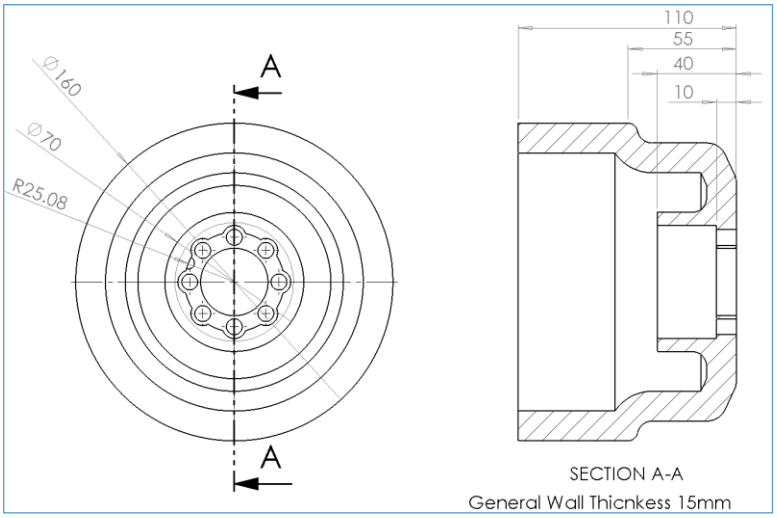

Figure D2: *General dimensions of permissible flywheel*

Reduced stiffness of shaft through rubber couplings. Additional rubber can be connected in series to the propshaft, reducing the stiffness of the system (Figure D3). However, off-the-shelf units do not match the required bolt configuration, increasing cost and lead time.

Figure D3: Flexible Propshaft Couplings available in rubber (left) or steel casings [107]

The spring stiffness of the coupling can be tailored through the hardness of the rubber used [108]. Assuming a shore hardness of 60ShA the addition of a rubber coupling at the engine-end of the system would reduce the average, primary and secondary engine speeds to 4918, 5943 and 3893 rev/min respectively. Heat management may however become a concern if the engine is heavily loaded for long periods of time, as the rubber dissipates a proportion of the cyclic torque loading.

Replacement of the Propshaft with a quill shaft. A quill shaft can be implemented to provide sufficiently low torsional stiffness whilst meeting torque specifications [109]. Designed to operate at higher stress levels these are typically 19-22mm in diameter for dynamometer applications, these shafts are sensitive to the concentricity of engine and dynamometer and may require additional rework of the test cell rig to accommodate.

Figure D4: Quill shaft intended for industrial machinery [109].